



This is to certify that the

dissertation entitled

Photoinduced Reductive Elimination From Binuclear Metal-Metal Complexes

presented by

Ann Marie Macintosh

has been accepted towards fulfillment of the requirements for

Ph.D. degree in Chemistry

Date April 3, 1997

0-12771

PLACE IN RETURN BOX to remove this checkout from your record. TO AVOID FINES return on or before date due.

DATE DUE	DATE DUE	DATE DUE

MSU Is An Affirmative Action/Equal Opportunity Institution stoictdatedus.pm3-p.1

# PHOTOINDUCED REDUCTIVE ELIMINATION FROM BINUCLEAR METAL-METAL COMPLEXES

By

**Ann Marie Macintosh** 

## **A DISSERTATION**

Submitted to

Michigan State University
in partial fulfillment of the requirements
for the degree of

**DOCTOR OF PHILOSOPHY** 

Department of Chemistry
1997

#### **ABSTRACT**

## PHOTOINDUCED REDUCTIVE ELIMINATION FROM BINUCLEAR METAL-METAL COMPLEXES

Вy

## Ann Marie Macintosh

A number of important reactions, such as small molecule activation, involve multielectron processes. As a result, considerable effort has been devoted to designing photochemical schemes in which the photoreagent effects a multielectron transformation. Although there are many examples of multielectron photoreactions, few photochemical systems have been developed where the photoreagent is regenerated. The multielectron photoproduct typically resides in deep thermodynamic or kinetic wells that hinder its conversion back to the photoactive state. However, in some cases it is possible to overcome these barriers by using the excited state of the photoproduct. This dissertation examines multielectron photoinduced reductive elimination from bimetallic complexes. The research focuses on the classes of bimetallic complexes that are known to possess excited states capable of undergoing multielectron transformations.

The quadruply bonded  $Mo_2Cl_2(6-mhp)_2(PR_3)_2$  (mhp = 2-hydroxy-6-methylpyridinato;  $PR_3$  = tertiary phosphine) possess a cis conformation of bridging ligands, which may engender a W-frame structure upon two-electron

oxidation to a Mo<sup>III</sup>Mo<sup>III</sup> complex. The W-frame geometry is important because the bridging halides are in close proximity to each other and may be predisposed to undergo concerted reductive elimination. However, well defined photoredox chemistry is obscured by facile photoinduced redistribution of mhp ligands to give Mo<sub>2</sub>Cl<sub>3</sub>(6-mhp)(PR<sub>3</sub>)<sub>3</sub> and Mo<sub>2</sub>Cl(6-mhp)<sub>3</sub>(PR<sub>3</sub>) as major photoproducts.

The photoinduced two-electron reductive elimination of halide has been realized for two different classes of bimetallic complexes. Photolysis of the dimolybdenum(III) edge-sharing bioctahedral complexes, Mo<sub>2</sub>X<sub>6</sub>(dppm)<sub>2</sub> (X= Cl, Br, I; dppm = bis(diphenylphosphino)methane), results in the photolytic cleavage of two metal-halide bonds to give the quadruply bonded Mo<sub>2</sub>X<sub>4</sub>(dppm)<sub>2</sub> complexes. This is an important result because it represents the first time a quadruply bonded metal-metal complex has been regenerated from a two-electron oxidized product with bioctahedral geometry.

The dirhodium singly bonded metal-metal complex  $Rh_2(dfpma)_3Br_2(\eta^1-dfpma)$  (dfpma = bis(difluorophosphinomethylamine) undergoes two-electron photoreductive elimination to yield a  $Rh^0Rh^0$  product. This reaction is significant because a metal-halide bond usually represents a kinetic and/or thermodynamic sink in a photochemical cycle. The  $d\sigma^*$  excited state of the two-electron mixed-valence complex can overcome such barriers and drive the photoinduced elimination of bromine.

To my parentnts,

Alan and Mary Macintosh

for all the love and support.

#### **ACKNOWLEDGMENTS**

First and foremost, I would like to thank my advisor, Prof. Daniel Nocera for his support and guidance as well as for teaching me how to see the big picture. I am grateful to my second reader, Prof. Kim Dunbar for sharing her special insights into the chemistry of metal-metal bonded complexes. I would also like to thank Prof. John Allison and Prof. John McCracken for serving on my guidance committee.

I am grateful to past and present members of the Nocera group for sharing their friendship and scientific expertise. Specifically, my fellow multielectron photochemists, Dr. Carolyn Hsu, Sara Helvoigt and Dan Engebretson. I would also like to thank Dr. Jeff Zaleski and Jim Roberts for their assistance with lifetime measurements. Dr. Al Barney's critical reading of this document is deeply appreciated. The friendship of Al, Jim, J. P., Sara and Wanda made the process of writing this dissertation bearable.

The Chemistry Department at Michigan State is blessed with a truly outstanding support staff. My graduate career would have been even longer without the prompt and highly competent assistance of glass shop and the electronics shop. The technical assistance of the staff of the Max T. Rogers NMR Facility is greatly appreciated. A special thank you goes to Linda Krause, secretary for the inorganic faculty, for her friendship and for taking care of the details. The figures in this dissertation are better owing to the help of Dr. Tom

Carter. I am grateful to the staffs of the MSU/NIH Mass Spec. Facility and the Macromolecular Structure Facility for their assistance in obtaining the mass spec data reported in this dissertation. The financial support of Michigan State University through a Herbert T. Graham scholarship and an Affirmative Action Scholarship are gratefully acknowledged. In closing, I would like to remember Chris Serafin who died tragically during the completion of this dissertation.

## TABLE OF CONTENTS

			Page
LIST OF TABLES	·····		x
LIST OF FIGURE	s		хi
LIST OF ABBREY	VIAT	IONS	xv
CHAPTER 1	INT	RODUCTION	1
	A.	Visible Absorption Characteristics	4
	В.	Multielectron Reactivity By Coupling One- Electron Steps	8
	C.	Regeneration Of The Photocatalyst	12
	D.	The Discrete Multielectron Approach	19
		1. Quadruply Bonded Metal-Metal Complexes	22
		2. Singly Bonded Metal-Metal Complexes	26
	E.	Dissertation Outline	26
CHAPTER 2	EXI	PERIMENTAL	29
	A.	Synthetic Procedures	29
		1. General Procedures	29
		2. Synthesis of Mo <sub>2</sub> Cl <sub>n</sub> (6-mhp) <sub>4-n</sub> (PR <sub>3</sub> ) <sub>n</sub> Complexes	30
		a. Precursors	30
		b. Mo <sub>2</sub> Cl <sub>2</sub> (6-mhp) <sub>2</sub> (PMe <sub>3</sub> ) <sub>2</sub>	30
		c. Mo <sub>2</sub> Cl <sub>2</sub> (6-mhp) <sub>2</sub> (PR <sub>3</sub> ) <sub>2</sub> (PR <sub>3</sub> =PEt <sub>3</sub> , PMe <sub>2</sub> Ph)	31
		d. Mo <sub>2</sub> Cl <sub>2</sub> (6-mhp) <sub>2</sub> (PMePh <sub>2</sub> ) <sub>2</sub>	31

			Page
		e. Mo <sub>2</sub> Cl <sub>3</sub> (6-mhp) <sub>2</sub> (PMe <sub>2</sub> Ph) <sub>2</sub>	31
		f. Mo <sub>2</sub> Cl(6-mhp) <sub>3</sub> (PMe <sub>2</sub> Ph)	32
		3. Mo <sub>2</sub> X <sub>6</sub> (dppm) <sub>2</sub>	32
		a. Precursors	32
		b. Mo <sub>2</sub> Cl <sub>6</sub> (dppm) <sub>2</sub>	32
		c. Mo <sub>2</sub> Br <sub>6</sub> (dppm) <sub>2</sub>	33
		d. Mo <sub>2</sub> I <sub>6</sub> (dppm) <sub>2</sub>	33
		4. $Rh_2(dfpma)_3Br_2(\eta^1-dfpma)$	33
	В.	Spectroscopic Instrumentation And Methods	34
		1. Electronic Absorption Spectroscopy	34
		2. Steady State Emission Spectroscopy	34
		3. Fluorescence Excitation Spectroscopy	36
		4. Time-Resolved Spectroscopy	36
		5. Nuclear Magnetic Resonance	36
		6. Infrared Spectroscopy	37
		7. Electrospray Mass Spectrometry	37
	C.	Photochemistry	37
CHAPTER 3	QUA	OTOINDUCED LIGAND REDISTRIBUTION OF ADRUPLY BONDED Mo <sub>2</sub> Cl <sub>2</sub> (6-mhp) <sub>3</sub> (PR <sub>3</sub> ) <sub>2</sub> MPLEXES	39
	A.	Background	39
	B.	Photophysical Properties	46
	C.	Photochemistry	55
	D.	Conclusions	70

	Га	ge
CHAPTER 4	PHOTOINDUCED REDUCTIVE ELIMINATION FROM EDGE-SHARING DIMOLYBDENUM COMPLEXES Mo <sub>2</sub> X <sub>6</sub> (dppm) <sub>2</sub>	73
	A. Background	73
	B. Photochemistry	78
	1. Mo <sub>2</sub> I <sub>6</sub> (dppm) <sub>2</sub>	78
	2. Mo <sub>2</sub> Br <sub>6</sub> (dppm) <sub>2</sub>	81
	3. Mo <sub>2</sub> Cl <sub>6</sub> (dppm) <sub>2</sub>	83
	C. Discussion and Conclusion	85
CHAPTER 5	PHOTOINDUCED TWO-ELECTRON REDUCTIVE ELIMINATION OF HALOGEN FROM A SINGLY	
	BONDED DIRHODIUM COMPLEX	90
	A. Background	90
	B. Photochemistry	97
	C. Conclusions	07
LIST OF REFER	ENCES 1	10

## LIST OF TABLES

		Page	
3.1	Photophysical Data for cis-Mo <sub>2</sub> Cl <sub>2</sub> (6-mhp) <sub>2</sub> (PR <sub>3</sub> ) <sub>2</sub> Complexes in CH <sub>2</sub> Cl <sub>2</sub> at Room Temperature		
3.2	Fluoresence lifetimes for solid samples of cis-Mo <sub>2</sub> Cl <sub>2</sub> (6-mhp) <sub>2</sub> (PMe <sub>2</sub> Ph) <sub>2</sub>	56	
3.3	Solvent Dependence of Selected Photophysical Data and Photolysis Quantum Yields for cis-Mo <sub>2</sub> Cl <sub>2</sub> (6-mhp) <sub>2</sub> (PMe <sub>2</sub> Ph) <sub>2</sub>	57	

## LIST OF FIGURES

		Page
1.1	The Z-scheme for oxygenic photosynthesis, which shows the pathway of electron flow from H <sub>2</sub> O to NADP <sup>+</sup> . (ref. 6)	3
1.2	Solar spectral distribution at normal incidence to the Earth's surface (air mass 1).	5
1.3	Structure of the charge transfer dye and a schematic representation of the principle of the dye-sensitized photovoltaic cell. S, sensitizer; S*, electronically excited sensitizer; S+, oxidized sensitizer; (R/R-), redox couple. (ref. 13)	7
1.4	Photochemistry of (a) "associative diradical" in d <sup>8</sup> and (b) "dissociative diradical" in d <sup>7</sup> and binuclear complexes	11
1.5	Reaction sequence for the photolysis ( $\lambda = 546$ nm) of Rh <sub>2</sub> (bridge) <sub>4</sub> <sup>2+</sup> (bridge = 1,3-diisocyanopropane) in concentrated HCl.	16
1.6	Advantages of using a discrete multi-electron excited state	20
1.7	Two strategies for designing two-electron mixed-valence excited states in binuclear metal-metal complexes.	21
1.8	Molecular orbital diagram for quadruply bonded metal-metal complexes with D <sub>4h</sub> symmetry.	23
1.9	Photochemistry of M <sub>2</sub> X <sub>4</sub> (PP) <sub>2</sub> complexes	25
3.1	Formation of (a) edge- and (b) face sharing bioctahedral photoproducts from quadruply bonded metal-metal complexes with D <sub>2h</sub> and D <sub>2d</sub> symmetry, respectively.	40

		Page
3.2	Three examples of metal-metal complexes with a W-frame geometry: (a) Rh <sub>2</sub> Cl <sub>4</sub> (dppm) <sub>2</sub> (ref. 86) (b) Re <sub>2</sub> (μ-SH) <sub>2</sub> Cl <sub>2</sub> (dppm) <sub>2</sub> (ref. 87) and (c) The Lewis acid induced coupling of bridging isocyanide ligands in Ir <sub>2</sub> (μ-CNR) <sub>2</sub> (CNR) <sub>2</sub> (dmpm) <sub>2</sub> to form Ir <sub>2</sub> (η <sup>2</sup> -CNR) <sub>2</sub> AlEt <sub>2</sub> )(CNR) <sub>2</sub> (dmpm) <sub>2</sub> (ref. 88).	43
3.3	Typical internuclear distances between ligands in (a) ESBO and (b) FSBO complexes.	45
3.4	Possible correlation between quadruply bonded metal-metal complexes with a cis arrangement of bridging ligands and W-frame complexes.	47
3.5	(a) Absorption, (b) fluorescence excitation and (c) emission spectra of $cis$ -Mo <sub>2</sub> Cl <sub>2</sub> (6-mhp) <sub>2</sub> (PMe <sub>2</sub> Ph) <sub>2</sub> in deoxygenated 2-methylpentane at room temperature. The absorption and excitation spectra are normalized to each other based on the intensity of the $\delta \to \delta^*$ transition. The open circles are the quantum yields for the photoreaction of $cis$ -Mo <sub>2</sub> Cl <sub>2</sub> (6-mhp) <sub>2</sub> (PMe <sub>2</sub> Ph) <sub>2</sub> in benzene at the specified wavelengths	50
3.6	Corrected emission spectrum of a solid sample of cis-Mo <sub>2</sub> Cl <sub>2</sub> (6-mhp) <sub>2</sub> (PEt <sub>3</sub> ) <sub>2</sub> at 10 K.	52
3.7	Electronic absorption spectral changes during the photolysis $(\lambda_{\rm exc} > 435  {\rm nm})$ of $cis$ -Mo <sub>2</sub> Cl <sub>2</sub> (6-mhp) <sub>2</sub> (PMe <sub>2</sub> Ph) <sub>2</sub> in deoxygenated benzene at 10 °C. Spectra were recorded at 0, 10, 30, 70, 170, 300 and 390 min.	58
3.8	Electronic absorption spectral changes during the photolysis $(\lambda_{\rm exc} > 435 \text{ nm})$ of $cis$ -Mo <sub>2</sub> Cl <sub>2</sub> (6-mhp) <sub>2</sub> (PMe <sub>2</sub> Ph) <sub>2</sub> with excess chloride in deoxygenated benzene at 10 °C. Spectra were recorded at 0, 5, 10, 15, 25, 35, and 60 min.	61
3.9	Electronic absorption spectral changes during the photolysis ( $\lambda_{\rm exc} > 435$ nm) of $cis$ -Mo <sub>2</sub> Cl <sub>2</sub> (6-mhp) <sub>2</sub> (PMe <sub>2</sub> Ph) <sub>2</sub> in deoxygenated DMF at 10 °C. Spectra were recorded at 0, 15, 45, 90, 180, 315, 435 and 1110 min.	62
3.10	Electronic absorption spectral changes during the photolysis ( $\lambda_{\rm exc} > 435$ nm) of $cis$ -Mo <sub>2</sub> Cl <sub>2</sub> (6-mhp) <sub>2</sub> (PMe <sub>2</sub> Ph) <sub>2</sub> in deoxygenated THF at 10 °C. Spectra were recorded at 0, 10, 30, 120 and 180 min.	64

		rage
3.11	Electronic absorption spectral changes recorded 30, 110, 210, 340, and 1260 min after the conclusion of the photolysis shown in Figure 3.10. The sample was stored in the dark at room temperature.	65
3.12	Summary of the overall photoreactivity of cis-Mo <sub>2</sub> Cl <sub>2</sub> (6-mhp) <sub>2</sub> (PMe <sub>2</sub> Ph) <sub>2</sub> in benzene, THF and DMF.	67
3.13	Two examples of quadruply bonded dimolybdenum complexes with tetradentate ligands that enforce a cis conformation of bridging ligands: (a) Mo <sub>2</sub> Cl <sub>4</sub> (eLTTP) (ref. 99) and (b) Mo <sub>2</sub> (N <sub>4</sub> )(O <sub>2</sub> CCH <sub>3</sub> ) <sub>2</sub> (ref. 100).	71
4.1	Qualitative molecular orbital diagram for ESBO complexes	75
4.2	Electronic absorption spectra of (a) $Mo_2I_6(dppm)_2$ , $(-\cdot -)$ (b) product from the irradiation ( $\lambda_{exc} > 435$ nm) of benzene solutions of $Mo_2I_6(dppm)_2$ with DMB (—) and (c) independently prepared $Mo_2I_4(dppm)_2$ , ().	80
4.3	Electronic absorption spectral changes during the photolysis ( $\lambda_{\rm exc} > 335$ nm) of $Mo_2Br_6({\rm dppm})_2$ in deoxygenated DMF at 20 °C. Spectra were recorded after 90 m, 3, 6, 16 h. The absorption spectrum of independently prepared $Mo_2Br_4({\rm dppm})_2$ is shown as a dashed line for comparison.	82
4.4	Electronic Absorption spectral changes during the photolysis $(\lambda_{\rm exc} > 335 \text{ nm})$ of $Mo_2Cl_6(dppm)_2$ with DMB in deoxygenated DMF at 20 °C. Spectra were recorded after 0, 4, 8, 13 and 19 h. The absorption spectrum of independently prepared $Mo_2Cl_4(dppm)_2$ is shown as a dashed line for comparison	84
5.1	A skeletal view of the inner coordination spheres of (a) $Rh_2(dfpma)_3(PF_3)_2$ (b) $Rh_2(dfpma)_3Br_2(\eta^1-dfpma)$ (c) $Rh_2(dfpma)_3Br_4$ (Ref. 60 and 61)	92
5.2	Qualitative energy level diagrams for Rh <sup>0</sup> Rh <sup>0</sup> , Rh <sup>0</sup> Rh <sup>II</sup> , and Rh <sup>II</sup> Rh <sup>II</sup> generated by the interaction of the appropriate C <sub>3V</sub> Rh <sup>0</sup> P <sup>4</sup> and C <sub>4V</sub> Rh <sup>II</sup> P <sub>3</sub> X <sub>2</sub> fragments	94

		Page
5.3	Electronic absorption spectrum of $Rh_2(dfpma)_3Br_2(\eta^1-dfpma)$ in THF. The corrected emission spectrum of the crystalline complex at 77 K is shown as a dashed line.	98
5.4	Electronic absorption spectral changes during the photolysis $(\lambda_{exc} > 305 \text{ nm})$ of $Rh_2(dfpma)_3Br_2(\eta^1-dfpma)$ in THF with excess dfpma. Spectra were recorded after 0, 5, 20, 50, 85, 210, 420, 1260 min. The spectrum of independently prepared $Rh_2(dfpma)_3(PF_3)_2$ is shown as a dashed line. The open circles are quantum yields for the photoreaction at the specified wavelengths.	101
5.5	ES-MS spectrum of the final products resulting from the photolysis ( $\lambda_{exc} > 305$ nm) of Rh <sub>2</sub> (dfpma) <sub>3</sub> Br <sub>2</sub> ( $\eta^{1}$ -dfpma) in THF with excess dfpma.	102
5.6	Electronic absorption spectral changes during the photolysis $(\lambda_{exc} > 305 \text{ nm})$ of Rh <sub>2</sub> (dfpma) <sub>3</sub> Br <sub>2</sub> ( $\eta^1$ -dfpma) in CH <sub>2</sub> Cl <sub>2</sub> in the presence of DMB. Spectra were recorded after 0, 10, 90, 180 and 240 min.	106

### LIST OF ABBREVIATIONS

AM air mass

bridge 1,3-diisocyanopropane

COD 1,5-cyclooctadiene

DMB 2,3-dimethyl-1,3-butadiene

DBU 1,8-diazabicyclo[5.4.0]undec-7-ene

dfpma- bis(difluorophosphino)methylamine

DMF dimethylformamide

dmpm bis(dimethylphosphino)methane

dppm bis(diphenylphosphino)methane

 $eLTTP \quad Et_2PCH_2CH_2P(Ph)CH_2P(Ph)CH_2CH_2PEt_2 \\$ 

ESBO edge-sharing bioctahedral

FSBO face-sharing bioctahedral

IR Infrared

LMCT ligand-to-metal charge transfer

LUMO lowest unoccupied molecular orbital

M-4-M quadruply bonded metal-metal complex

mhp 2-hydroxy-6-methylpyridinato

MMCT metal-to-metal charge transfer

N<sub>4</sub> 5, 7, 12, 14,tetramethyldibenzo-[b,i][1,4, 8, 11]tetraazotetradecine

NADPH nicotinamide adenine dinucleotide phosphate (reduced form)

NBD norbornadiene

OEC oxygen evolving complex

PR<sub>3</sub> tertiary phosphine

pop pyrophosphite, (HO<sub>2</sub>P)<sub>2</sub>O

pz pyrazoyl

Q quadricyclene

 $Rh^{0}Rh^{0}$   $Rh_{2}[F_{2}P)_{2}N(CH_{3})]_{3}(L)$  (L=  $\eta^{1}$ -dfpma or PF<sub>3</sub>

 $Rh^{0}Rh^{II}X_{2} \quad Rh_{2}[F_{2}P)_{2}N(CH_{3})]_{3}(L)X_{2} \ \ (L=\eta^{1}\text{-dfpma or }PF_{3};\ X=Cl,\ Br.\ I)$ 

 $Rh^{II}Rh^{II}X_4$   $Rh_2[F_2P)_2N(CH_3)]_3(L)X_4$  (L=  $\eta^1$ -dfpma or  $PF_3$ ; X = Cl, Br. I)

THF tetrahydrofuran

UV- ultraviolet

vis- visible

## CHAPTER 1

#### INTRODUCTION

The energy crises of the 1970s generated considerable interest in finding alternative sources of energy. This search has focused primarily on developing ways to harness and efficiently use the enormous amount of energy available directly from the sun.<sup>1-5</sup> The advantage of using solar energy is that it is abundant, environmentally sound and not subject to embargo.

Nature uses the process of photosynthesis<sup>6</sup> to convert solar energy into the chemical fuels that sustain life on this planet. The net result of photosynthesis is the conversion of water and carbon dioxide into molecular oxygen and carbohydrates. The photosynthetic reaction center is remarkably efficient, harnessing between 98 and 100 percent of the energy from the photons that it absorbs.<sup>7</sup> Photosynthetic organisms are able to store about fifty percent of the energy of incident photons in the form of the stored, separated charges that is used for the small molecule activation chemistry. The remainder of the energy is sacrificed in driving the charge separation of the holes and electrons.

Oxygen-evolving organisms contain two coupled photosynthetic systems, Photosystems I and II (PS I and PS II). Photosynthesis in all green plants utilizes the solar energy collected and funneled to the reaction center,  $P_{680}$  (a

specialized chlorophyll a molecule) by the light-harvesting complex (LHC-II) associated with PS II. The unique structure of LHC-II<sup>8</sup> results in energy transfer into the reaction center on a sub-picosecond timescale. Within a few picoseconds of the excitation of the P<sub>680</sub>, electron transfer results in a reduced pheophytin and the radical cation of the reaction center, P<sub>680</sub><sup>+</sup>. The pheophytin radical anion reduces a bound plastoquinone QA, which transfers the electron further to a second plastoquinone Q<sub>B</sub>. The reduction of Q<sub>B</sub> by a second electron results in the production of plastoquinol which then leaves the binding site. Plastoquinol is reoxidized by cytochrome  $b_0 f$ , delivering its electrons to Photosystem I via plastocyanin. P680<sup>+</sup> is reduced by a nearby tyrosine residue, Y<sub>z</sub>. The tyrosine radical returns to the diamagnetic state by oxidizing a cluster of four manganese ions in the oxygen evolving complex (OEC).9 The Z-scheme, pictured in Figure 1.1, shows the pathway of electron flow in oxygen-evolving photosynthetic organisms. The OEC goes through a cycle of five oxidation states, the most oxidized of which results in the evolution of molecular oxygen. The Mn cluster serves as an electron hole accumulator that enables O2 to be formed without generating partially oxidized intermediates that would be deleterious to the biological milieu. Photoexcitation and charge separation in Photosystem I produces NADPH, which is used to reduce carbon dioxide to carbohydrates in the Calvin cycle.

The above discussion highlights three major challenges for the design of artificial solar energy conversion schemes based on molecular transition metal complexes. The photosensitizer/catalyst (1) must efficiently absorb visible light, (2) effect multielectron reactions such as the endergonic four-electron oxidation

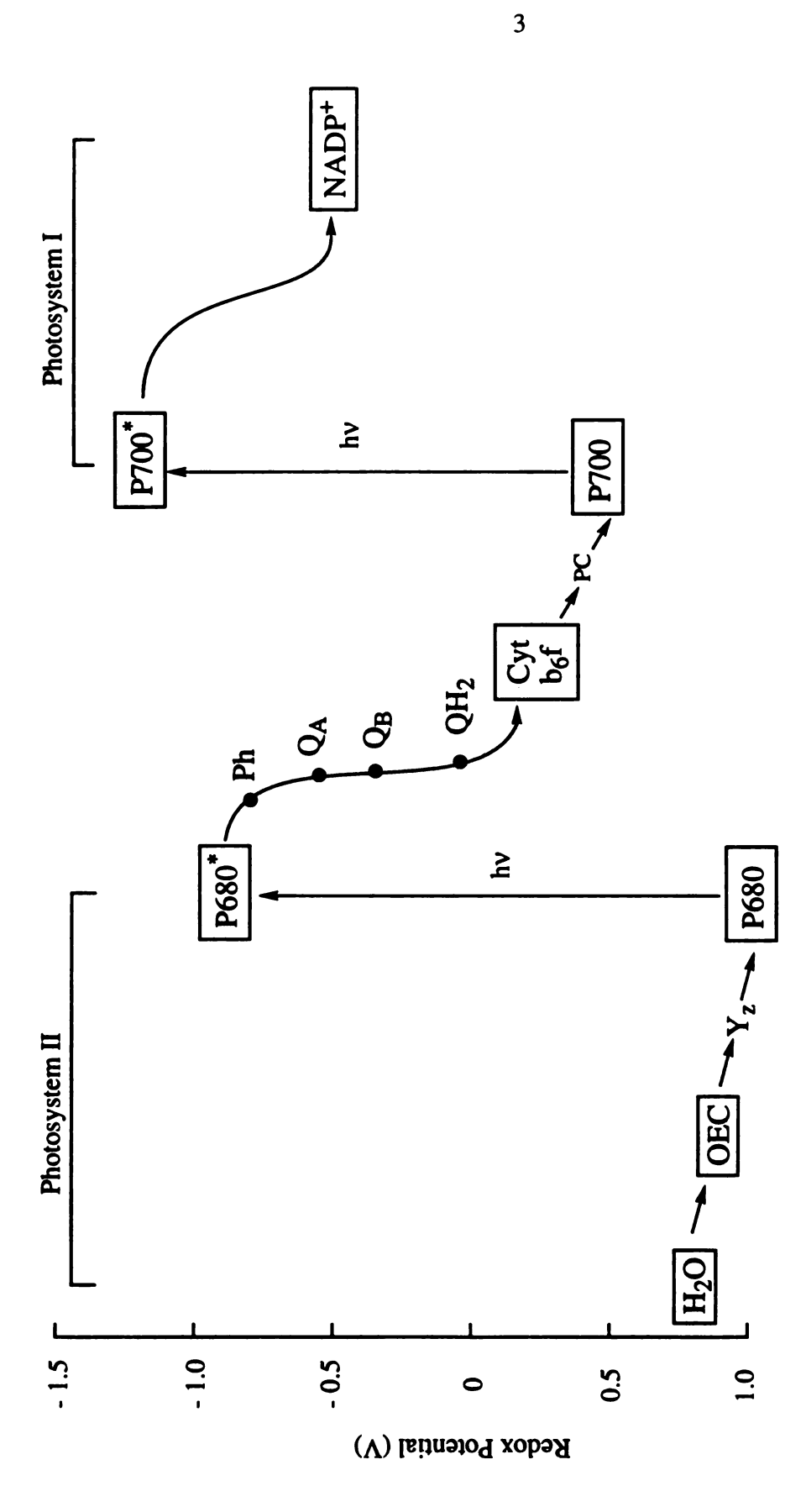


Figure 1.1 The Z-scheme for oxygenic photosynthesis, which shows the pathway of electron flow from H<sub>2</sub>O to NADP<sup>+</sup>. (ref. 6)

of water to molecular oxygen and protons, and (3) be capable of undergoing many turnovers without any significant degradation of the system. These requirements for energy conversion cycles, as they pertain to transition metal chemistry, are discussed below.

## A. Visible Absorption Characteristics

In order to be practical, any proposed energy conversion scheme must be capable of operating over a significant portion of the solar spectrum. Figure 1.2 shows the spectral distribution of sunlight at normal incidence to the Earth's surface (AM = 1).<sup>10</sup> The sunlight reaching the earth's surface is most intense in the visible region of the spectrum. The short-wavelength cutoff is due to absorption by O, N, O<sub>2</sub>, N<sub>2</sub> and O<sub>3</sub>, while the long-wavelength cutoff is the result of absorption by water vapor and CO<sub>2</sub>. The requirement that the photosensitizer/catalyst absorb efficiently in the visible region has limited the utility of several otherwise promising systems.

An example of a system limited by its absorption characteristics is the conversion of norbornadiene, NBD, to its metastable valence isomer quadricyclene, Q.<sup>2,11</sup> The irradiation of a 1:1 complex of CuCl and NBD with UV light affords Q with high quantum efficiency. The addition of an appropriate catalyst facilitates the reversion of Q to NBD, which results in the release of the stored energy as heat. The high quantum efficiency, large storage capacity, capability for long term storage and the ability to control the reverse reaction make this system exceedingly attractive as a model for photochemical energy

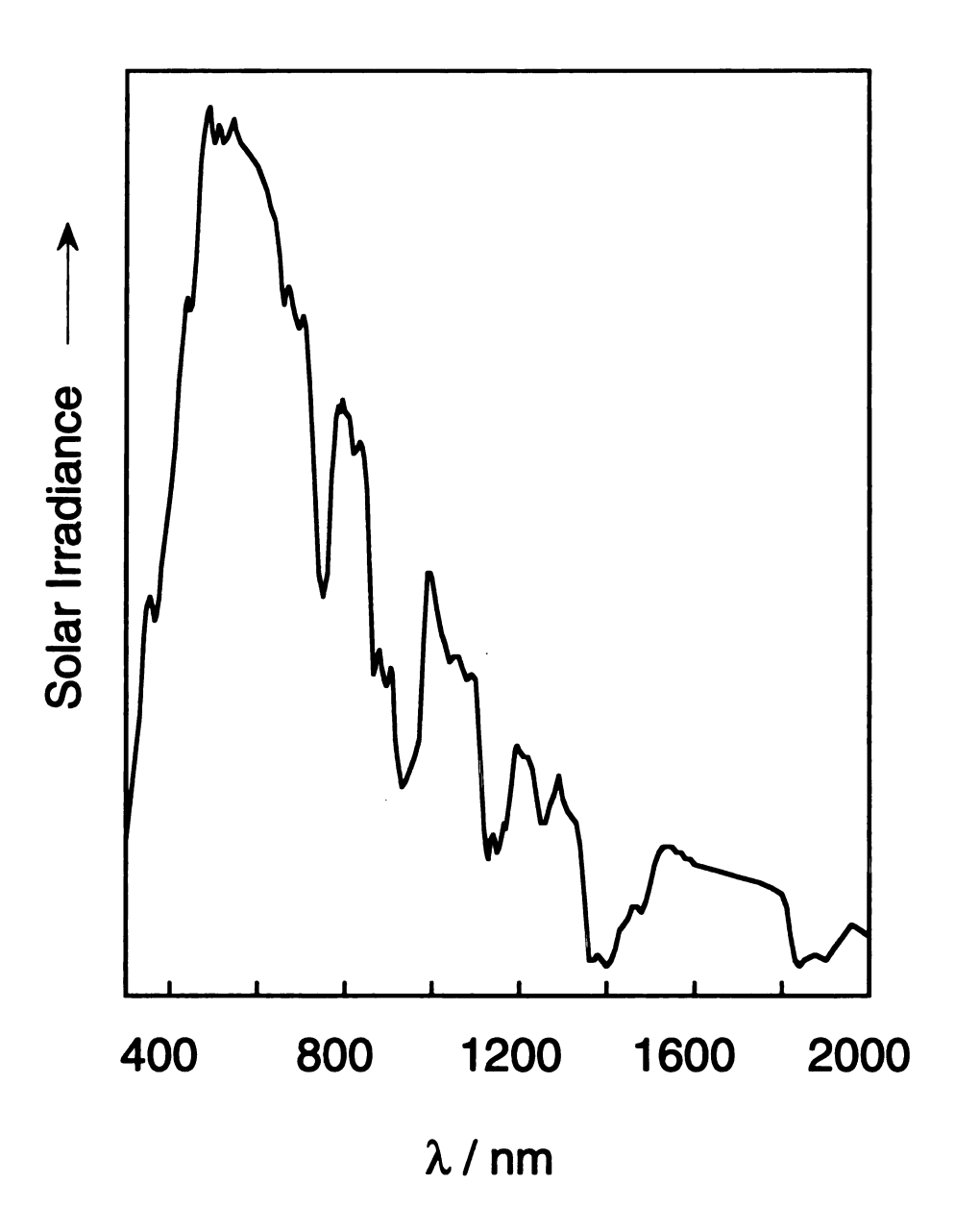


Figure 1.2 Solar spectral distribution at normal incidence to the Earth's surface (air mass 1).

storage. However, since the reaction cannot be driven with wavelengths longer than 450 nm, the system is capable of storing only a small fraction of the available solar energy.<sup>2</sup>

The inability to efficiently absorb a large portion of the solar spectrum is also a major constraint in the development of semiconductor based solar energy conversion devices. Semiconductors possess a definite threshold for light absorption known as the band gap energy. Therefore, large band gap materials such as TiO<sub>2</sub> (band gap 3.2 eV) are only able to capture a small percentage of the sunlight striking it.<sup>12</sup> The problem of the poor light harvesting ability of TiO<sub>2</sub> semiconductor devices has been addressed by developing dye-sensitized photovoltaic cells. These cells differ from the conventional semiconductor devices in that they separate the function of light absorption from charge carrier transport.

O'Regan and Grätzel<sup>13</sup> have developed a solar cell based on a thin, high surface area  $TiO_2$  film coated with a monolayer of the charge transfer dye,  $RuL_2(\mu$ -(CN)Ru(CN)L'<sub>2</sub>)<sub>2</sub> (L' = 2,2'-bipyridine, 4,4'-dicarboxylic acid; L = 2,2'-bipyridine). Figure 1.3 shows the structure of the dye as well as a schematic representation of the photovoltaic device. The two 'antenna' bis(bipyridyl) ruthenium moieties of this trimeric dye complex, serve to funnel excitation energy to the bis(dicarboxybipyridyl) sensitizer. The dye complex system harvests 46% of the incident solar flux. The excited sensitizer injects an electron into the conduction band of the  $TiO_2$  film. The conduction band electrons travel very rapidly across the film and are directed through a charge collector into the external circuit where electrical work is done. The electrons are subsequently

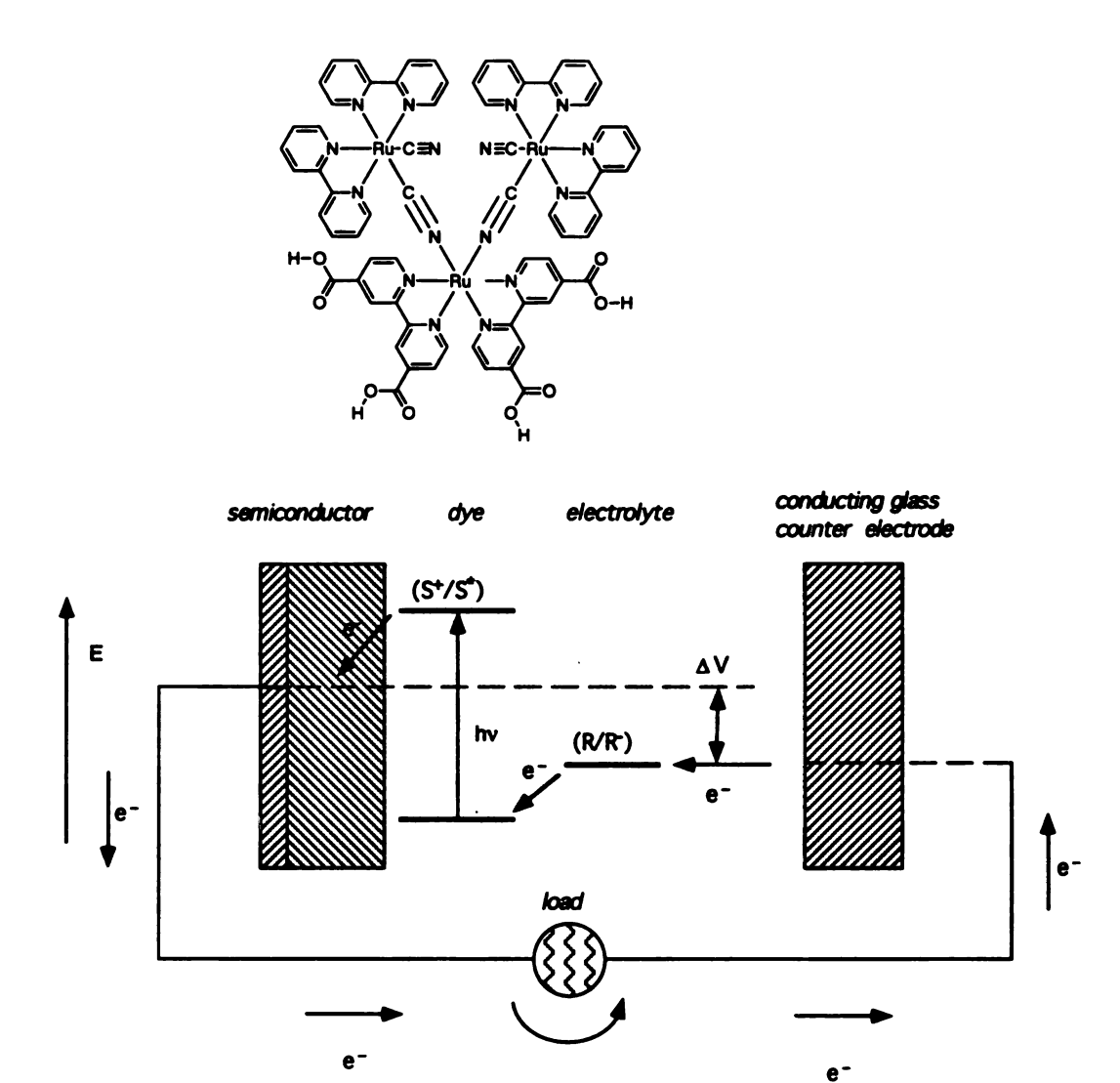


Figure 1.3 Structure of the charge transfer dye and a schematic representation of the principle of the dye-sensitized photovoltaic cell. S, sensitizer; S\*, electronically excited sensitizer; S+, oxidized sensitizer; (R/R-), redox couple. (ref. 13)

returned to the cell via a counter electrode. The sensitizer is regenerated by electron transfer from a redox active species in solution, which is in turn reduced at the counter electrode, to complete the circuit. The overall light-to-electrical energy conversion yield is 7.1-7.9% in simulated sunlight, which surpasses the performance of natural photosynthesis.

## **B.** Multielectron Reactivity by Coupling One-Electron Steps

Photointiated electron transfer, which transforms excitation energy into chemical potential in the form of long-lived transmembrane charge separation, is at the heart of photosynthetic energy conversion. These one-electron charge separating events are then stored in catalytic bookends (e.g. OEC) that effect the overall multielectron process. Accordingly, photoinduced electron transfer is a primary process in the design of many chemical solar energy storage systems. An electronically excited state, induced in a molecule by the absorption of a photon, possesses excess energy that can promote reactions that are either kinetically or thermodynamically unfavorable in the ground state. The increased internal energy of the excited state complex makes it both a better oxidant and a better reductant than its ground state parent complex. Electronically excited states can participate in intermolecular electron transfer reactions if they live long enough, in solution, to encounter a molecule of another solute.

The main challenge in these systems is to control the kinetics of the energy wasting back electron transfer. The primary photoproducts are often so reactive that they recombine before productive photochemistry can occur.

Natural photosynthetic systems prevent charge recombination by spatially separating the electron far enough away from its hole that even though recombination is still thermodynamically favorable, it is kinetically slow. A common strategy for suppressing the back reaction in artificial systems is the use a sacrificial donor<sup>14</sup> or sacrificial acceptor<sup>15</sup> to rapidly scavenge one of the photoproducts. However, the consumption of a sacrificial reagent limits both the economic and environmental benefits of these reactions.<sup>3</sup> Another method for slowing the back electron transfer process is the use of microscopic assemblies such as ionic micelles, <sup>16</sup> microemulsions <sup>17</sup> or vesicles. <sup>18</sup> An especially important characteristic of these aggregates is the presence of a charged lipid-water interface that can be exploited to control the kinetics of the electron transfer process. 19 In yet another approach, pigments, electron donors and acceptors similar to those found in natural photosynthetic systems are used but covalent bonds replace the protein as the organizing precept. The molecular pentads of Gust and Moore<sup>20</sup> exemplify this approach. At the center of these pentads are two covalently linked synthetic porphyrin moieties (P-P). One of these porphyrins serves as a model for chlorophyll and is attached to a carotenoid polyene (C) whereas the other is linked to a rigid diquinone (Q-Q). Photoinitated electron transfer ultimately leads to the C\*+—P—P—Q—Q\*charge separated state. The charge separated states can be formed with quantum yields of up to 0.83, have lifetimes as long as 0.5 ms and store about one-half of the energy of the excited singlet state.

Because most research has focused on single electron/hole charge separation, efforts have been directed toward coupling the primary one-electron events to effect multielectron transformations.  $^{21-23}$  Ingenious schemes have been designed to couple successive excited state one-electron transfers via relay catalysts or by photochemically generating reactive intermediates that can undergo subsequent multielectron oxidation-reduction reactions.  $^{1,22,23,24}$  One popular example of this approach is predicated on the chemistry of  $d^8 \cdots d^8$  complexes. The lowest energy  $d\sigma^* \to p\sigma$  transition of  $d^8 \cdots d^8$  complexes yields an "associative diradical" pair  $^{25}$ , as shown in Figure 1.4 (a), wherein the electrons of this triplet-configured lowest-energy excited state are localized formally on the metal atoms. The associative nature of the diradical allows the individual metal centers of the bimetallic core to cooperatively interact such that atom abstraction reactions can be coupled to effect the selective multielectron transformation of substrates.

A classic example of substrate activation by  $d^8 \cdots d^8$  binuclear complexes is the photoinduced catalytic conversion of isopropyl alcohol to acetone and hydrogen by  $Pt_2(P_2O_5H_2)_4^{4-}$ ,  $Pt_2(pop)_4^{4-}.^{25,26}$  In the initial step of this transformation the  ${}^3(d\sigma^*p\sigma)$  excited state of  $Pt_2(pop)_4^{4-}$  abstracts the methine hydrogen from isopropyl alcohol, yielding  $Pt_2(pop)_4^{4-}$  and a  $(CH_3)_2COH$  radical. Subsequently,  $(CH_3)_2COH$  reacts with a second equivalent of  $Pt_2(pop)_4^{4-}$  leading to the production of acetone and the Pt(II)Pt(III) mixed-valent  $Pt_2(pop)_4^{4-}$  intermediate, which undergoes disproportionation to give  $Pt_2(pop)_4^{4-}$  and  $Pt_2(pop)_4^{4-}$ . The photocatalytic cycle is completed by reductive elimination of hydrogen from  $Pt_2(pop)_4^{4-}$ . This reactivity is summarized in eqs. 1.1 to 1.4.

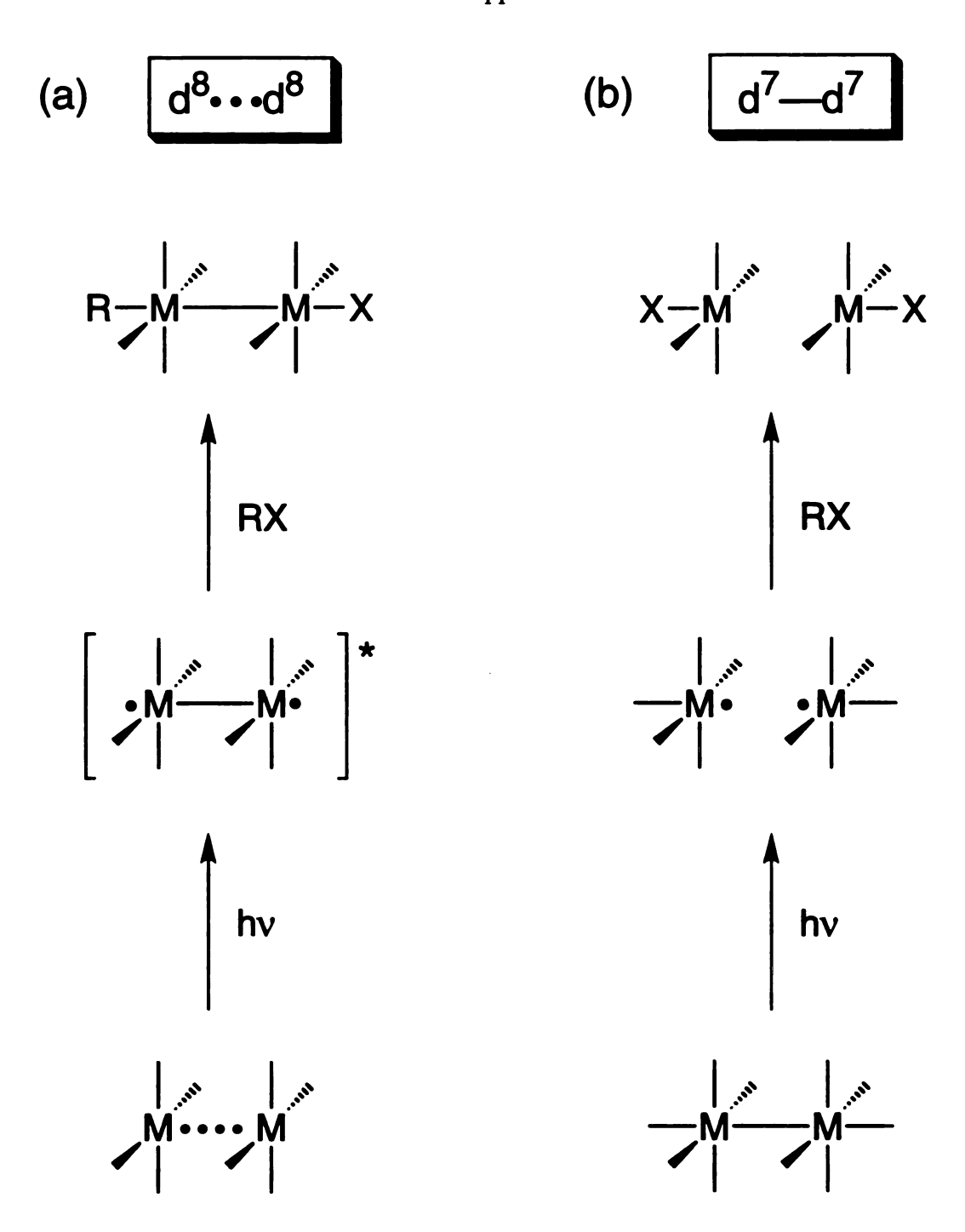


Figure 1.4 Photochemistry of (a) "associative diradical" in d<sup>8</sup> and (b) dissociative diradical in d<sup>7</sup> binuclear complexes.

$$Pt_2(pop)_4^{4-} + (CH_3)_2CHOH \longrightarrow Pt_2(pop)_4H^{4-} + (CH_3)_2COH$$
 (1.1)

$$Pt_2(pop)_4^{4-} + (CH_3)_2COH \longrightarrow Pt_2(pop)_4H^{4-} + (CH_3)_2CO$$
 (1.2)

$$Pt_2(pop)_4H^{4-} \longrightarrow Pt_2(pop)_4^{4-} + Pt_2(pop)_4H_2^{4-}$$
 (1.3)

$$Pt_2(pop)_4H_2^{4-} \longrightarrow Pt_2(pop)_4^{4-} + H_2$$
 (1.4)

The photoinduced reductive elimination of  $H_2$  from  $Pt_2(pop)_4H_2^{4-}$  was investigated by Gray and co-workers. Irradiation into the  $\sigma \to d\sigma^*$  absorption band of  $Pt_2(pop)_4H_2^{4-}$  ( $\lambda=313$  nm) results in the quantitative production of  $H_2$  and  $Pt_2(pop)_4^{4-}$ . The dihydride species,  $Pt_2(pop)_4H_2^{4-}$ , is also formed by atom transfer reactions of the  $^3(d\sigma^*p\sigma)$  excited state of  $Pt_2(pop)_4^{4-}$  with H-atom donors such as alcohols with  $\alpha(C-H)$  bonds, triorganosilanes, -germanes and -stannanes.  $^{28-30}$ 

## C. Regeneration of the Photocatalyst

The ability to regenerate the photocatalyst is essential to the development of an artificial solar energy conversion systems. In the  $Pt_2(pop)_4^{4-}$  H-atom chemistry, the photocatalyst is regenerated by  $H_2$  elimination, which can be a facile process. This process is typical to organometallic chemistry, where it generally proceeds via a non-polar, non-radical, three centered transition state. The reaction follows a concerted pathway where the formal oxidation state and coordination number of the metal are both reduced by two. Concerted photoinduced reductive elimination reactions are common for mononuclear diand polyhydride complexes of V, Mo, W, Re, Fe, Ru, Co and Ir that contain a

diverse array of ligands.<sup>31</sup> A specific example of the photochemistry of transition metal hydride complexes is the elimination  $H_2$  from  $IrClH_2(PPh_3)_3$ . The reaction occurs upon irradiation with light  $\lambda < 400$  nm, and has a quantum yield of 0.56 at 254 nm.<sup>32</sup> The elimination of  $H_2$  was unambiguously shown to occur in a concerted fashion by irradiating a mixture of  $IrClH_2(PPh_3)_3$  and  $IrClD_2(PPh_3)_3$ , only  $H_2$  and  $D_2$  were produced with no evidence for HD.<sup>32</sup> This experiment clearly eliminates the possibility of stepwise loss of one hydrogen as either  $H^+$ ,  $H^-$  or  $H^+$ , since substantial amounts of HD should have been produced if these mechanisms were operative. The process is readily reversed by the addition of  $H_2$ .

The IrClH<sub>2</sub>(PPh<sub>3</sub>)<sub>3</sub>/IrCl(PPh<sub>3</sub>)<sub>3</sub> system serves as a model for hydrogen and energy storage. The complex IrCl(PPh<sub>3</sub>)<sub>3</sub> readily takes up H<sub>2</sub> to store it as IrClH<sub>2</sub>(PPh<sub>3</sub>)<sub>3</sub> and then releases it on demand by irradiating it with UV light or sunlight. Furthermore, when hydrogen adds to IrCl(PPh<sub>3</sub>)<sub>3</sub> approximately 15-20 kcal/mol of energy is released.<sup>32</sup> The system is limited not only by the high cost of iridium but also by the requirement of UV light to drive the reverse reaction, meaning only a small portion of the solar spectrum can be utilized. The photochemistry of Ir monomers is not limited to the reductive elimination of H<sub>2</sub>. Irradiation of solutions of HCIIrClCO(PPh<sub>3</sub>)<sub>2</sub> under purge with an inert gas induces the loss HCl<sup>33</sup> and the production of IrClCO(PPh<sub>3</sub>)<sub>2</sub>. Photolysis of air saturated benzene solutions of O<sub>2</sub>IrClCO(PPh<sub>3</sub>)<sub>2</sub> induces the loss of oxygen<sup>33</sup> and regeneration of the square planar species, IrClCO(PPh<sub>3</sub>)<sub>2</sub>.

The photoinduced reductive elimination of H<sub>2</sub> from transition metal hydride complexes is a significant reaction because it can yield highly reactive

organometallic species, many of which cannot be obtained thermally. The work of Green *et al.*<sup>34</sup> and Bergman *et al.*<sup>35</sup> illustrates the synthetic utility of intermediates generated by photochemical  $H_2$  elimination. The highly reactive tungstenocene  $W(\eta^5-C_5H_5)_2$  intermediate is produced upon photolysis of  $W(\eta^5-C_5H_5)_2$ . The tungstenocene complex is very reactive and is 'carbene-like' in its ability to insert into the C—H bond of both aromatic and aliphatic complexes. The irradiation of  $(\eta^5-C_5H_5)(PR_3)IrH_2$  in saturated hydrocarbons, R'—H, leads to the production of  $(\eta^5-C_5H_5)(PR_3)Ir(R')(H)$ . The mechanism of the formation of  $(\eta^5-C_5H_5)(PR_3)Ir(R')(H)$  is believed to involve the concerted loss of hydrogen to form  $(\eta^5-C_5H_5)(PR_3)Ir$  followed by oxidative addition across the C—H bond of the hydrocarbon. The oxidative addition step is also thought to proceed in a concerted fashion via a 3-centered transition state.

In view of the facile  $H_2$  elimination from metal complexes, the challenge in designing a photocatalytic cycle is not the generation of hydrogen but rather the generation of the complementary energy storing constituent. Specifically, most important cycles (e.g.  $2 H_2O \rightarrow H_2$  and  $O_2$ ;  $2 HX \rightarrow H_2 + X_2$ ) involve the formation of metal-halide or metal-oxo bonds in addition to the metal-hydride bond. Because these bonds often represent kinetic and/or thermodynamic sinks, photocatalytic reactivity is typically circumvented upon their formation. For instance, the problems posed by metal-halide bond formation in the design of energy conversion chemistry is best exemplified by the dirhodium isocyanide work of Gray and co-workers in the 1970s and  $80s.^{36}$  In this work, the role of the metal-halide bond in circumventing the photochemical splitting of hydrochloric acid ( $2 HCl \rightarrow H_2 + Cl_2$ ), a highly desirable reaction because of the

substantial amount of energy stored by the transformation, is readily apparent.<sup>35</sup> Gray and co-workers have shown that protons are reduced to hydrogen when aqueous HCl solutions of Rh<sub>2</sub>(bridge)<sub>4</sub><sup>2+</sup> (bridge = 1,3-disocyanopropane) are irradiated with 546 nm light.<sup>36</sup> As shown in Figure 1.5, the reaction proceeds in two stages. In the first step Rh<sub>2</sub>(bridge)<sub>4</sub><sup>2+</sup> reacts thermally with HCl to generate the tetrameric Rh<sub>4</sub>(bridge)<sub>8</sub>Cl<sub>2</sub><sup>4+</sup> and one-half an equivalent of hydrogen. Subsequently, Rh<sub>4</sub>(bridge)<sub>8</sub>Cl<sub>2</sub><sup>4+</sup> reacts photochemically with HCl resulting in the production of an additional one-half an equivalent of hydrogen and Rh<sub>2</sub>(bridge)<sub>4</sub>Cl<sub>2</sub><sup>2+</sup>. This reaction is noteworthy because it achieves the desired two electron transformation of protons to hydrogen and because it can be driven with visible light. However, due to the fact that Rh<sub>2</sub>(bridge)<sub>4</sub>Cl<sub>2</sub><sup>2+</sup> does not undergo reductive elimination to regenerate Rh<sub>2</sub>(bridge)<sub>4</sub><sup>2+</sup> this reaction cannot form the basis for an energy conversion chemistry.

The barriers imposed by the metal-halide bond are present in the multielectron photochemistry of other transition metal systems. The two-electron photoreduction of dichloroethane to ethylene by  $[Ir(\mu-pz)(COD)]_2$  (COD = 1,5-cyclooctadiene and pz = pyrazoyl)<sup>37</sup> is not catalytic owing to the formation of the Ir(II)—Cl bond. The initial step in this reaction is the abstraction of a chlorine atom by an electronically excited  $[Ir(\mu-pz)(COD)]_2$  to yield the a mixed valence complex and the alkyl radical. The mixed valence complex then abstracts a second chlorine atom from the alkyl radical producing ethylene and  $[Ir(COD)(\mu-pz)Cl]_2$ . The absence of radical recombination or disproportionation products indicates that the organic radical intermediates are effectively trapped within the

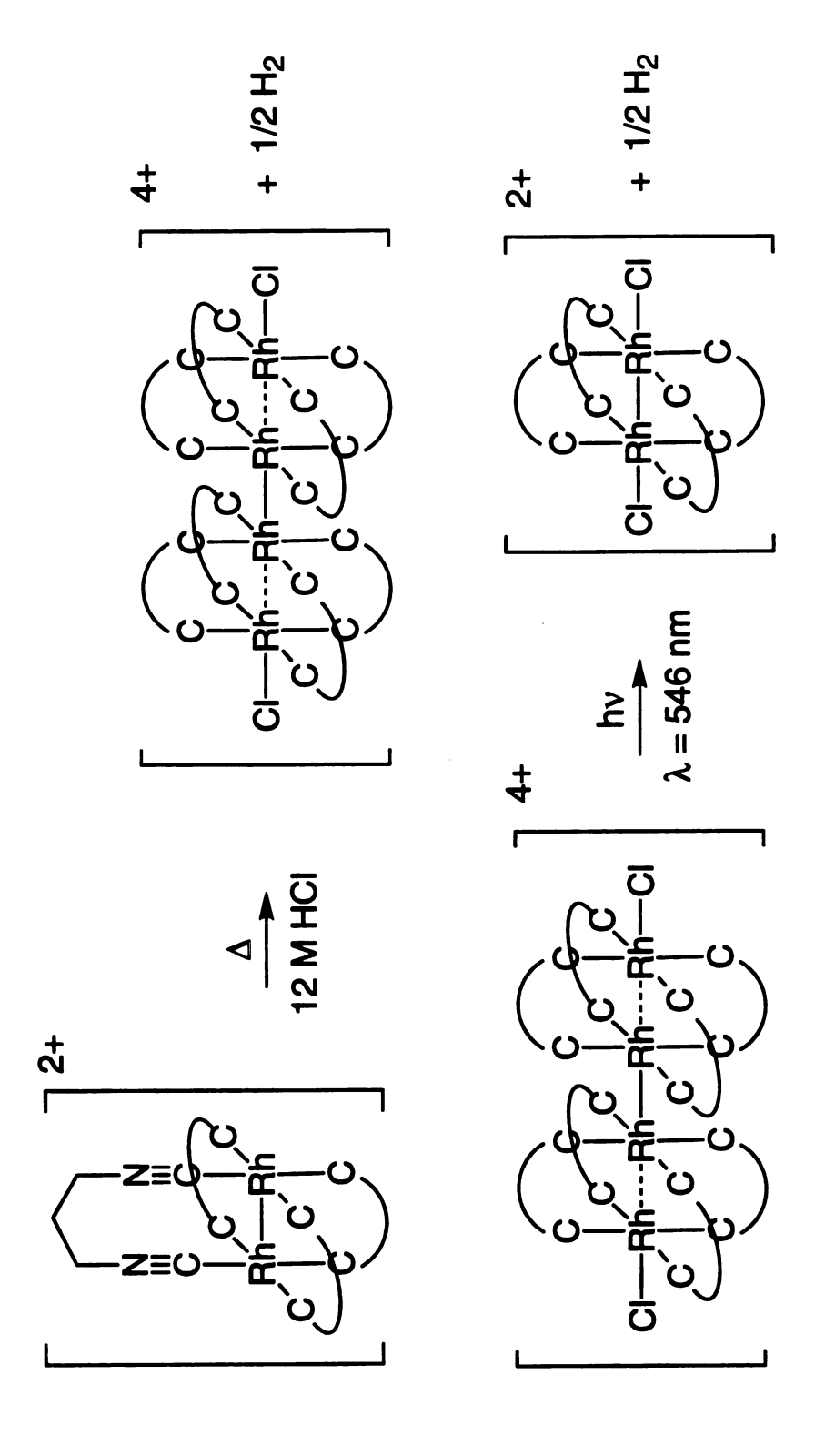


Figure 1.5 Reaction sequence for the photolysis  $(\lambda > 546 \text{ nm})$  of  $Rh_2(bridge)_4^{2+}$  (bridge = 1,3-diisocyanopropane) in concentrated HCl.

be regenerated from  $[Ir(COD)(\mu-pz)Cl]_2$ . The process can be summarized by the following equations:

$$Ir_2(COD)_2(\mu-pz)_2 + ClCH_2CH_2Cl \longrightarrow Ir_2(COD)_2(\mu-pz)_2Cl + \bullet CH_2CH_2Cl \quad (1.5)$$

$$Ir_2(COD)_2(\mu-pz)_2Cl + \bullet CH_2CH_2Cl \longrightarrow Ir_2(COD)_2(\mu-pz)_2Cl_2 + C_2H_4 \quad (1.6)$$

The photochemistry of  $Rh_2(bridge)_4^{2+}$  and  $[Ir(\mu-pz)(COD)]_2$  emphasizes the need to develop methods of regenerating the photocatalyst from metalhalide complexes. Photocatalysts have been successfully regenerated by using the energy of an excited state to overcome metal-halide dissociation barriers. An example of this is the regeneration of  $Pt_2(pop)_4^{4-}$  from  $Pt_2(pop)_4X_2^{4-}$  ( $X_2 = Cl_2$ , Br<sub>2</sub>, I<sub>2</sub>, SCN, CH<sub>3</sub>I, Im<sub>2</sub> (ImH= imidazole).<sup>38</sup> Irradiation of methanolic solutions of  $Pt_2(pop)_4X_2^{4}$  leads to reduction to  $Pt_2(pop)_4^{4}$ . Two isobestic points are maintained during the photolysis of  $Pt_2(pop)_4X_2^{4-}$ , except in the case of X = SCN, which indicates that no intermediate is formed in appreciable quantity during the course of the reaction. The conversion of  $Pt_2(pop)_4X_2^4$  to Pt<sub>2</sub>(pop)<sub>4</sub><sup>4</sup> is essentially quantitative. Thermal reactions were generally insignificant under the conditions that the photochemical experiments were run. The results of flash photolysis experiments strongly suggest that the primary photochemical process for Pt<sub>2</sub>(pop)<sub>4</sub>X<sub>2</sub><sup>4</sup> complexes is the homolytic cleavage of the Pt—X bond resulting in the formation of Pt<sup>II</sup>Pt<sup>III</sup>(pop)<sub>4</sub>X<sup>4</sup> and X<sup>\*</sup>. The quantum yields,  $\Phi_r$ , for the photoreduction of  $Pt_2(pop)_4X_2^{4-}$  complexes are highest when the excitation wavelengths are coincident with the  $\sigma \to d\sigma^*$  ( $\sigma$ refers to a combination of  $\sigma_x$  and d $\sigma$  orbitals). The higher  $\Phi_r$  values observed upon  $\sigma \to d\sigma^*$  excitation are due primarily to the X  $\to$  Pt(III) charge-transfer

character of the  $(\sigma)^1(d\sigma^*)^1$  state, which should promote redox reactions leading to the production of X—Pt(III)—Pt(II) and X\*. species. The photolytic cleavage of the platinum-chloride bond was also observed with PtCl<sub>6</sub><sup>2-</sup>. The transformation of PtCl<sub>6</sub><sup>2-</sup> to PtCl<sub>4</sub><sup>2-</sup> has been shown to occur via a radical pathway. Flash photolysis<sup>39</sup> into the LMCT band of aqueous solutions of PtCl<sub>6</sub><sup>2-</sup> resulted in the formation of PtCl<sub>5</sub><sup>2-</sup> and a chlorine atom. The PtCl<sub>5</sub><sup>2-</sup> ion subsequently underwent disproportionation to PtCl<sub>6</sub><sup>2-</sup> and PtCl<sub>4</sub><sup>2-</sup> with a second-order rate constant of  $4.6 \times 10^6 \, \mathrm{M}^{-1} \mathrm{s}^{-1}$ .

Photoinduced reductive elimination of halogen from metal centers has also been observed in the photochemistry of coordination compounds of main group metals. 40-45 The elimination of Cl<sub>2</sub> from PbCl<sub>4</sub> has been postulated, on the basis of flash photolysis studies,<sup>41</sup> to occur via a radical mechanism. The primary products of the flash photolysis of PbCl<sub>4</sub> are PbCl<sub>3</sub> and Cl<sup>6</sup>. LMCT excitation of the octahedral anion, PbCl<sub>6</sub><sup>2-</sup>, likewise leads to the elimination of Cl<sub>2</sub>.<sup>42</sup> However, the PbCl<sub>4</sub><sup>2-</sup> product is unstable and reacts further to produce PbCl<sub>3</sub><sup>-</sup> and Cl<sup>-</sup>. The UV-vis spectral changes that occur during photolysis indicate that the reaction is clean and can be driven to completion. Although no attempt was made to detect the intermediates of this reaction, the results of flash photolysis studies of PbCl<sub>4</sub> suggest that the primary photochemical step yields a Pb(III) species. Other examples of X<sub>2</sub> photoelimination from main group metal complexes include the production of I<sub>2</sub> from Sn(IV)I<sub>4</sub>,<sup>43</sup> Cl<sub>2</sub> from Sb(V)Cl<sub>6</sub><sup>-44</sup> and TlCl<sub>4</sub>-,<sup>42</sup> and X<sub>2</sub> from TeX<sub>6</sub>-. <sup>42,45</sup> The mechanisms of these reactions have not been elucidated but it is likely that these reactions also proceed via a halogen atom intermediate.

#### D. The Discrete Multielectron Approach

Over the past decade, the Nocera group has tackled the issue of energy conversion from a conceptually new direction. As opposed to coupling one-electron pathways to drive a multielectron process, excited states have been designed that undergo discrete multielectron reactivity. The two approaches are contrasted schematically in Figure 1.6. The motivation for designing multielectron reactivity, in the context of the above discussion, is many-fold. If more than one electron can be moved from a discrete excited state, then the structural complexity required for charge separation may be eased. Moreover, multielectron reaction from an electronically excited core obviates the necessity for charge storage coupled to catalytic redox centers.

Because of the diradical character of the excited states of d<sup>7</sup>—d<sup>7</sup> and d<sup>8</sup>···d<sup>8</sup> binuclear complexes, multielectron transformations of substrates by these systems, is limited to the coupling sequential one-electron reactions.<sup>21,46</sup> This diradical chemistry is summarized in Figure 1.4. Nevertheless, the photochemistry of d<sup>7</sup>—d<sup>7</sup> and d<sup>8</sup>···d<sup>8</sup> binuclear complexes is instructive, suggesting a correlation between diradical excited states and one-electron chemistry. This discovery raised the question - can multielectron excited state reactions be emphasized when two metal-localized electrons are singlet coupled within a bimetallic core? The approach taken by the Nocera group to the design of multielectron chemistry is based on two-electron mixed valence excited states,<sup>47</sup> is summarized in Figure 1.7. Two-electron mixed-valence complexes can be generated from two distinctly different classes of binuclear complexes. If electrons are weakly

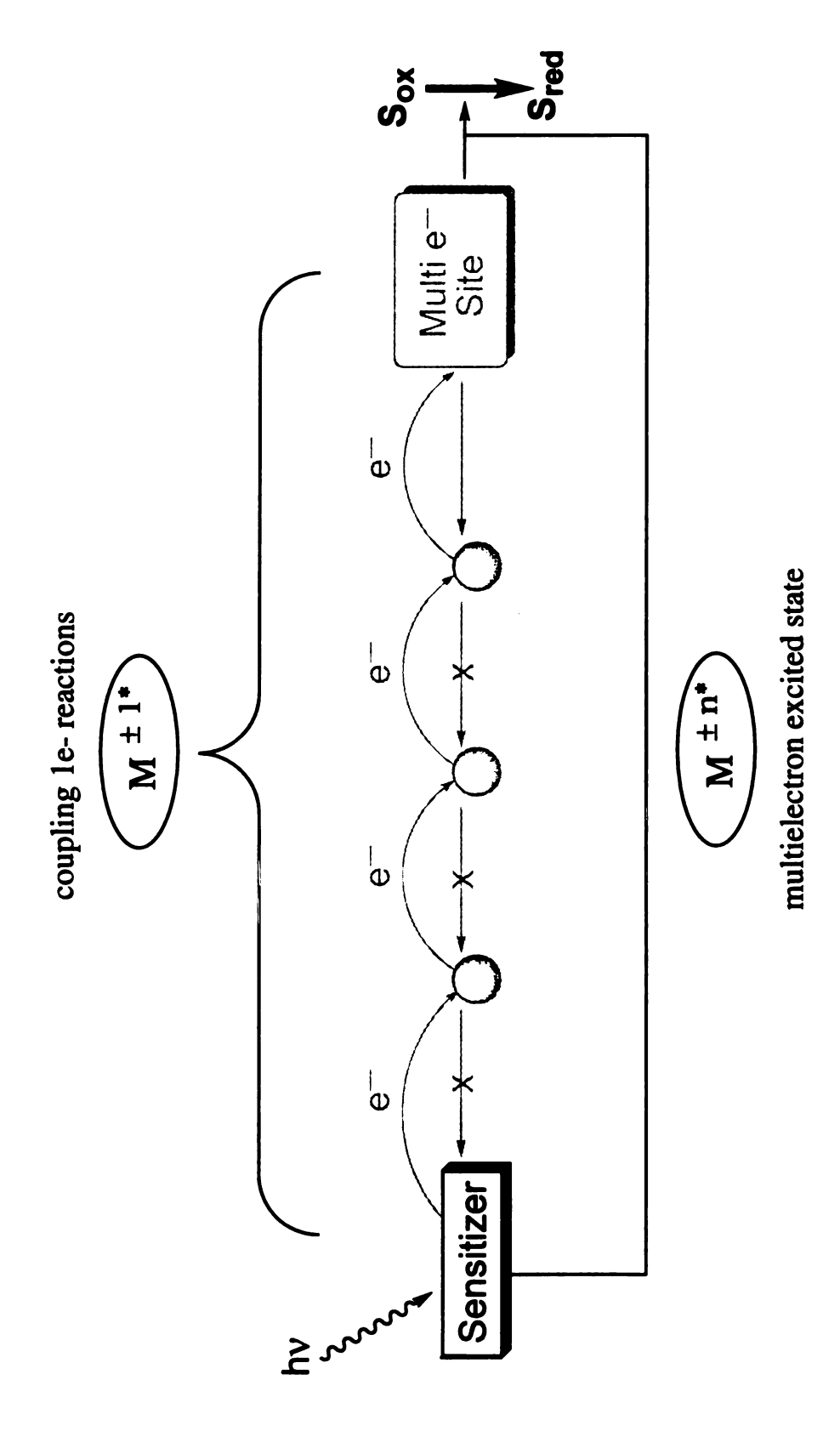


Figure 1.6 Advantages of using a discrete multi-electron excited state.

 $M^n$ — $M^{n+2}$ 

 $-M = M^n - M^n$ 

\ **∑** 

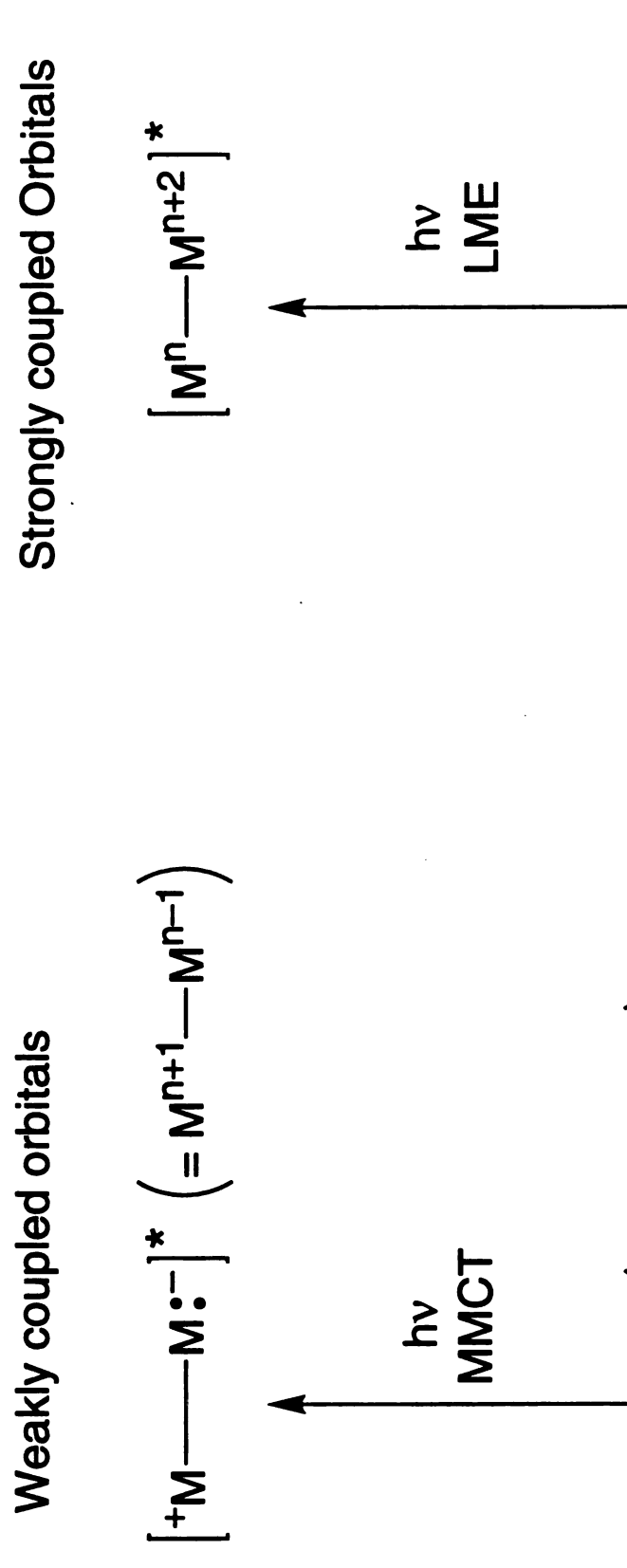


Figure 1.7 Two strategies for designing two-electron mixed-valence excited states in binuclear metal-metal complexes.

coupled within a binuclear complex, a multielectron excited state may be prepared by exciting a metal-to-metal charge transfer (MMCT) transition. In this case, electrons that are localized on individual metal centers of a bimetallic core in the ground state are paired upon the absorption of a photon to produce an excited state that is zwitterionic, M<sup>+</sup>—M<sup>-</sup> in nature. The result is that a two-electron mixed valence, M<sup>n+1</sup>—M<sup>n-1</sup>, excited state is photogenerated from a M<sup>n</sup>—M<sup>n</sup> ground state. The other approach to obtaining two-electron mixed-valence excited states, centers on building the two-electron mixed-valence character into the corresponding ground state.<sup>47</sup> This can be accomplished by synthesizing complexes where the formal oxidation states of the metals within a bimetallic core differ by two. Utilizing this approach, the absorption of a photon produces a more energetic excited state that is predisposed to react in two-electron steps at the individual metal centers of the bimetallic core.

# 1. Quadruply Bond Metal-Metal Complexes

Ironically, one place to find two electrons in weakly coupled metal orbitals is in complexes that feature the shortest distances between metal atoms, quadruply bonded metal-metal complexes. The quadruple bond is formed by the overlap of the  $d_z^2$ ,  $(d_{xz},d_{yz})$  and  $d_{xy}$  orbitals of two  $d^4$  metals, which results in a  $\sigma^2\pi^4\delta^2$  ground state electronic configuration, as shown in Figure 1.8.<sup>48</sup> The spectroscopy of these complexes is dominated by metal-localized transitions with the lowest energy excited states arising from the promotion of electrons from the  $\delta$  to the  $\delta$ \* orbital.<sup>49</sup> Theoretical studies carried out on the

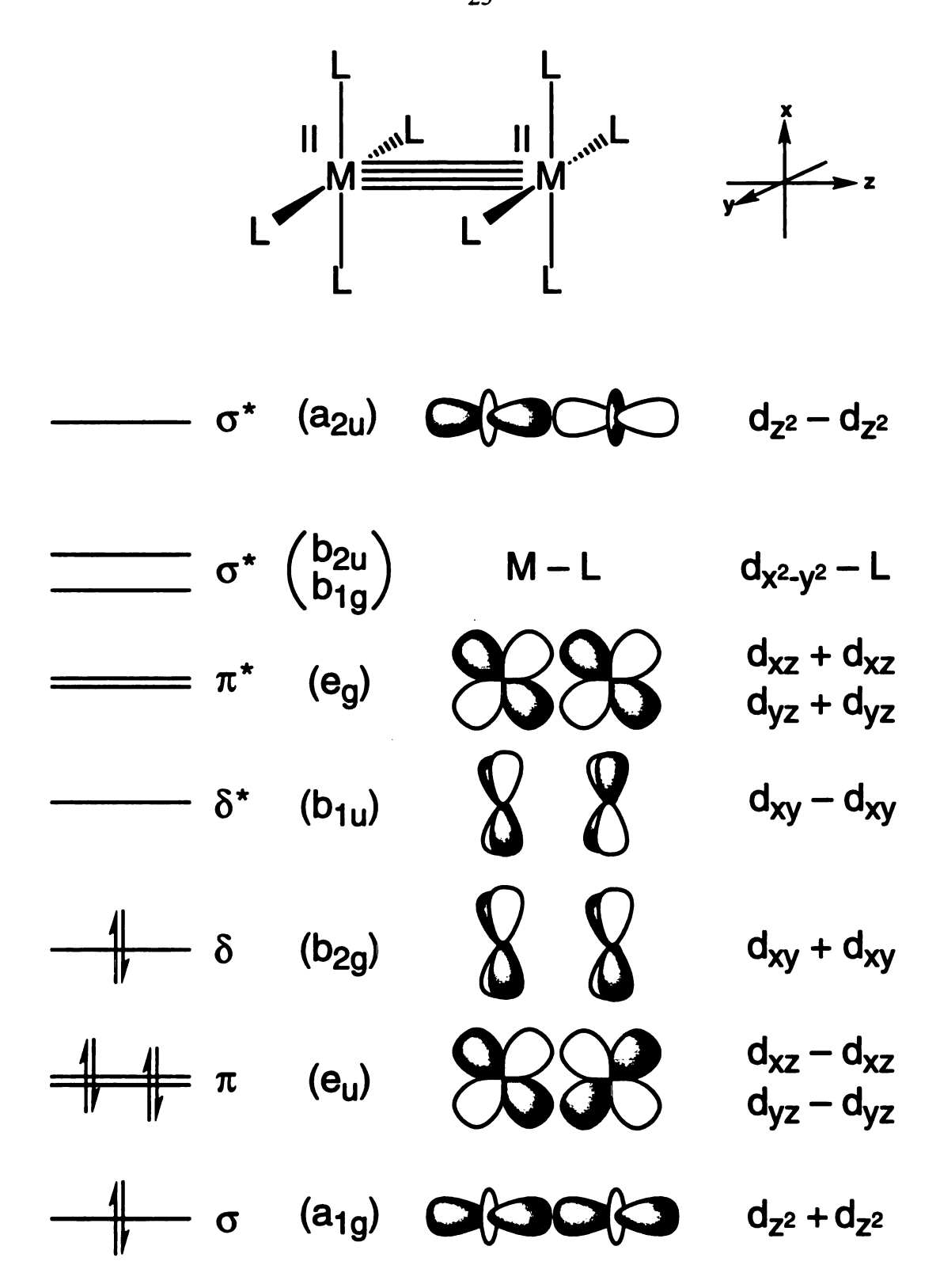


Figure 1.8 Molecular orbital diagram for quadruply bonded metal-metal complexes with  $D_{4h}$  symmetry.

octachlorodirhenate ion  $Re_2Cl_8^{2-}(D_{4h})$  establish that the  $d_{xy}$  orbitals on adjacent metal centers of the bimetallic core have poor overlap owing to their parallel disposition to each other, and consequently the electrons residing in these orbitals are weakly coupled.<sup>50</sup>

The two-electron character of the excited state can be trapped by intramolecular distortions within the ligation sphere. In the M<sup>+</sup>—M<sup>-</sup> excited state, one metal of the binuclear core is oxidized. Oxidation of quadruply bonded metal-metal complexes results in the rearrangement of the ligating sphere to either face or edge sharing bioctahedral geometries. 48,51,52 Transient absorption spectroscopy of  $M_2X_4(PP)_2$  (M = Mo or W; X= halide; and PP = bridging phosphine) complexes indicates that a bioctahedral intermediate is indeed produced in the excited state. These complexes exhibit long-lived transients<sup>53</sup> whose absorption spectra are similar to those of M<sub>2</sub>Cl<sub>6</sub>(PP)<sub>2</sub> edgesharing bioctahedral complexes<sup>54,55</sup> As Figure 1.9 illustrates, the absorption of a photon, by a M<sub>2</sub>X<sub>4</sub>(PP)<sub>2</sub> complex, produces a charge-separated state of singlet character and simultaneously provides an open coordination site at the reduced metal center. The oxidative addition<sup>55-57</sup> and atom transfer<sup>58</sup>hemistry of this reactive intermediate has been elaborated by the Nocera group. The photochemistry of the  $M_2Cl_4(dppm)_2$ (M=Mo. W: dppm bis(diphenylphosphino)methane) is consistent with classic oxidative-addition reactivity. Excitation of solutions of M<sub>2</sub>Cl<sub>4</sub>(dppm)<sub>2</sub> and alkyl halides<sup>56,57</sup> or aryl disulfides,<sup>55</sup> with wavelengths that are energetically coincident with those required for the production of the long-lived transient yield M<sup>III</sup>M<sup>III</sup> edgesharing bioctahedral photoproducts.

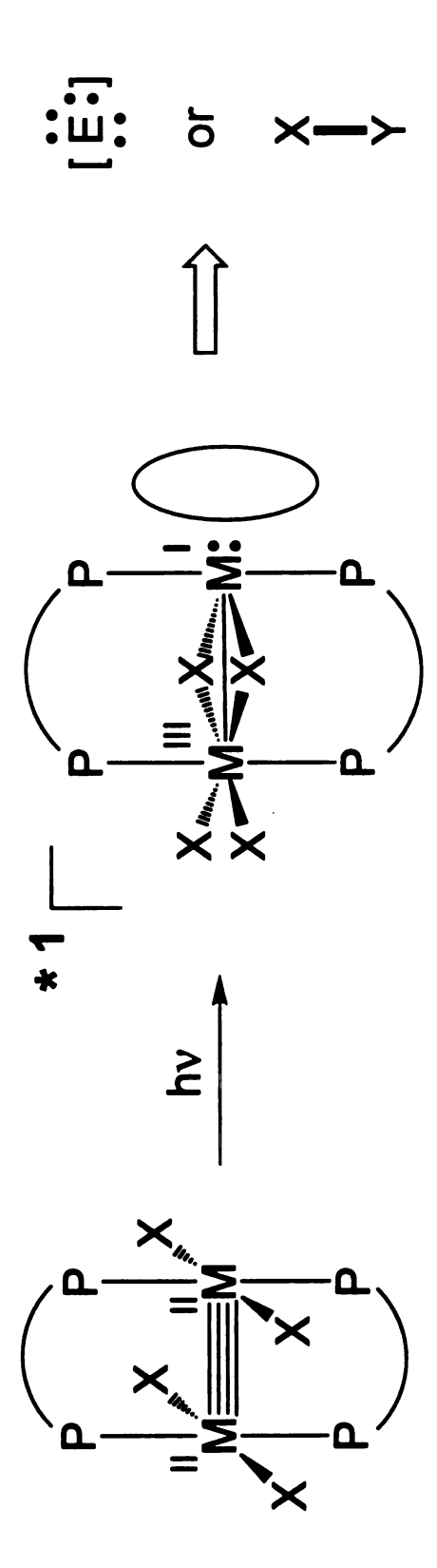


Figure 1.9 Photochemistry of M<sub>2</sub>X<sub>4</sub>(PP)<sub>2</sub> complexes.

# 2. Singly Bonded Metal-Metal Complexes

The series of dirhodium complexes  $Rh_2(dfpma)_3X_2L$  (X = Cl, Br, I; dfpma = bis(difluorophosphino)methylamine;  $L = PF_3$  or  $\eta^1$ -dfpma)<sup>59-61</sup> contain singly bonded metals whose oxidation states differ by two. The two-electron mixed-valence  $Rh^0Rh^{II}$  core is established by the coordination sphere about each of the dirhodium centers. Low temperature glasses and solids of  $Rh^0Rh^{II}X_2$  complexes exhibit red luminescence that is strongly temperature dependent. Spectroscopic and photophysical studies are consistent with the luminescence arising from a  $d\sigma^*$  excited state. The  $d\sigma^*$  excited state of  $Rh^0Rh^{II}X_2$  complex can be synthetically tailored into a homologous four-electron series. The  $Rh^0Rh^{II}X_2$  complex can be oxidized to the symmetrical  $X_2Rh^{II}Rh^{II}X_2$  complex. Alternatively, the two-electron reduction of the mixed-valence complex yields the  $Rh^0Rh^0$  species. Because the  $d\sigma^*$  excited state presents the possibility for interconverting among the  $Rh^0Rh^0$ ,  $Rh^0Rh^{II}X_2$  and  $X_2Rh^{II}Rh^{II}X_2$  complexes in two-electron steps, the series provides a foundation for the design of four-electron photocatalytic schemes.

#### E. Dissertation outline

As the two-electron oxidation pathways have emerged for bimetallic complexes in the Nocera group, attention has turned to developing elimination pathways that effect overall multielectron transformations. Specifically, the elimination of halides from bimetallic excited states has become a central issue of

inquiry. The goal of the research described in this dissertation is to study concerted and radical photoinduced reductive elimination chemistry from bimetallic complexes. The research focuses on the types of multielectron electron photoreagents already developed in Nocera group.

Chapter 3 describes the photophysics and photochemistry of  $Mo_2Cl_2(6-mhp)_2(PR_3)_2$ . These complexes were chosen because of the cis conformation of bridging mhp ligands and the presence of a long-lived  $\delta\delta^*$  state which, in principle, permits the excited state oxidation chemistry of this series of complexes to be studied. The cis conformation of bridging ligands may engender a W-frame structure upon two-electron oxidation to  $Mo^{III}Mo^{III}$ . This W-frame geometry is highly desirable because the bridging halide ligands in these structures are in close proximity to each other and therefore may be predisposed to undergo photoinduced reductive elimination via a concerted mechanism. The photoinduced redistribution of mhp ligands, which prevents the formation of the desired W-frame complex, is discussed in detail.

Chapter 4 details the photoreductive elimination of halide ligands from the edge-sharing bioctahedral Mo<sup>III</sup>Mo<sup>III</sup> complexes, Mo<sub>2</sub>X<sub>6</sub>(dppm)<sub>2</sub> (X = halide; dppm = bis-(diphenylphosphino)methane). These complexes were studied because the edge-sharing bioctahedron is a common geometry for the two-electron oxidation products of quadruply bonded metal-metal complexes. From the standpoint of photocatalysis, it would be desirable to develop oxidative addition and reductive elimination photochemistry for a complementary class of metal-metal complexes.

The photochemistry of  $Rh_2(dfpma)_3Br_2(\eta^1-dfpma)$  is described in Chapter 5. A two-electron mixed-valence excited state of these complexes is produced upon excitation of the  $Rh^0Rh^{II}$  ground state. The  $d\sigma^*$  excited state engenders the two-electron reduction of the  $Rh^0Rh^{II}Br_2$  species. The effect of excitation wavelength, solvent and reaction conditions on the photochemistry is discussed in detail.

### **CHAPTER 2**

#### **EXPERIMENTAL**

## A. Synthetic Procedures

#### 1. General Procedures

All manipulations, unless otherwise noted, were carried out under an atmosphere of dry argon by using standard Schlenk-line techniques. All solvents were refluxed under N<sub>2</sub> for no less than 8 hours prior to use. Benzene, toluene, tetrahydrofuran and diethyl ether were refluxed over sodium. Benzophenone was added to all of the above solvents, except diethyl ether, as an indicator of water content. Hexane, pentane and dichloromethane were refluxed over P<sub>2</sub>O<sub>5</sub>; methylcyclohexane and acetonitrile were refluxed over calcium hydride. Methanol was refluxed over Mg(OMe)<sub>2</sub>, prepared by initially refluxing 50 mL of methanol containing 5.0 g of magnesium turnings and 0.5 g iodine. Once the color of I<sub>2</sub> disappeared, an additional 1 liter of methanol was added.

# 2. Synthesis of $Mo_2Cl_n(6-mhp)_{4-n}(PR_3)_n$ Complexes

The syntheses of Mo<sub>2</sub>Cl<sub>2</sub>(6-mhp)<sub>2</sub>(PEt<sub>3</sub>)<sub>2</sub>, Mo<sub>2</sub>Cl<sub>2</sub>(6-mhp)<sub>2</sub>(PMe<sub>2</sub>Ph<sub>2</sub>)<sub>2</sub>, Mo<sub>2</sub>Cl<sub>2</sub>(6-mhp)<sub>2</sub>(PMePh<sub>2</sub>)<sub>2</sub>, Mo<sub>2</sub>Cl<sub>3</sub>(6-mhp)(PMe<sub>2</sub>Ph)<sub>3</sub> were carried out by using literature methods, <sup>62</sup> which are described below. The previously unknown complexes Mo<sub>2</sub>Cl<sub>2</sub>(6-mhp)<sub>2</sub>(PMe<sub>3</sub>)<sub>2</sub> and Mo<sub>2</sub>Cl(6-mhp)<sub>3</sub>(PMe<sub>2</sub>Ph) were prepared by modifying existing procedures.

- a. Precursors. Trimethylsilyl chloride and 2-hydroxy-6-methylpyridine (Hmhp) were purchased from Aldrich Chemical Co. and used without further purification. Tertiary phosphines were obtained from Strem Chemicals Inc. and stored under argon. The complexes Mo<sub>2</sub>Cl<sub>4</sub>(PMe<sub>2</sub>Ph)<sub>4</sub><sup>63</sup>, Mo<sub>2</sub>Cl<sub>4</sub>(PMePh<sub>2</sub>)<sub>4</sub><sup>63</sup> and Mo<sub>2</sub>Cl<sub>4</sub>(PEt<sub>3</sub>)<sub>4</sub><sup>64</sup> were prepared by published procedures as was Mo<sub>2</sub>(mhp)<sub>4</sub>.65
- b.  $Mo_2Cl_2(6\text{-mhp})_2(PMe_3)_2$ . The complex  $Mo_2Cl_2(6\text{-mhp})_2(PMe_3)_2$  was obtained by refluxing a mixture of 0.5 g (0.82 mmol) of  $Mo_2(mhp)_4$ , 0.2 mL (1.6 mmol) of trimethylsilyl chloride and 0.15 mL (1.4 mmol) of  $PMe_3$  in THF for 3 hours, as described for the synthesis of  $Mo_2Cl_2(6\text{-mhp})_2(PEt_3)_2$ . The THF was removed under reduced pressure at the conclusion of the reaction. The resulting dark red product was chromatographed twice on silica gel with  $CH_2Cl_2$  as an eluant. The  $^1H$  NMR spectrum of the product is consistent with the proposed stoichiometry, and the presence of a singlet at -6.99 ppm,  $CDCl_3$ , in the  $^{31}P\{^1H\}$  NMR is consistent with the results obtained for the complex  $PR_3 = PEt_3$ .

- c. Mo<sub>2</sub>Cl<sub>2</sub>(6-mhp)<sub>2</sub>(PR<sub>3</sub>)<sub>2</sub> (PR<sub>3</sub> = PEt<sub>3</sub>, PMe<sub>2</sub>Ph). A solution that contained an equimolar mixture of Mo<sub>2</sub>Cl<sub>4</sub>(PR<sub>3</sub>)<sub>4</sub> and Mo<sub>2</sub>(mhp)<sub>4</sub> in 25 mL of toluene was refluxed for 6 hours and then stirred while still warm (50 70 °C) for 12 hours. The reaction mixture was evaporated to dryness under reduced pressure and then purified by column chromatography as described above. The spectroscopic properties are consistent with those reported in the literature.<sup>62,66</sup>
- d. Mo<sub>2</sub>Cl<sub>2</sub>(6-mhp)<sub>2</sub>(PMePh<sub>2</sub>)<sub>2</sub>. This complex was synthesized by refluxing 0.9 g (0.79 mmols) of Mo<sub>2</sub>Cl<sub>4</sub>(PMePh<sub>2</sub>)<sub>4</sub> in 25 mL of toluene for 4 hours in the presence of excess Hmhp (0.35 g, 3.2 mmol). The solution was kept warm for an additional 12 hours with stirring, evaporated to dryness under reduced pressure and purified by column chromatography, as described above. The spectroscopic properties are consistent with those previously reported in the literature.<sup>62</sup>
- e. Mo<sub>2</sub>Cl<sub>3</sub>(6-mhp)(PMe<sub>2</sub>Ph)<sub>3</sub>. The complex was prepared upon refluxing a solution of Mo<sub>2</sub>Cl<sub>4</sub>(PMe<sub>2</sub>Ph)<sub>4</sub> (0.23 g, 0.29 mmol) and Mo<sub>2</sub>Cl<sub>2</sub>(6-mhp)<sub>2</sub>(PMe<sub>2</sub>Ph)<sub>2</sub> in 25 mL of toluene for 4 hours. The suspension was stirred while warm for an additional 12 hours. The product was evaporated to dryness under reduced pressure. The residue was then chromatographed twice, silica gel/CH<sub>2</sub>Cl<sub>2</sub>. The <sup>31</sup>P{<sup>1</sup>H} NMR and UV-vis spectra were identical those reported by Walton *et al.*. <sup>62</sup>

f. Mo<sub>2</sub>Cl(6-mhp)<sub>3</sub>(PMe<sub>2</sub>Ph). The literature procedure for the preparation of Mo<sub>2</sub>Cl(6-mhp)<sub>3</sub>(PMePh<sub>2</sub>)<sup>62</sup> was modified by refluxing Mo<sub>2</sub>Cl<sub>2</sub>(6-mhp)<sub>2</sub>(PMe<sub>2</sub>Ph)<sub>2</sub> (0.126 g, mmol) and 1 equiv of Hmhp in toluene. The redorange product was collected by suction filtration in air, washed with 3 × 10 mL of methanol and then vacuum dried. The UV-vis spectrum displayed maxima at 528 and 417 nm in THF. The <sup>31</sup>P{<sup>1</sup>H} NMR spectrum consists of a singlet at 3.2 ppm, CDCl<sub>3</sub>.

## 3. $Mo_2X_6(dppm)_2$

The syntheses of Mo<sub>2</sub>Cl<sub>6</sub>(dppm)<sub>2</sub>,<sup>67</sup> Mo<sub>2</sub>Br<sub>6</sub>(dppm)<sub>2</sub><sup>68</sup> and Mo<sub>2</sub>I<sub>6</sub>(dppm)<sub>2</sub><sup>68</sup> were carried out using published procedures; a brief description of their preparation is given below.

- a. Precursors. Bis(diphenylphosphino)methane (dppm) and chlorine were purchased from Aldrich Chemical Co. and used without further purification. Bromine was obtained from Fisher and used as received. The iodine was purchased from Mallinkrodt and purified by sublimation prior to use. The complexes Mo<sub>2</sub>Cl<sub>4</sub>(dppm)<sub>2</sub>,<sup>69</sup> Mo<sub>2</sub>Br<sub>4</sub>(dppm)<sub>2</sub><sup>70</sup> and Mo<sub>2</sub>I<sub>4</sub>(dppm)<sub>2</sub><sup>71</sup> were prepared according to literature methods.
- b. Mo<sub>2</sub>Cl<sub>6</sub>(dppm)<sub>2</sub>. To a dichloromethane solution (25 mL) of Mo<sub>2</sub>Cl<sub>4</sub>(dppm)<sub>2</sub> (0.21 g, 0.18 mmol) was added 5 mL of chlorine via a gas tight syringe. The color of the solution immediately changed from blue-green to bright red. The solution volume was then reduced to 5 mL under reduced pressure. The

product was collected by filtration and washed with  $4 \times 8$  mL of diethyl ether and dried. The absorption spectrum is consistent with the one reported in the literature.<sup>67</sup>

c. Mo<sub>2</sub>Br<sub>6</sub>(dppm)<sub>2</sub>. A sample of Mo<sub>2</sub>Br<sub>4</sub>(dppm)<sub>2</sub> (0.4 g, 0.312 mmol) was dissolved in CH<sub>2</sub>Cl<sub>2</sub> (30 mL) and treated with liquid bromine (1 equiv, 18 μL). The solution was stirred at room temperature for 18 hours. The pine green solid was collected by filtration and dried *in vacuo*. The UV-vis spectrum is identical to the one previously reported by Cotton and co-workers.<sup>68</sup>

d. Mo<sub>2</sub>I<sub>6</sub>(dppm)<sub>2</sub>. A dichloromethane solution (10 mL) of Mo<sub>2</sub>I<sub>4</sub>(dppm)<sub>2</sub> (0.20 g, 0.136 mmol) was treated with 1 equiv (0.035 g) of elemental iodine. The solution color immediately changed from olive to an orange-brown. The reaction mixture was stirred at room temperature for 3 hours and filtered through Celite. The filtrate was refrigerated at -10 °C for 2 days after the addition of 15 mL of toluene. The brown solid was collected by filtration, washed with cold toluene and dried. The IR and electronic spectra are virtually identical to the previously published spectra.<sup>68</sup>

# 4. $Rh_2(dfpma)_3(\eta^1-dfma)Br_2^{61}$

The bis(difluorophosphino)methylamine ligand was synthesized according to the method of Nixon<sup>72</sup> and characterized by <sup>1</sup>H and <sup>31</sup>P{<sup>1</sup>H} NMR spectroscopy. The complex Rh<sub>2</sub>Cl<sub>2</sub>(PF<sub>3</sub>)<sub>4</sub><sup>73</sup> was prepared using a previously published procedure. The starting material Rh<sub>2</sub>Br<sub>2</sub>(PF<sub>3</sub>)<sub>4</sub><sup>73</sup> was obtained by reacting Rh<sub>2</sub>Cl<sub>2</sub>(PF<sub>3</sub>)<sub>4</sub> with excess LiBr. To a toluene solution (15 mL) of

Rh<sub>2</sub>Br<sub>2</sub>(PF<sub>3</sub>)<sub>4</sub> (0.2 g, 0.28 mmol) was added 0.18 mL of CH<sub>3</sub>N(PF<sub>2</sub>)<sub>2</sub>. The yellow solution instantaneously darkened and began to evolve PF<sub>3</sub> gas. The solution color lightened again in a few seconds. The reaction mixture was then allowed to stir at room temperature for three hours. The red-orange precipitate was then collected by filtration, washed with toluene and dried *in vacuo*. The absorption spectrum is identical to the one reported in the literature. The <sup>31</sup>P{<sup>1</sup>H} NMR and <sup>1</sup>H NMR are consistent with those obtained previously.<sup>74</sup>

## **B. Spectroscopic Instrumentation and Methods**

## 1. Electronic Absorption Spectroscopy

Electronic absorption spectra were recorded on either an OLIS-modified Cary 17-D or a Cary 2300 UV-Vis-near-IR spectrometer. Extinction coefficients were calculated from Beer-Lambert plots composed of at least seven points.

# 2. Steady State Emission Spectroscopy

The steady-state emission spectra were obtained by exciting samples with the 200 W Hg/Xe lamp of a high resolution emission spectrometer designed and constructed at Michigan State University.<sup>75</sup> Emission quantum yields of Mo<sub>2</sub>Cl<sub>2</sub>(6-mhp)<sub>2</sub>(PMe<sub>2</sub>Ph)<sub>2</sub> were measured on the instrument featuring National Instruments hardware and LabVIEW software upgrades of the instrument control and interfacing. These changes will be described elsewhere.<sup>76</sup> These modifications did not alter the optical path or the detection system. The

excitation wavelength (546 nm) was selected using a double monochromator in conjunction with an Oriel 546 nm interference filter. The emitted light from the sample was directed through a single monochromator and onto a dry ice cooled PMT (Hamamatsu R-1104). A 570 nm longpass filter was placed in front of the emission monochromator. For solution samples slit widths were 2.5 mm/2.5 mm and 3 mm/3 mm for excitation and emission monochromators, respectively. For low temperature spectra, 1 mm slit widths were used for the emission monochromator. Temperature-dependent emission spectra were obtained by controlling the temperature of microcrystalline solids with an Air Products cryogenic system. Absolute emission quantum yields were measured for optically dilute samples (A < 0.1 at excitation wavelength) using Ru(bpy)<sub>3</sub>Cl<sub>2</sub> in water as the quantum yield standard ( $\Phi_e = 0.042$  at 300 K).<sup>77</sup> The quantum yields were calculated by using the following equation:<sup>78</sup>

$$\Phi_{\mathbf{x}} = \Phi_{\mathbf{r}} \times \frac{\mathbf{A}_{\mathbf{r}} \quad \eta_{\mathbf{x}}^2 \quad \mathbf{D}_{\mathbf{x}}}{\mathbf{A}_{\mathbf{x}} \quad \eta_{\mathbf{r}}^2 \quad \mathbf{D}_{\mathbf{r}}} \tag{2.1}$$

where x and r designate the unknown and standard solutions, respectively, A is the absorbance at the exciting wavelength,  $\eta$  is the average refractive index of the solution and D is the integrated area under the corrected emission spectrum.

## 3. Fluorescence Excitation Spectroscopy

Unpolarized fluorescence excitation spectra were recorded on the high-resolution emission spectrometer with the following modifications: a quartz beam splitter was placed in the excitation path to direct a portion of the excitation light from a 150 W Xe lamp to a photodiode, which was used to monitor the intensity profile of the excitation source thereby permitting excitation intensity to be normalized; the phase-modulated intensities of the excitation and emission light were detected with individual lock-in amplifiers. The outputs of the lock-in amplifiers and the photodiode were fed to a microcomputer, which permitted the emission intensity to be simultaneously corrected for excitation intensity and photodiode responses.

# 4. Time-Resolved Spectroscopy

Luminescence lifetime measurements were made utilizing a previously described time-correlated single-photon-counting instrument,<sup>79</sup> housed in the LASER Laboratory at Michigan State. Fluorescence decays were obtained with exciting and detecting wavelengths of 580 and 640 nm, respectively.

# 5. Nuclear Magnetic Resonance Spectroscopy

The NMR spectra were recorded at the Max T. Rogers NMR Facility at Michigan State University. Both <sup>31</sup>P and <sup>1</sup>H NMR spectra were recorded on a

Varian VXR-300S spectrometer at 121 and 300 MHz, respectively. <sup>1</sup>H NMR spectra were referenced to the residual protons of incompletely deuterated solvents and <sup>31</sup>P{<sup>1</sup>H} NMR spectra were referenced to an external sample of 85 % aqueous H<sub>3</sub>PO<sub>4</sub>.

## **6. Infrared Spectroscopy**

Infrared spectra were obtained as Nujol mulls on a Nicolet IR/42 spectrometer.

## 7. Electrospray Mass Spectrometry

Electrospray mass spectrometric analyses were performed on a Finnegan mat (San Jose, CA) quadrupole mass spectrometer, housed in the Macromolecular Structure Facility at Michigan State University, by using a CH<sub>3</sub>CN mobile phase. An acetonitrile solution of the sample was infused directly into the vaporization nozzle of the electrospray ion source at a flow rate of 3 mL min<sup>-1</sup>. Nitrogen was used as the nebulizing gas at a pressure of 35 psi.

# C. Photochemistry

Sample irradiations were performed using an Oriel 1000 W Hg/Xe high pressure lamp, powered by an Oriel 1 kW power supply. The beam was collimated and passed through a circulating water bath and wavelengths were

selected with Schott high-energy cutoff filters. The experimental apparatus is described in further detail elsewhere. 80 Photolysis experiments were performed in two-arm evacuable cells equipped with Kontes quick release Teflon valves. The sample temperatures were thermostatted using a Neslab Ex 211 water circulator/heater in conjunction with a Neslab En 850 chiller. photochemical quantum yields were determined by using an identical setup except that Oriel interference filters were used in place of cutoff filters. The intensity of the lamp was determined by using a ferrioxylate actinometer.81,82 Measurements were made under optically dense conditions, A > 2 at the exciting wavelengths. Photoproduct concentrations were limited to less than 10 % to avoid inner filter effects and competing product absorption. The quantum yields were determined by monitoring the disappearance of the  $\delta \to \delta^*$  ( $\lambda_{max} = 548$ nm) or  $d\pi^* \rightarrow d\sigma^*$  ( $\lambda_{max} = 417$  nm) for  $Mo_2Cl_2(6-mhp)_2(PR_3)_2$  and  $Rh_2(dfpma)_3(\eta^1-dfpma)Br_2$  respectively. The procedure for calculating photochemical quantum yields is described in detail in the dissertation of Dr. I-Jy Chang.<sup>83</sup> The overall chemical yields for Mo<sub>2</sub>Cl<sub>2</sub>(6-mhp)<sub>2</sub>(PMe<sub>2</sub>Ph)<sub>2</sub> were determined from electronic absorption spectra of photolyzed solutions by simultaneously solving Beer's law at three wavelengths.

#### **CHAPTER 3**

# PHOTOINDUCED LIGAND REDISTRIBUTION CHEMISTRY OF QUADRUPLY BONDED Mo<sub>2</sub>Cl<sub>2</sub>(6-mhp)<sub>2</sub>(PR<sub>3</sub>)<sub>2</sub> COMPLEXES

## A. Background

The multielectron photochemistry of quadruply bonded metal-metal complexes is intimately related to the coordination environment of the bimetallic core. A case in point is the two-electron photooxidative chemistry of  $M^{-4}$ -M complexes previously elaborated in the Nocera group. The different geometries enforced in the photoproducts, shown in Figure 3.1, are determined by the coordination geometry of the parent  $M^{-4}$ -M complex. The two-electron photooxidative addition of substrate to  $M^{-4}$ -M complexes featuring two bridging phosphines trans to each other  $(D_{2h})$  is promoted by the terminal halide ligands folding into edge-bridging positions to form edge-sharing bioctahedral photoproducts (ESBOs). For example, trans- $M_2X_4(PP)_2$  (PP = bridging phosphine, M = Mo(II), W(II), X = halide) complexes photooxidatively add a variety of substrates (YZ) to yield  $M_2X_4YZ(PP)_2$  ESBOs. So Conversely, the absence of bridging ligands in  $M_2X_4P_4$  ( $D_{2d}$ ) complexes (X = halide, P = tertiary

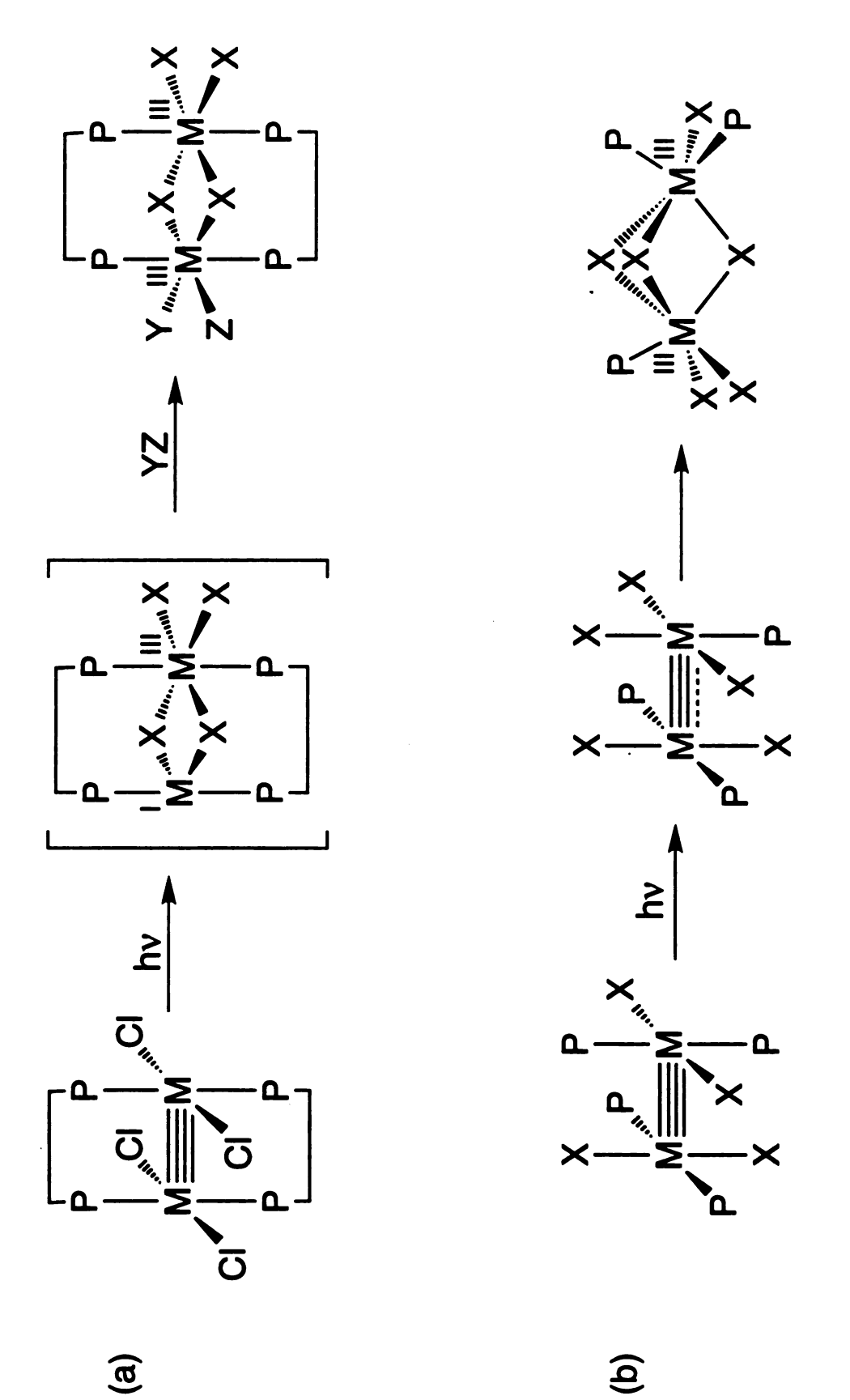


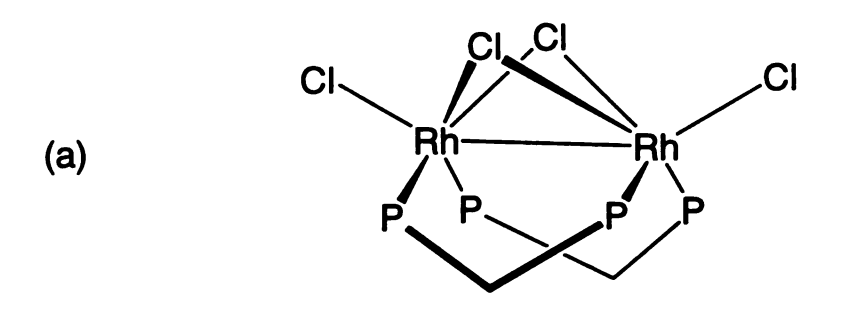
Figure 3.1 Formation of (a) edge- and (b) face-sharing bioctahedral photoproducts from quadruply bonded metal-metal-complexes with D<sub>2h</sub> and D<sub>2d</sub> symmetry, respectively.

(a)

phosphine) allows three terminal halides to move into bridging positions about the photooxidized bimetallic core to afford face-sharing bioctahedral products (FSBOs).<sup>85</sup> This observation raised the question of whether different photoproduct coordination geometries might be important in promoting photoreductive elimination reactions. Specifically, is the coordination geometry of Mo(III)—Mo(III) multiply bonded complexes important for photochemical conversions to Mo(II)—Mo(II) quadruply bonded complexes? The discovery of complexes that are predisposed to undergo concerted elimination reactions is of particular interest in this study.

One important consideration in the design of complexes predisposed to undergo reductive elimination is the internuclear distance between leaving groups, this is especially true if the elimination reaction is to occur via a concerted process. In the case of a concerted mechanism, the leaving groups must be sufficiently close to each other to allow coupling to take place. The crucial role internuclear distance plays in achieving concerted reductive elimination reactions led to a search for a structure type that places two ligands in the closest proximity to each other. The class of complexes that have the shortest nonbonded ligand-ligand distances are W-frame or cradle type structures. In the W-frame structure type, two metals are supported by two bidentate ligands, which span the metal centers in a cis,cis conformation, and four additional ligands, two of which occupy bridging sites. Figure 3.2 shows several examples of W-frame complexes. The two bridging chloride ligands in the singly bonded metal-metal dirhodium W-frame complex, Rh<sub>2</sub>Cl<sub>4</sub>(dppm)<sub>2</sub> (Figure 3.2a) are 3.14Å apart, <sup>86</sup> which is shorter than the internuclear distance

Figure 3.2 Three examples of metal-metal complexes with a W-frame geometry: (a)  $Rh_2Cl_4(dppm)_2$  (ref. 86) (b)  $Re_2(\mu-SH)_2Cl_2(dppm)_2$  (ref. 87) and (c) The Lewis acid induced coupling of bridging isocyanide ligands in  $Ir_2(\mu-CNR)_2(CNR)_2(dmpm)_2$  to form  $Ir_2(\eta^2-CNR)_2AlEt_2)(CNR)_2(dmpm)_2$  (ref. 88).



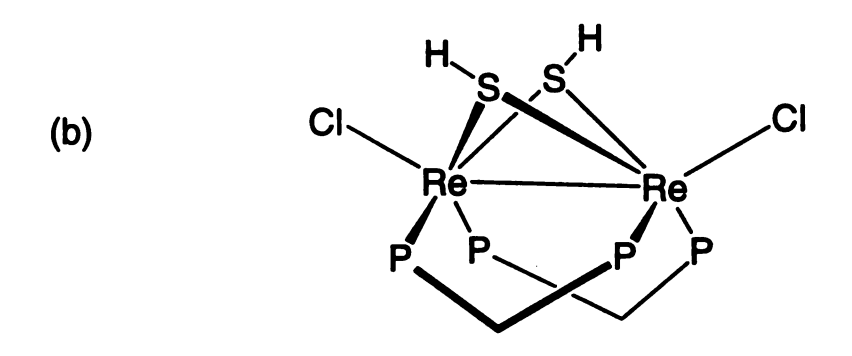


Figure 3.2

between adjacent ligands in other oxidized metal-metal bonded complexes such as ESBOs and FSBOs. Typical internuclear distances, between ligands, in ESBO and FSBO complexes are shown in Figure 3.3. W-frame structures are observed not only for singly bonded metal-metal complexes, but for multiply bonded metal-metal complexes as well. The nonredox reaction of Re<sub>2</sub>(O<sub>2</sub>CR)<sub>2</sub>Cl<sub>2</sub>(dppm)<sub>2</sub> with gaseous H<sub>2</sub>S in the presence of a strong acid results in the formation of the W-frame complex Re<sub>2</sub>(μ-SH)<sub>2</sub>Cl<sub>2</sub>(dppm)<sub>2</sub>, Figure 3.2b. The Re—Re bond distance in Re<sub>2</sub>(μ-SH)<sub>2</sub>Cl<sub>2</sub>(dppm)<sub>2</sub> is consistent with the presence of a Re—Re triple bond.

The importance of a W-frame structure in promoting elimination reaction chemistry is demonstrated in the Lewis acid induced reductive coupling of the two  $\mu$ -isocyanide ligands in Ir<sub>2</sub>( $\mu$ -CNR)<sub>2</sub>(CNR)<sub>2</sub>(dmpm)<sub>2</sub> (R= 2,6-Me<sub>2</sub>-C<sub>6</sub>H<sub>3</sub>)<sup>88</sup> to form Ir<sub>2</sub>( $\eta^2$ -(CNR)<sub>2</sub>AlEt<sub>2</sub>)(CNR)<sub>2</sub>(dmpm)<sub>2</sub>, Figure 3.2c. The carbon atoms of the  $\mu$ -isocyanide ligands in Ir<sub>2</sub>( $\mu$ -CNR)<sub>2</sub>(CNR)<sub>2</sub>(dmpm)<sub>2</sub> have a very short nonbonded contact of 2.37 Å. The isocyanide coupled product, Ir<sub>2</sub>( $\eta^2$ -(CNR)<sub>2</sub>AlEt<sub>2</sub>)(CNR)<sub>2</sub>(dmpm)<sub>2</sub>, contains a new carbon-carbon bond between the two bridging isocyanide ligands of 1.48 Å. An important issue is whether such factors could be exploited in photochemical reactions of W-frames. However, to date there has been no report of a triply bonded W-frame metal complex, that correlates to a M-4-M species.

Because a trans arrangement of two bridging ligands typically leads to ESBO photoproducts, *vide supra*, a logical starting point for the development of W-frames is M-4-M complexes with a cis arrangement of bridging ligands. The possible correlation between M-4-M complexes with two bridging ligands cis to

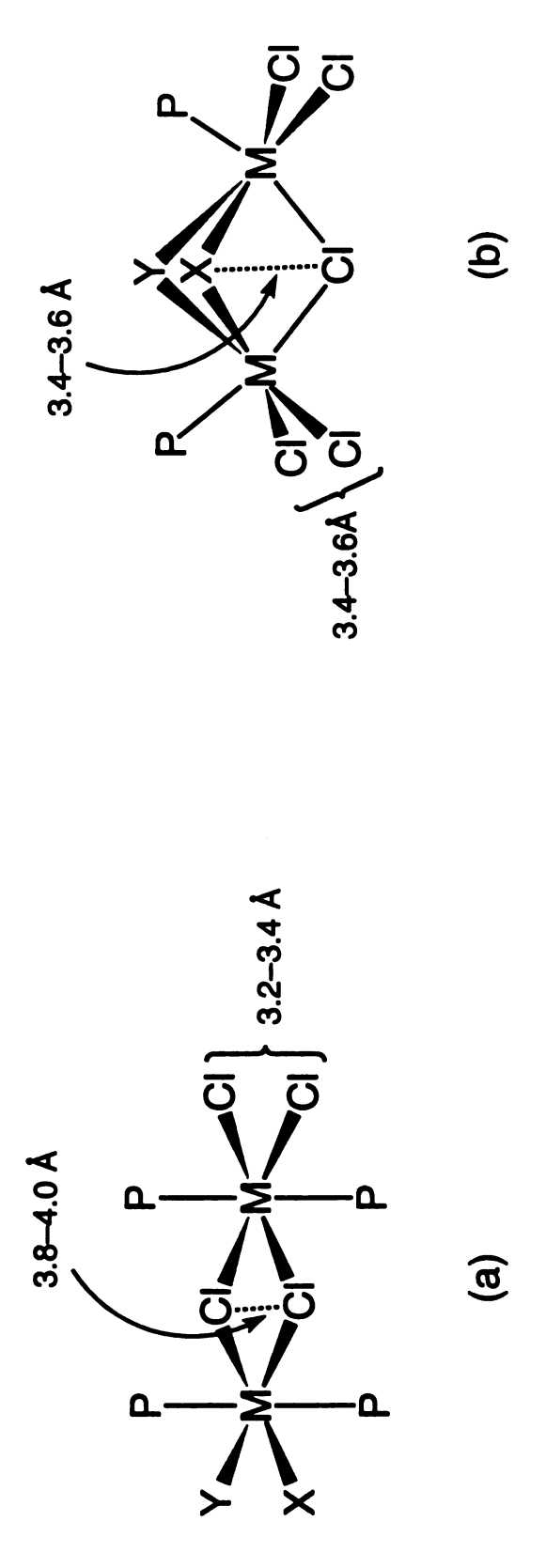


Figure 3.3 Typical internuclear distances between ligands in (a) ESBO and (b) FSBO complexes.

each other and W-frame structures is illustrated in Figure 3.4. Within this context, the quadruply bonded  $Mo_2Cl_2(6-mhp)_2(PR_3)_2$  (mhp = 2-hydroxy-6methylpyridinato; PR<sub>3</sub> = tertiary phosphine) complexes were attractive candidates for study because they were potentially photoactive M-4-M complexes possessing bidentate ligands in a cis conformation. The complexes with PR<sub>3</sub> = PEt<sub>3</sub>, PMe<sub>2</sub>Ph, PMePh<sub>2</sub>, <sup>62,66</sup> have been previously reported and the crystal structure of the PEt<sub>3</sub> complex reveals that the mhp ligands assume a cis conformation with the methyl groups of the pyridinato ligand in a head-to-tail arrangement.<sup>66</sup> Low-temperature spectroscopy is consistent with a  $\delta \rightarrow \delta^*$ assignment for the lowest-energy absorption band,  $^{66}$  arising from a  $\delta$ -HOMO and a  $\delta^*$ -LUMO of a  $\sigma^2 \pi^4 \delta^2$  ground state electronic configuration.<sup>49</sup> The presence of a long-lived  $\delta \delta^*$  excited state ( $\tau_0 = 34$  ns for the PEt<sub>3</sub> complex<sup>66</sup>) in principle permits the excited state oxidation chemistry for this series of complexes to be elaborated. However, as this Chapter describes the cis-Mo<sub>2</sub>Cl<sub>2</sub>(6-mhp)<sub>2</sub>(PR<sub>3</sub>)<sub>2</sub> series of complexes, which has been extended to include the complex with PR<sub>3</sub> = PMe<sub>3</sub>, well-defined photoredox chemistry is obscured by facile photoinduced redistribution of the mhp ligands.

# **B. Photophysical Properties**

Dichloromethane solutions of *cis*-Mo<sub>2</sub>Cl<sub>2</sub>(6-mhp)<sub>2</sub>(PR<sub>3</sub>)<sub>2</sub> exhibit characteristic absorption profiles dominated by a lowest energy absorption in the ~550 nm spectral range. With the exception of the PMe<sub>3</sub> complex, the absorption spectra of *cis*-Mo<sub>2</sub>Cl<sub>2</sub>(6-mhp)<sub>2</sub>(PR<sub>3</sub>)<sub>2</sub> complexes have previously

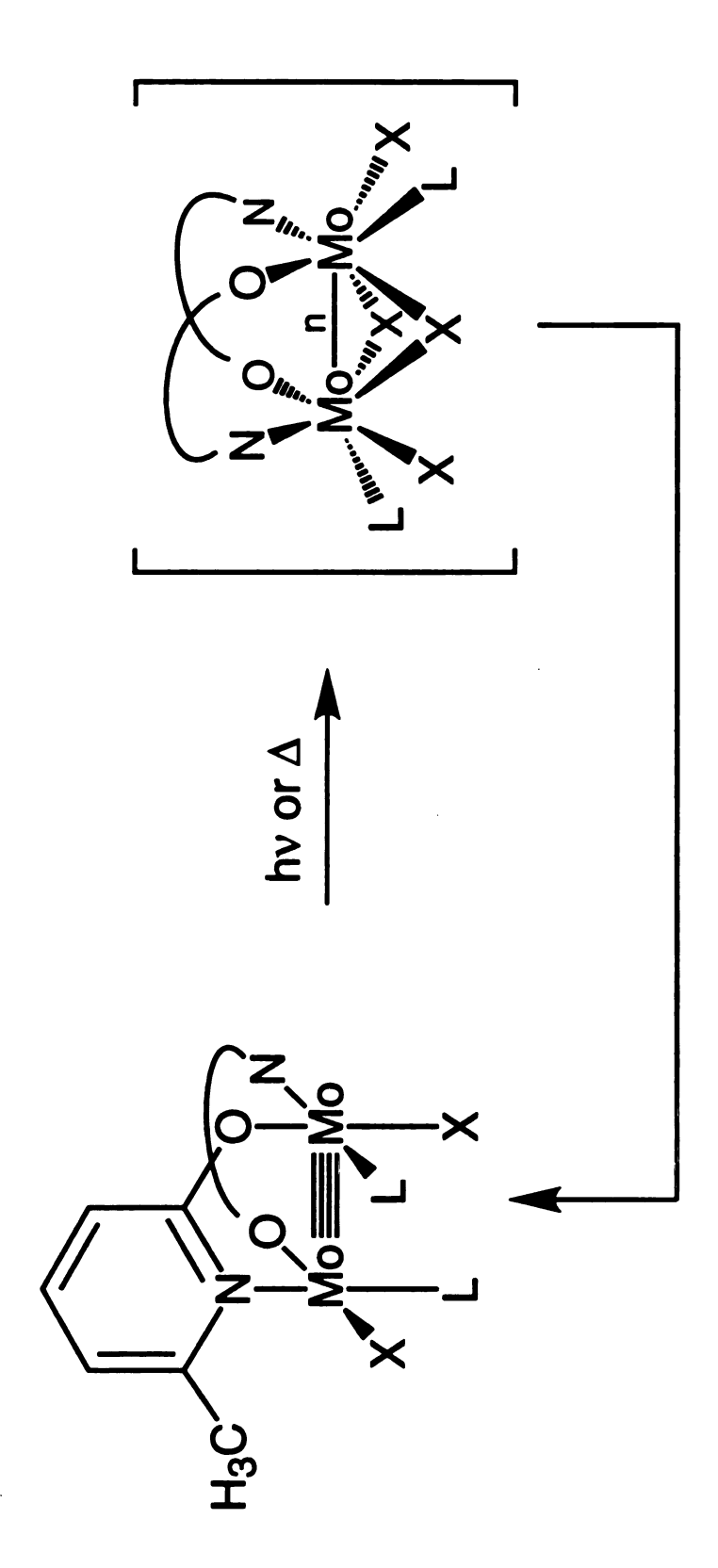


Figure 3.4 Possible correlation between quadruply bonded metal-metal complexes with a cis arrangement of bridging ligands and W-frame complexes.

been investigated.<sup>62,66</sup> The prominent low-energy feature is consistent with a  $\delta \to \delta^*$  transition. Deconvolution of the electronic absorption spectrum of the PEt<sub>3</sub> complex suggests the presence of at least five other bands,<sup>66</sup> and tentative assignments for some of these transitions have been made by comparison to the assigned spectra of Mo<sub>2</sub>(mhp)<sub>4</sub> and Mo<sub>2</sub>Cl<sub>4</sub>(PR<sub>3</sub>)<sub>4</sub>. Important to the studies discussed in this Chapter, the intense absorption bands at 300 and 280 nm have been assigned<sup>66</sup> to ligand-to-metal charge transfer (LMCT) and mhp-localized  $\pi \to \pi^*$  transitions.

Figure 3.5 shows the absorption, fluorescence excitation, and emission spectra for the PMe<sub>2</sub>Ph complex. Excitation into the  $\delta \rightarrow \delta^*$  transition of room temperature solutions and solids of the complexes produces bright luminescence that is easily observed, even in ambient light. As the wavelength of excitation is decreased, the overall emission emanating from the complex is severely attenuated. This is most easily observed by comparing the excitation and absorption spectra. Using the  $\delta \rightarrow \delta^*$  transition to standardize intensities, the intensity of the excitation profile is attenuated significantly in the 325-425 nm spectral region and disappears almost completely when the excitation wavelength is coincident with the near-UV charge transfer transitions ( $\lambda$ <325 nm).

Upon cooling to 10 K, the emission of the PMe<sub>2</sub>Ph, and PEt<sub>3</sub> complexes blue-shifts and sharpens with the fwhm of the emission band changing from ~1500 to ~990 cm<sup>-1</sup>. These data suggest that the emission profile is inhomogeneously broadened owing to luminescence from different conformers of the complex. With cooling, the conformer contributing the higher energy

Figure 3.5 (a) Absorption, (b) fluorescence excitation and (c) emission spectra of cis-Mo<sub>2</sub>Cl<sub>2</sub>(6-mhp)<sub>2</sub>(PMe<sub>2</sub>Ph)<sub>2</sub> in deoxygenated 2-methylpentane at room temperature. The absorption and excitation spectra are normalized to each other based on the intensity of the  $\delta \to \delta^*$  transition. The open circles are the quantum yields for the photoreaction of cis-Mo<sub>2</sub>Cl<sub>2</sub>(6-mhp)<sub>2</sub>(PMe<sub>2</sub>Ph)<sub>2</sub> in benzene at the specified wavelengths.

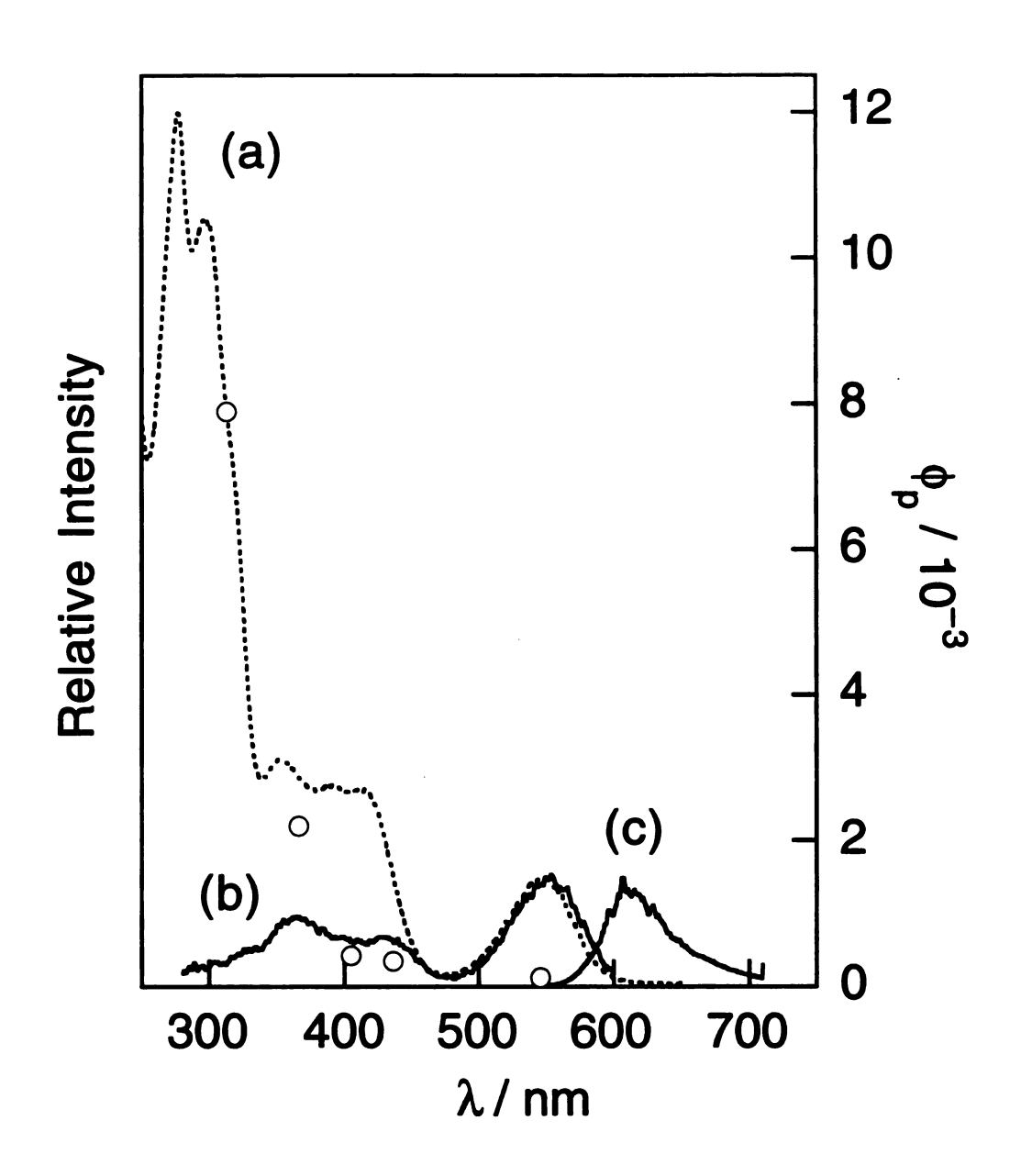


Figure 3.5

luminescence to the overall emission profile is favored. Interestingly, the emission profile of the PMePh<sub>2</sub> complex shows very little temperature dependence, suggesting that emission profile is not broadened by contributions from different conformers. The Stokes shifts between the absorption and emission profiles of room temperature solution spectra are modest, ranging from  $1850 \text{ cm}^{-1} \text{ for } PR_3 = PMe_3 \text{ to } 2010 \text{ cm}^{-1} \text{ for } PR_3 = PMe_2Ph, \text{ and smaller than}$ those observed in the  $Mo_2Cl_4(PR_3)_4$  series (2210 cm<sup>-1</sup> for  $PR_3 = PMe_3$ , <sup>89</sup> 2210 cm<sup>-1</sup> for PR<sub>3</sub> = PBu<sub>3</sub>,<sup>90</sup> and 2250 cm<sup>-1</sup> for PR<sub>3</sub> = PEt<sub>3</sub><sup>91</sup>). This result suggests less distortion in cis-Mo<sub>2</sub>Cl<sub>2</sub>(6-mhp)<sub>2</sub>(PR<sub>3</sub>)<sub>2</sub> excited states owing to more hindered elongation of the metal-metal bond when it is spanned by the rigid, bidentate mhp ligands as compared to the Mo<sub>2</sub>Cl<sub>4</sub>(PR<sub>3</sub>)<sub>4</sub> series where the metalmetal bond is unsupported by bridging ligands. Luminescence spectra feature sharp vibrational fine structure when solid samples of cis-Mo<sub>2</sub>Cl<sub>2</sub>(mhp)<sub>2</sub>(PR<sub>3</sub>)<sub>2</sub> are cooled to T < 50 K. The emission spectrum for cis-Mo<sub>2</sub>Cl<sub>2</sub>(6-mhp)<sub>2</sub>(PEt<sub>3</sub>)<sub>2</sub> at 10 K (Figure 3.6) is representative of the data obtained for the cis-Mo<sub>2</sub>Cl<sub>2</sub>(6mhp)<sub>2</sub>(PR<sub>3</sub>)<sub>2</sub> series of complexes. The  $\delta \rightarrow \delta^*$  absorption band is a mirror image of the emission band and the 0-0 components of the two profiles overlap, indicating the absence of a Duschinsky effect.<sup>92</sup> These results are consistent with emission originating from the  $\delta\delta^*$  excited state in which distortion occurs along a coordinate common to both excited and ground states; the prominent vibrational progression is a signature of distortion along the metal-metal bond. The frequency of the progression for cis-Mo<sub>2</sub>Cl<sub>2</sub>(6-mhp)<sub>2</sub>(PR<sub>3</sub>)<sub>2</sub> (389  $\pm$  4, 387  $\pm$ 4,  $383 \pm 15$  cm<sup>-1</sup> for PR<sub>3</sub> = PEt<sub>3</sub>, PMe<sub>2</sub>Ph and PMePh<sub>2</sub>, respectively) reasonably lies between the 358 and 425 cm<sup>-1</sup> frequencies of the  $v_{a_1}(Mo-Mo)$  symmetric

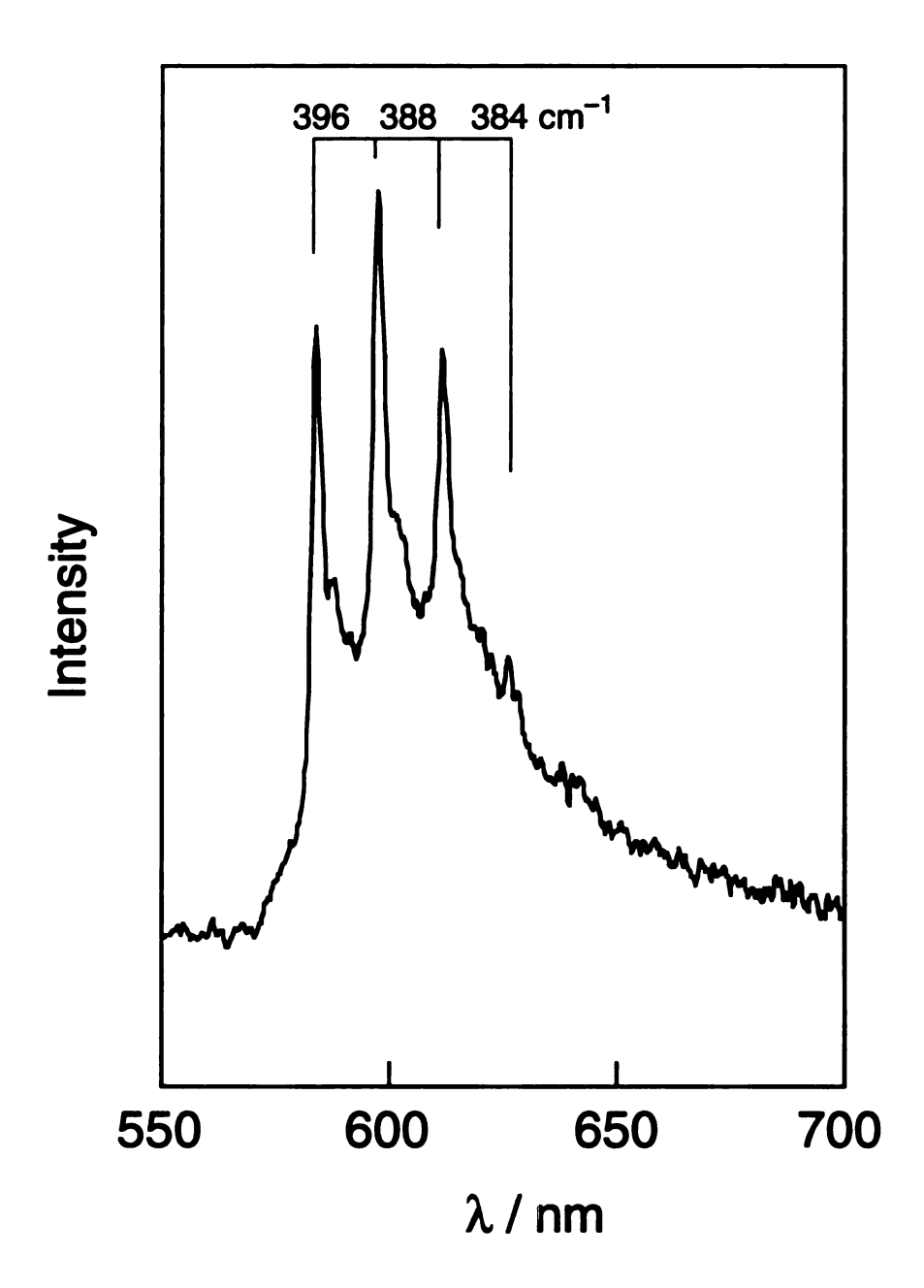


Figure 3.6 Corrected emission spectrum of a solid sample of cis-Mo<sub>2</sub>Cl<sub>2</sub>(6-mhp)<sub>2</sub>(PEt<sub>3</sub>)<sub>2</sub> at 10 K.

stretch of Mo<sub>2</sub>Cl<sub>4</sub>(PMe<sub>3</sub>)<sub>4</sub> and Mo<sub>2</sub>(mhp)<sub>4</sub>, respectively.<sup>89,93</sup> Low-temperature absorption spectra of the  $\delta \rightarrow \delta^*$  transition of the PEt<sub>3</sub> complex place  $v_{a_1}$  (Mo— Mo) at 370 cm<sup>-1</sup>. A 19 cm<sup>-1</sup> reduction of the metal-metal frequency in the  $\delta\delta^*$ excited state of cis-Mo<sub>2</sub>Cl<sub>2</sub>(6-mhp)<sub>2</sub>(PEt<sub>3</sub>)<sub>2</sub> is in good agreement with the 22 cm<sup>-1</sup> decrease of  $v_{a_1}(Mo-Mo)$  in electronically excited  $Mo_2Cl_4(PMe_3)_4$ , and is within the 10-50 cm<sup>-1</sup> range typically observed for M-4-M complexes.<sup>48</sup> The Mo-Mo bond distances in the ground and excited states can be calculated from the vibronic progressions of the low temperature emission and absorption spectra, respectively, by using Woodruff's modification of Badger's relation.<sup>94</sup> The 389 cm<sup>-1</sup> progression in the emission spectrum of the PEt<sub>3</sub> complex corresponds to a ground state Mo—Mo bond distance of 2.10 Å, which is in excellent agreement with the 2.103 Å distance obtained from the crystal structure.<sup>66</sup> Moreover a 0.048 Å increase of the Mo-Mo bond distance in the excited state, as determined from the 370 cm<sup>-1</sup> progression in the low temperature absorption spectrum, results from the elimination of the weak  $\delta$  bond upon  $\delta \rightarrow \delta^*$  excitation. This elongation coincides with the ~0.025-0.050 Å increase in M—M bond length when the  $\delta$  bond is weakened or eliminated by chemical redox 95,96

The luminescence quantum yields ( $\Phi_e$ ) of cis-Mo<sub>2</sub>Cl<sub>2</sub>(6-mhp)<sub>2</sub>(PR<sub>3</sub>)<sub>2</sub> in CH<sub>2</sub>Cl<sub>2</sub> are listed in Table 3.1. Generally they are greater than those observed for the corresponding Mo<sub>2</sub>Cl<sub>4</sub>(PR<sub>3</sub>)<sub>4</sub> complexes. Similarly, the lifetimes of cis-Mo<sub>2</sub>Cl<sub>2</sub>(6-mhp)<sub>2</sub>(PR<sub>3</sub>)<sub>2</sub> complexes are also longer than their Mo<sub>2</sub>Cl<sub>4</sub>(PR<sub>3</sub>)<sub>4</sub> congeners. Although solutions of the complexes exhibit clean monoexponential luminescence decays, the lifetimes of solid samples at room temperature and at

$\mathbb{R}_3$	Amax,abs/nm	Amax,em/nm	Ф <sub>еш</sub>	τ/ns
Me <sub>3</sub>	545	009	0.084	50
Et3	542	909	0.22	75
Me <sub>2</sub> Ph	545	209	0.18	45
MePh <sub>2</sub>	549	614	0.18	74

Mo<sub>2</sub>Cl<sub>2</sub>(6-mhp)<sub>2</sub>(PR<sub>3</sub>)<sub>2</sub> and the relative contribution of each component are listed in Table 3.2. In view of the monoexponential behavior of these solids when dissolved in solution, the second component does not appear to arise from an impurity but is a consequence of localized heating of the lattice or some other crystal lattice effect. In addition to CH<sub>2</sub>Cl<sub>2</sub>, luminescence lifetimes and emission quantum yields, listed in Table 3.3, were measured in the solvents in which photochemical studies were performed. These data reveal no discernible trend with respect to solvent properties.

#### C. Photochemistry

The irradiation of solutions of cis-Mo<sub>2</sub>Cl<sub>2</sub>(6-mhp)<sub>2</sub>(PR<sub>3</sub>)<sub>2</sub> complexes with visible and near-UV light results in a prompt reaction. In the absence of light, no reaction is observed, although a thermal reaction does occur for DMF solutions at elevated temperatures (> 60 °C). Because all members of this series photoreact in a similar manner, this Chapter will focus on the photochemistry of only one of these complexes, cis-Mo<sub>2</sub>Cl<sub>2</sub>(6-mhp)<sub>2</sub>(PMe<sub>2</sub>Ph)<sub>2</sub>. Irradiation of the benzene solutions of cis-Mo<sub>2</sub>Cl<sub>2</sub>(6-mhp)<sub>2</sub>(PMe<sub>2</sub>Ph)<sub>2</sub> with visible light ( $\lambda$  > 435 nm) causes the bright red solution to turn plum. The spectral changes associated with this photochemistry are displayed in Figure 3.7. The disappearance of the  $\delta \rightarrow \delta^*$  absorption at 548 nm is accompanied by the appearance of an absorption band at slightly longer wavelengths. Photolyzed solutions eluted on silica gel with

**Table 3.2** Fluoresence lifetimes for solid samples of *cis*-Mo<sub>2</sub>Cl<sub>2</sub>(6-mhp)<sub>2</sub>(PMe<sub>2</sub>Ph)<sub>2</sub>

R <sub>3</sub>	τ/ns 298 K	τ/ns 77 K
Et <sub>3</sub>	2.9, 5.9 (25.2 %)	2.9, 12.5 (41.7 %)
Me <sub>2</sub> Ph	35.6, 117.8 (35.8 %)	37.3, 67.1 (54.9 %)
MePh <sub>2</sub>	4.1, 5.5 (35.0) %	3.9, 18.2 (23.6 %)

**Table 3.3** Solvent Dependence of Selected Photophysical Data and Photolysis Quantum Yields for *cis*-Mo<sub>2</sub>Cl<sub>2</sub>(6-mhp)<sub>2</sub>(PMe<sub>2</sub>Ph)<sub>2</sub>

solvent	$\Phi_{ m em}$	<b>t</b> ∕ns	$10^4 \Phi_{\rm p}{}^a$
DMF	0.064	23	9.7
THF	0.18	60	6.4
C <sub>6</sub> H <sub>6</sub>	0.20	55	4.2

<sup>&</sup>lt;sup>a</sup> Photolysis Quantum Yields for disappearance of *cis*-Mo<sub>2</sub>Cl<sub>2</sub>(6-mhp)<sub>2</sub>(PMe<sub>2</sub>Ph)<sub>2</sub> with 405-nm irradiation.

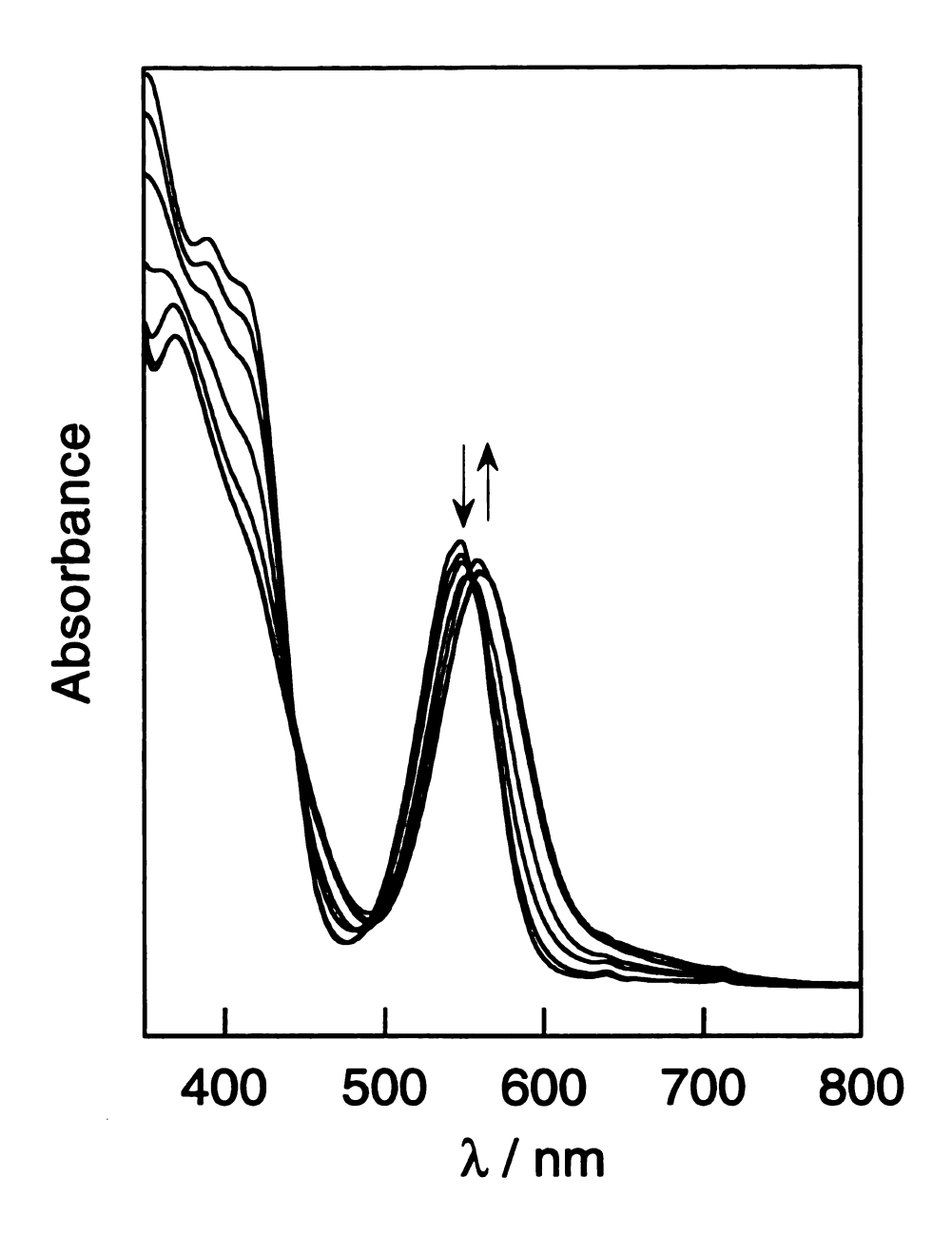


Figure 3.7 Electronic absorption spectral changes during the photolysis ( $\lambda_{\rm exc} > 435\,$  nm) of cis-Mo<sub>2</sub>Cl<sub>2</sub>(6-mhp)<sub>2</sub>(PMe<sub>2</sub>Ph)<sub>2</sub> in deoxygenated benzene at 10 °C. Spectra were recorded at 0, 10, 30, 70, 170, 300 and 390 min.

CH<sub>2</sub>Cl<sub>2</sub> yield major components that are red and purple, and minor components that are blue and orange.

All the components observed by column chromatography have been identified. The red component is unreacted starting material, identified on the basis of its <sup>31</sup>P{<sup>1</sup>H} NMR and electronic absorption spectra. The UV-vis spectrum of the purple product exhibits maxima at 573 and 329 nm, with shoulders observed at 417 and 367 nm. The <sup>31</sup>P{<sup>1</sup>H} NMR spectrum of the purple component exhibits two resonances, a doublet at 1.35 and a triplet at 0.88 ppm (J(P-P) = 12.8 Hz; ratio of doublet:triplet is 2:1). These UV-vis and <sup>31</sup>P{<sup>1</sup>H} NMR spectra identically match the corresponding spectra of the independently prepared complex, Mo<sub>2</sub>Cl<sub>3</sub>(6-mhp)(PMe<sub>2</sub>Ph)<sub>3</sub>.<sup>62</sup> This complex was first observed as an impurity in the synthesis of cis-Mo<sub>2</sub>Cl<sub>2</sub>(6mhp)<sub>2</sub>(PMe<sub>2</sub>Ph)<sub>2</sub> and can be directly synthesized by reacting cis-Mo<sub>2</sub>Cl<sub>2</sub>(6mhp)<sub>2</sub>(PMe<sub>2</sub>Ph)<sub>2</sub> with Mo<sub>2</sub>Cl<sub>4</sub>(PMe<sub>2</sub>Ph)<sub>4</sub> in refluxing toluene. The blue, minor product is also readily identified from its spectroscopic signatures; the electronic absorption and NMR spectral features are identical to those of Mo<sub>2</sub>Cl<sub>4</sub>(PMe<sub>2</sub>Ph)<sub>4</sub>. The orange product was present in smaller amounts and decomposed before eluting from the column. Nevertheless the product was determined to be Mo<sub>2</sub>Cl(6-mhp)<sub>3</sub>(PMe<sub>2</sub>Ph) on the basis of TLC, using an independently prepared sample as a standard.

The disappearance quantum yield of the photolysis reaction of *cis*-Mo<sub>2</sub>Cl<sub>2</sub>(6-mhp)<sub>2</sub>(PMe<sub>2</sub>Ph)<sub>2</sub> in benzene was measured at several wavelengths; these are shown overlaid on the absorption spectrum in Figure 3.5. The quantum yield changes only slightly over the excitation wavelength range from 546 to

405 nm and increases dramatically for  $\lambda_{\rm exc}$  < 366 nm. In the presence of a 20-fold excess of Hmhp, the quantum yield decreases from  $2.2 \times 10^{-3}$  to  $4.7 \times 10^{-4}$  at  $\lambda$  = 366 nm. Interestingly, the photoreaction is accelerated by Cl<sup>-</sup> (the quantum yield increased by almost a factor of 10). The addition of excess chloride not only markedly increases the rate of the reaction but also the extent to which the photoreaction occurs. The spectral changes due to the photolysis of *cis*-Mo<sub>2</sub>Cl<sub>2</sub>(6-mhp)<sub>2</sub>(PMe<sub>2</sub>Ph)<sub>2</sub> ( $\lambda$  > 435 nm) with excess Cl<sup>-</sup> in benzene are shown in Figure 3.8. The addition of excess PMe<sub>2</sub>Ph does not have a noticeable effect on the photochemistry. Similar photoreaction quantum yields are observed for the other complexes in this series. For instance,  $\Phi_p^{366}$  =  $7.8 \times 10^{-4}$  for *cis*-Mo<sub>2</sub>Cl<sub>2</sub>(6-mhp)<sub>2</sub>(PEt<sub>3</sub>)<sub>2</sub> in benzene. Photochemical substitution of mhp in benzene is also observed for *cis*-Mo<sub>2</sub>Cl<sub>2</sub>(6-mhp)<sub>2</sub>(PMePh<sub>2</sub>)<sub>2</sub>. However, its low solubility precludes an accurate quantum yield determination.

The photolysis reaction of cis-Mo<sub>2</sub>Cl<sub>2</sub>(6-mhp)<sub>2</sub>(PMe<sub>2</sub>Ph)<sub>2</sub> is strongly solvent dependent. As opposed to the plum-colored benzene-photolyzed solutions, irradiation in DMF ( $\lambda_{exc} > 435$  nm) leads to bright orange solutions, the spectral changes for which are displayed in Figure 3.9. The reaction, to produce a photoproduct whose absorption spectrum compares well with that of Mo<sub>2</sub>Cl(6-mhp)<sub>3</sub>(PMe<sub>2</sub>Ph) is complete within a day. If the irradiation is continued for several more hours, the peak at 528 nm shifts to 514 nm and the 417-nm band grows in intensity but is energetically invariant. This secondary photoreaction is identical to the one that occurs when solutions of the independently synthesized Mo<sub>2</sub>Cl(6-mhp)<sub>3</sub>(PMe<sub>2</sub>Ph) are irradiated ( $\lambda > 435$  nm) in DMF.

Photolysis of cis-Mo<sub>2</sub>Cl<sub>2</sub>(6-mhp)<sub>2</sub>(PMe<sub>2</sub>Ph)<sub>2</sub> in THF ( $\lambda_{exc} > 435$  nm)

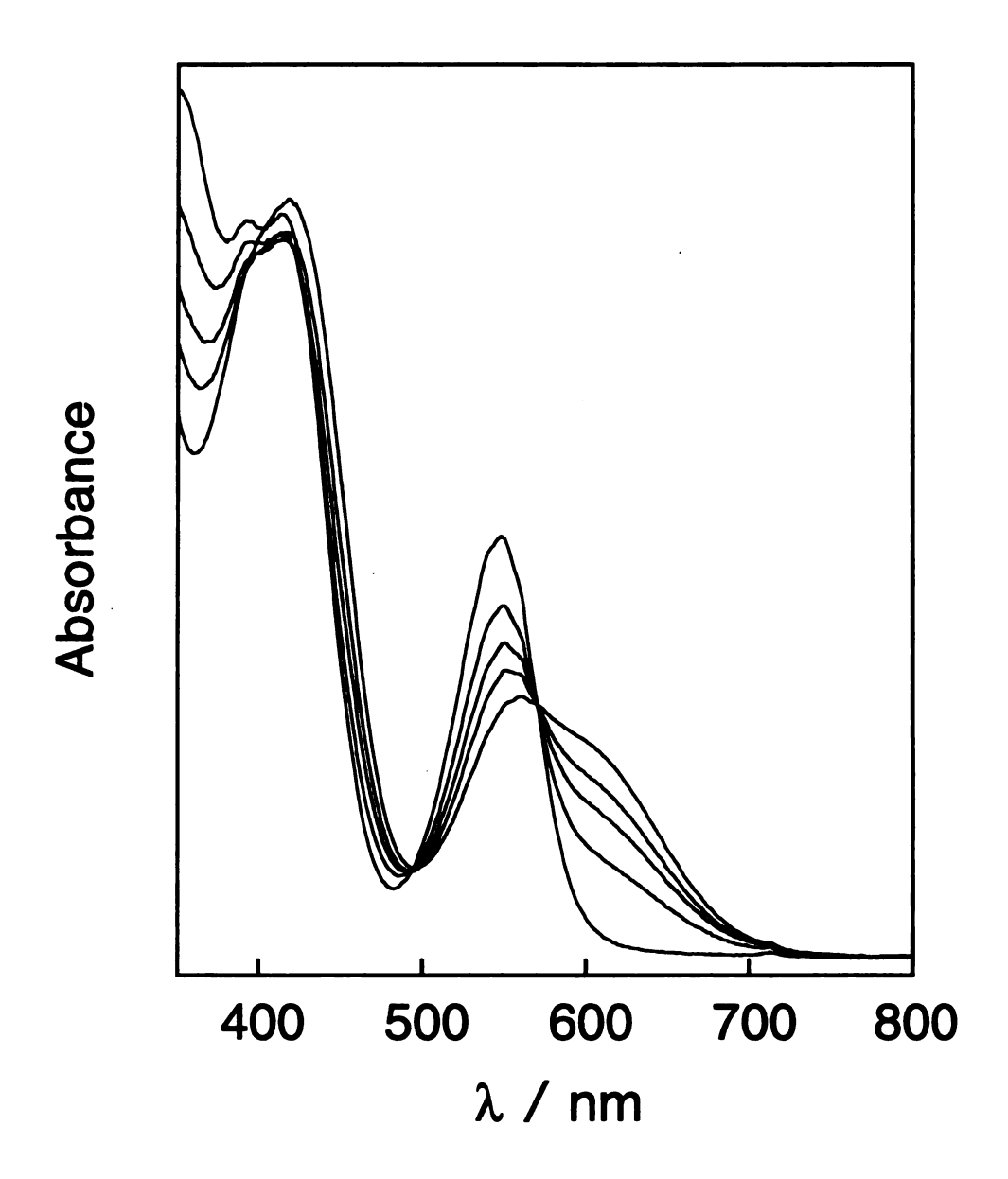


Figure 3.8 Electronic absorption spectral changes during the photolysis ( $\lambda_{\rm exc} > 435$  nm) of cis-Mo<sub>2</sub>Cl<sub>2</sub>(6-mhp)<sub>2</sub>(PMe<sub>2</sub>Ph)<sub>2</sub> with excess chloride in deoxygenated benzene at 10 °C. Spectra were recorded at 0, 5, 10, 15, 25, 35, and 60 min.

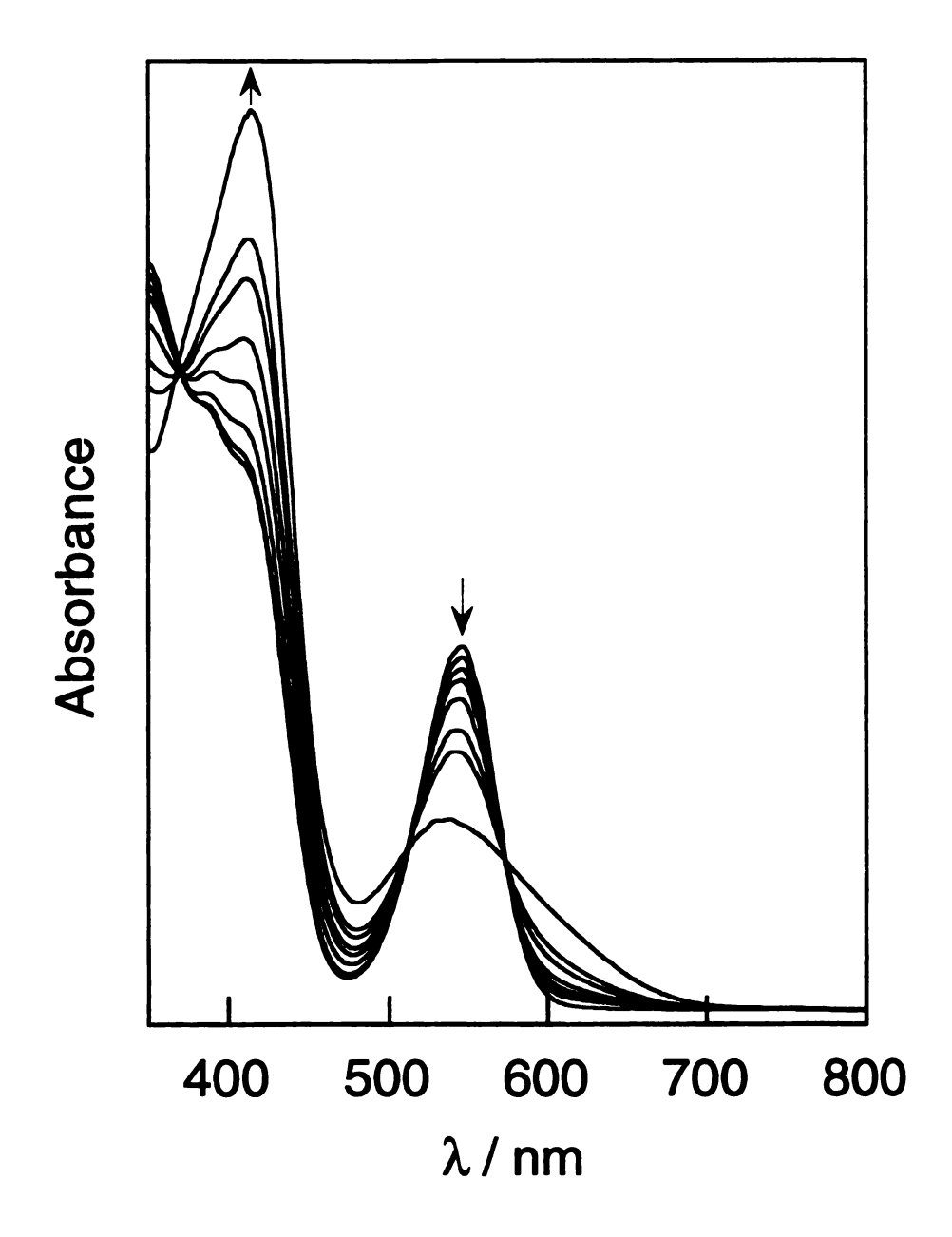
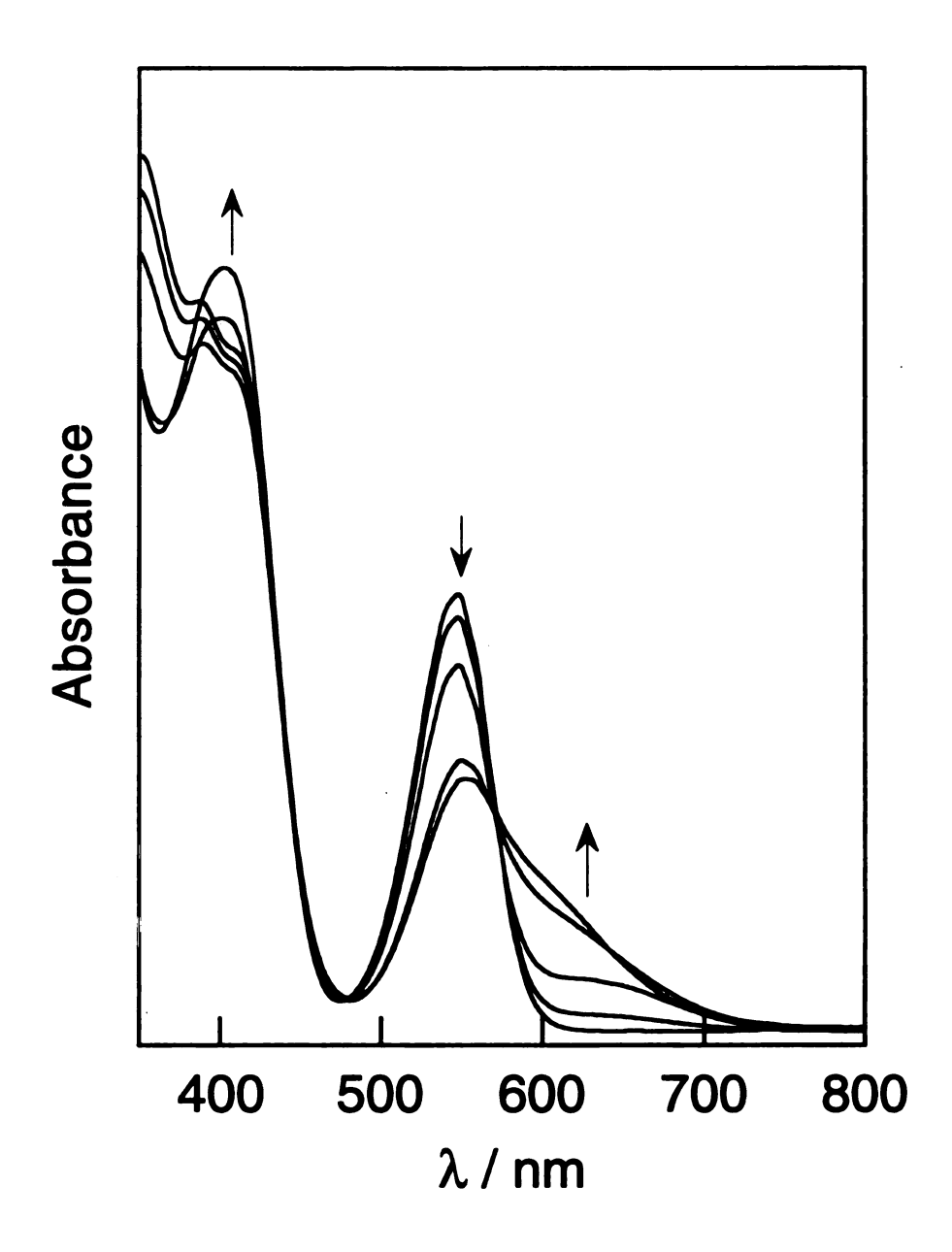


Figure 3.9 Electronic absorption spectral changes during the photolysis  $(\lambda_{\rm exc} > 435 \text{ nm})$  of  $cis\text{-Mo}_2\text{Cl}_2(6\text{-mhp})_2(\text{PMe}_2\text{Ph})_2$  in deoxygenated DMF at 10 °C. Spectra were recorded at 0, 15, 45, 90, 180, 315, 435 and 1110 min.

yields a blue-gray solution, and as Figure 3.10 shows, the low energy tail of the  $\delta \rightarrow \delta^*$  absorption increases in intensity and a broad prominent absorption appears at 403 nm. An isosbestic point is maintained at low energy; however, the absence of an isosbestic point in the near-ultraviolet spectral region indicates the presence of a minor impurity. The two major photoproducts were separated by column chromatography as described above. The purple and red-orange photoproducts, Mo<sub>2</sub>Cl<sub>3</sub>(6-mhp)(PMe<sub>2</sub>Ph)<sub>3</sub> and Mo<sub>2</sub>Cl(6-mhp)<sub>3</sub>(PMe<sub>2</sub>Ph), were obtained in nearly equal yields in addition to unreacted starting material.

The photoproducts exhibit different stabilities in the various solvents used to carry out the photochemistry. In THF both the Mo<sub>2</sub>Cl<sub>3</sub>(6mhp)(PMe<sub>2</sub>Ph)<sub>3</sub> and Mo<sub>2</sub>Cl(6-mhp)<sub>3</sub>(PMe<sub>2</sub>Ph) photoproducts are stable. When solutions are allowed to stand at room temperature, protected from light, the absorption spectrum of the starting complex reappears over hours. As indicated by electronic absorption spectra in Figure 3.11, this back reaction to give cis-Mo<sub>2</sub>Cl<sub>2</sub>(6-mhp)<sub>2</sub>(PMe<sub>2</sub>Ph)<sub>2</sub> appears to be clean and is reproduced by mixing equimolar amounts of Mo<sub>2</sub>Cl<sub>3</sub>(6-mhp)(PMe<sub>2</sub>Ph)<sub>3</sub> and Mo<sub>2</sub>Cl(6-mhp)<sub>3</sub>(PMe<sub>2</sub>Ph) in the presence of free ligand. The reaction is accelerated when the conjugate base of the ligand is generated addition by the bis(dimethylamino)naphthalene to solution. Similarly, the reaction is accelerated when the tetrabutylammonium salt of the mhp anion is added to solution. No thermal reaction is observed in the absence of free ligand or its conjugate base. In benzene, the back reaction only partially occurs because Mo<sub>2</sub>Cl(6mhp)<sub>3</sub>(PMe<sub>2</sub>Ph) is depleted by a competing, albeit slow, secondary photochemical reaction. A secondary photoreaction of Mo<sub>2</sub>Cl(6-mhp)<sub>3</sub>(PMe<sub>2</sub>Ph)



**Figure 3.10** Electronic absorption spectral changes during the photolysis ( $\lambda_{\rm exc} > 435\,$  nm) of *cis*-Mo<sub>2</sub>Cl<sub>2</sub>(6-mhp)<sub>2</sub>(PMe<sub>2</sub>Ph)<sub>2</sub> in deoxygenated THF at 10 °C. Spectra were recorded at 0, 10, 30, 120 and 180 min.

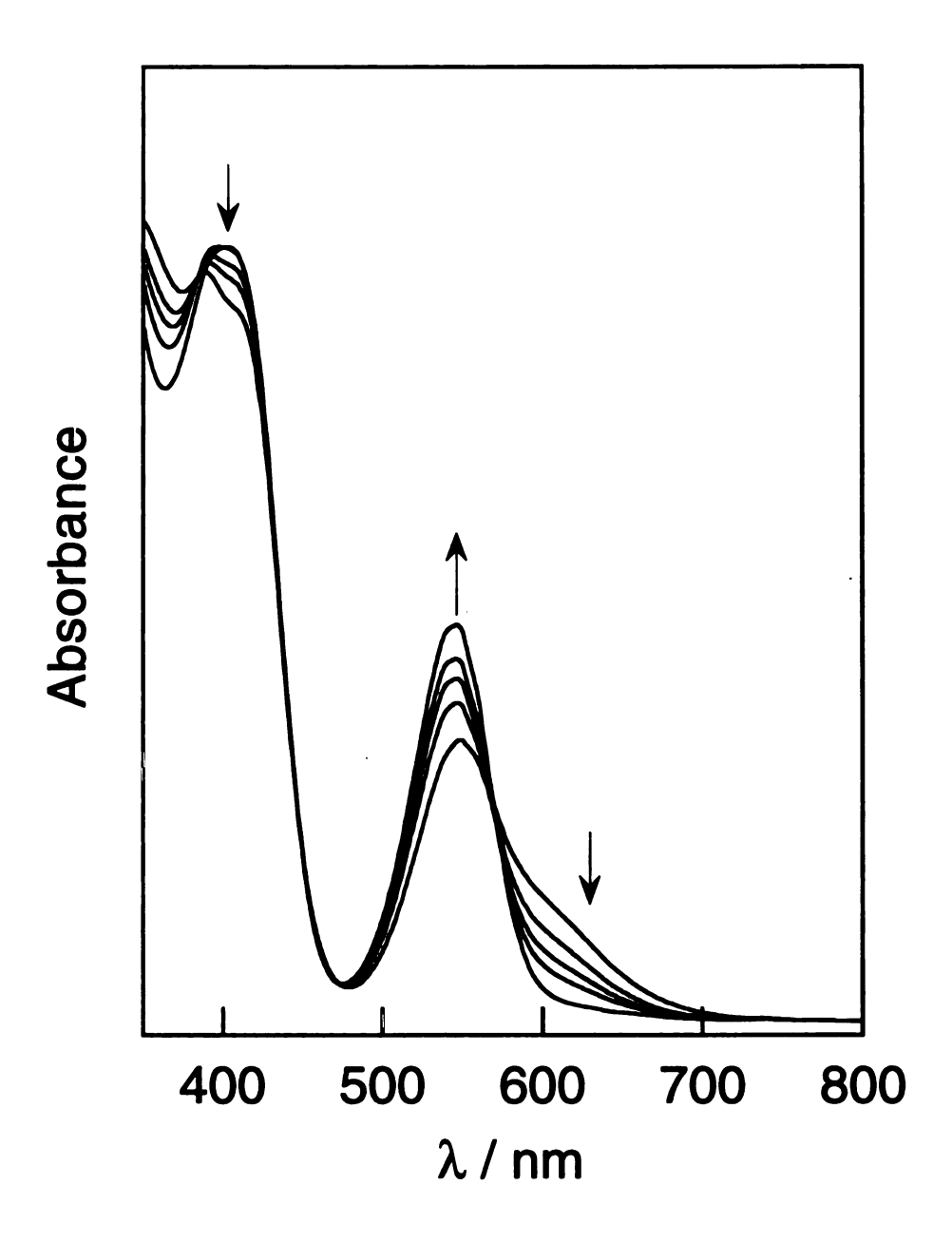


Figure 3.11 Electronic absorption spectral changes recorded 30, 110, 210, 340, and 1260 min after the conclusion of the photolysis shown in Figure 3.10. The sample was stored in the dark at room temperature.

was verified by photolyzing benzene solutions of the independently prepared complex. Conversely in DMF, whereas Mo<sub>2</sub>Cl<sub>(6</sub>-mhp)<sub>3</sub>(PMe<sub>2</sub>Ph) is stable, Mo<sub>2</sub>Cl<sub>3</sub>(6-mhp)(PMe<sub>2</sub>Ph)<sub>3</sub> is not. DMF solutions of independently prepared Mo<sub>2</sub>Cl<sub>3</sub>(6-mhp)(PMe<sub>2</sub>Ph)<sub>3</sub> undergo slow thermal and rapid photochemical decomposition thereby explaining the complete absence of a thermal back reaction for DMF-photolyzed solutions.

In addition to the three solvents studied in detail the photochemistry of cis-Mo<sub>2</sub>Cl<sub>2</sub>(6-mhp)<sub>2</sub>(PMe<sub>2</sub>Ph)<sub>2</sub> ( $\lambda > 435$  nm) was examined in a number of other solvents. The photochemistry of cis-Mo<sub>2</sub>Cl<sub>2</sub>(6-mhp)<sub>2</sub>(PMe<sub>2</sub>Ph)<sub>2</sub> in toluene is identical to that observed in benzene. Photolysis in pyridine results in spectral changes that are very similar to those observed for DMF. The photochemical behavior of cis-Mo<sub>2</sub>Cl<sub>2</sub>(6-mhp)<sub>2</sub>(PMe<sub>2</sub>Ph)<sub>2</sub> in acetone, acetonitrile and benzonitrile is closely related that found in THF. Dichloromethane solutions of the complex photoreact much slower than any of the other solvents studied.

The photochemistry of *cis*-Mo<sub>2</sub>Cl<sub>2</sub>(6-mhp)<sub>2</sub>(PR<sub>3</sub>)<sub>2</sub> complexes in homogeneous solution is ligand redistribution to give Mo<sub>2</sub>Cl<sub>3</sub>(6-mhp)(PR<sub>3</sub>)<sub>3</sub> and Mo<sub>2</sub>Cl(6-mhp)<sub>3</sub>(PR<sub>3</sub>) as major photoproducts. Depending on the solvent, the overall photochemistry of the system varies owing to different stabilities of the mono- and tri-substituted mhp species. Figure 3.12 summarizes the overall photoreactivity. The mono- and tri-substituted photoproducts are stable in THF solutions and they back react in the dark over hours to produce the red parent complex of *cis*-Mo<sub>2</sub>Cl<sub>2</sub>(6-mhp)<sub>2</sub>(PR<sub>3</sub>)<sub>2</sub>. The overall chemical yield for each of the photoproducts in THF is 45(±10)%. This is not the case in DMF solutions where the monosubstituted mhp product is thermally and photochemically unstable.



Figure 3.12 Summary of the overall photoreactivity of cis-Mo<sub>2</sub>Cl<sub>2</sub>(6-mhp)<sub>2</sub>(PMe<sub>2</sub>Ph)<sub>2</sub> in benzene, THF and DMF.

Thus only the orange solution of Mo<sub>2</sub>Cl(6-mhp)<sub>3</sub>(PR<sub>3</sub>) is obtained for photolysis reactions performed in DMF. The facile decomposition of the monosubstituted complex circumvents its reaction with the tri-substituted complex to regenerate starting complex. Conversely, in benzene, the tri-substituted product undergoes a secondary photoreaction and only the purple solution of Mo<sub>2</sub>Cl<sub>3</sub>(6-mhp)(PR<sub>3</sub>)<sub>3</sub> is obtained. Because the ensuing photoreaction of Mo<sub>2</sub>Cl(6-mhp)<sub>3</sub>(PR<sub>3</sub>) is slow, a partial back reaction to *cis*-Mo<sub>2</sub>Cl<sub>2</sub>(6-mhp)<sub>2</sub>(PR<sub>3</sub>)<sub>2</sub> is observed over days. The determination of chemical yields from the photolysis spectra of DMF and benzene solutions are compromised by the presence of absorption contributions from the decomposition products.

The wavelength dependence of the quantum yield shows that the reaction is efficiently promoted by  $\lambda_{\rm exc}$  < 366 nm. Specifically,  $\Phi_{\rm p}$  appears to track the absorption profile of the 300 nm absorption band, which is in the region for  $\sigma_{\rm MP} \to \delta^*$  LMCT transitions of molybdenum-halide M<sup>4</sup>-M complexes. The photochemistry is appreciably maintained at 366 nm because the excitation wavelength clearly lies within the low energy tail of this intense near-UV transition. Photoreactivity from the LMCT excited state is also consistent with the excitation spectrum of cis-Mo<sub>2</sub>Cl<sub>2</sub>(6-mhp)<sub>2</sub>(PMe<sub>2</sub>Ph)<sub>2</sub> in hydrocarbon solvent. The intensity of the excitation profile is attenuated in the 325-400 nm range and is negligible at wavelengths coincident with the  $\sigma_{\rm MP} \to \delta^*$  LMCT transition. The higher energy transition centered at 280 nm is consistent with a mhp-localized  $\pi \to \pi^*$  transition for cis-Mo<sub>2</sub>Cl<sub>2</sub>(6-mhp)<sub>2</sub>(PR<sub>3</sub>)<sub>2</sub>, as it is energetically coincident with this transition in the Mo<sub>2</sub>(mhp)<sub>4</sub> complex. The photochemical studies discussed in this Chapter did not include this spectral

region. This type of behavior implies that a unimolecular photoreaction is a significant process for the high energy excited states of these complexes. It is noteworthy that the luminescence excitation and absorption spectra are identical for excitation wavelengths as short as 220 nm for hydrocarbon solutions of  $Mo_2X_4L_4$  complexes,  $^{98}$  which are photoinert under these conditions. The photochemistry reported here is consistent with a LMCT parentage to the extent that a  $\sigma_{MP} \rightarrow \delta^*$  excitation would lead to a weakening of the metal-ligand bonds as the formal oxidation state of the metal is reduced. The photoreaction quantum yield decreases significantly as the excitation wavelength is moved into the visible spectral region. A low photoreaction quantum yield is observed for wavelengths coincident with the  $\delta \rightarrow \delta^*$  transition. Presumably, the photoreaction proceeds inefficiently with excitation of the metal-localized excited states.

The loss of mhp from the metal core is reflected in the solvent dependence of the photolysis quantum yields. Dissociation of mhp leads to ionic intermediates that will be stabilized by increasingly polar solvents. This is born out by the monotonic increase of  $\Phi_p$  at a given wavelength along the series  $C_6H_6 < THF < DMF$  (see Table 3.3). Interestingly, the emission quantum yields and lifetimes do not show a parallel trend. Inasmuch as photodissociation of a mhp ligand is a single contributing factor to the overall nonradiative decay pathway for cis-Mo<sub>2</sub>Cl<sub>2</sub>(6-mhp)<sub>2</sub>(PR<sub>3</sub>)<sub>2</sub> complexes, the inability to correlate  $\Phi_p$  with  $\Phi_e$  (or  $\tau_0$ ) indicates that the overall nonradiative decay is influenced by other factors in addition to ligand dissociation from the excited state. Moreover, mhp loss may be more complicated than direct excited state dissociation, as

evidenced by the Cl<sup>-</sup> enhancement of the observed photoreactivity. A primary photoprocess involving Cl<sup>-</sup> dissociation can in principle catalyze the dissociation of the mhp ligand.

#### **D.** Conclusions

The results described here suggest that any potential photochemistry of these complexes to yield new products such as Mo<sup>III</sup><sub>2</sub> W-frame complexes will be circumvented by photosubstitution of the bidentate mhp ligands. This obstacle might be overcome by the substitution of the mhp ligands with tetradentate ligands that enforce the same cis conformation. Several examples of quadruply bonded dimolybdenum complexes that contain tetradentate ligands in the desired cis conformation have been reported recently in the literature.<sup>99</sup>-<sup>101</sup> Cotton and coworkers reported that the complex Mo<sub>2</sub>Cl<sub>4</sub>(eLTTP) (eLTTP = Et<sub>2</sub>PCH<sub>2</sub>CH<sub>2</sub>P(Ph)CH<sub>2</sub>P(Ph)CH<sub>2</sub>CH<sub>2</sub>PEt<sub>2</sub>) is formed upon reaction of Mo<sub>2</sub>(O<sub>2</sub>CCF<sub>3</sub>)<sub>4</sub> with 1 equiv of meso-eLTTP and excess Me<sub>3</sub>SiCl. The spectroscopic data are consistent with the structure shown in Figure 3.13a. This complex possesses the desired arrangement of ligands however, oxidation by CH<sub>2</sub>Cl<sub>2</sub> results in the production of Mo<sub>2</sub>Cl<sub>6</sub>(eLTTP) which has an ESBO structure rather than the desired W-frame geometry.<sup>99</sup> The flexibility of this bischelating/single-bridging ligand apparently permits rearrangement upon oxidation. The flexibility of the tetradentate ligand should not be a problem in the case of the Schiff base complex Mo<sub>2</sub>(N<sub>4</sub>)(O<sub>2</sub>CCH<sub>3</sub>)<sub>2</sub> where N<sub>4</sub> is 5,7,12,14tetramethyldibenzo-[b,i][1,4,8,11]tetraazocyclotetradecine, 100 the structure of this

$$\begin{array}{c|c} Et_2P & Et_2P \\ Ph & P & P \\ \hline \\ CI & CI \\ \hline \\ CI & CI \\ \end{array}$$

Figure 3.13 Two examples of quadruply bonded dimolybdenum complexes with tetradentate ligands that enforce a cis conformation of bridging ligands: (a)  $Mo_2Cl_4(eLTTP)$  (ref. 99) and (b)  $Mo_2(N_4)(O_2CCH_3)_2$  (ref. 100).

complex is shown in Figure 3.13b. Several unsuccessful attempts were made to synthesize Mo<sub>2</sub>(N<sub>4</sub>)Cl<sub>2</sub>(PR<sub>3</sub>)<sub>2</sub>. The treatment of Mo<sub>2</sub>(N<sub>4</sub>)(O<sub>2</sub>CCH<sub>3</sub>)<sub>2</sub> with trimethylsiyl chloride and excess tertiary phosphine in an effort to replace the two acetate ligands with two chloride and two phosphine ligands resulted instead in the decomposition of Mo<sub>2</sub>(N<sub>4</sub>)(O<sub>2</sub>CCH<sub>3</sub>)<sub>2</sub>. The reaction of Mo<sub>2</sub>X<sub>4</sub>(PMe<sub>3</sub>)<sub>4</sub> (X= Cl, Br) with N<sub>4</sub> in the presence of the noncoordinating base DBU (DBU = 1,8-diazabicyclo[5.4.0]undec-7-ene) did not produce any reaction. The addition of one equivalent of doubly deprotonated N<sub>4</sub>, two equiv of Br<sup>-</sup> and two equiv of PMe<sub>3</sub> to Mo<sub>2</sub>(CH<sub>3</sub>CN)<sub>10</sub> produced mainly Mo<sub>2</sub>Br<sub>4</sub>(PMe<sub>3</sub>)<sub>4</sub> and unreacted N<sub>4</sub>. Despite the failure of initial attempts to synthesize Mo<sub>2</sub>(N<sub>4</sub>)Cl<sub>2</sub>(PR<sub>3</sub>)<sub>2</sub>, the idea of producing complexes with a W-frame geometry by the two-electron oxidation of M<sup>4</sup>M complexes that contain a tetradentate ligand enforcing a cis conformation of bridging ligands is still, in principle, a good one.

Alternatively, the desired Mo<sup>III</sup><sub>2</sub> W-frame complex might be obtained by thermally oxidizing *cis*-Mo<sub>2</sub>Cl<sub>2</sub>(6-mhp)<sub>2</sub>(PR<sub>3</sub>)<sub>2</sub> with X<sub>2</sub>. However, as the photochemical studies described in this Chapter suggest, the photochemistry of the oxidized products of these species would likely be complicated by ligand substitution chemistry. In fact, attempts to thermally oxidize *cis*-Mo<sub>2</sub>Cl<sub>2</sub>(6-mhp)<sub>2</sub>(PMe<sub>2</sub>Ph)<sub>2</sub> with iodobenzene dichloride, under ambient lighting conditions, resulted in the production significant quantities of ligand substitution products. The next two chapters describe successful strategies for engendering photoinduced reductive elimination from bimetallic complexes.

### **CHAPTER 4**

# PHOTOINDUCED REDUCTIVE ELIMINATION FROM EDGE-SHARING BIOCTAHEDRAL COMPLEXES Mo<sub>2</sub>X<sub>6</sub>(dppm)<sub>2</sub>

## A. Background

The results described in Chapter 3 suggest that any potential photochemical oxidation of cis-Mo<sub>2</sub>Cl<sub>2</sub>(6-mhp)<sub>2</sub>(PR<sub>3</sub>)<sub>2</sub> complexes to produce Mo<sub>2</sub><sup>III</sup> W-frame products will be circumvented by the photolability of the bidentate mhp ligands. The difficulties experienced in obtaining dimolybdenum(III) W-frames led to a search for multiply bonded dimolybdenum(III) complexes with other structure types that might engender photoinduced reductive elimination. As mentioned in Chapter 3, an important consideration in photoinduced reductive elimination chemistry is the ligand-ligand distances. The two most common geometries for dimolybdenum(III) complexes are ESBO and FSBO. Figure 3.3 shows representative internuclear distances for ligands in ESBO and FSBO complexes. The internuclear distances in FSBOs are relatively large, therefore, it is difficult to imagine reductive elimination from these complexes occurring via a concerted process. ESBOs are more promising candidates because the internuclear distance between adjacent

terminal ligands is significantly shorter in ESBOs than it is in FSBOs. Specifically, the internuclear distances between adjacent terminal X ligands in the  $Mo_2X_6(dppm)_2$  ESBO complexes (Cl···Cl = 3.22 Å, Br···Br = 3.37 Å and I···I = 3.66 Å)<sup>68,102</sup> are all significantly smaller than the sum of van der Waals radii for two X atoms (Cl = 3.62 Å, Br = 3.90 Å and I = 4.30 Å). These internuclear distances are sufficiently short that reductive elimination from  $Mo_2X_6(dppm)_2$  complexes could, in principle, occur.

The metal-metal bonding in ESBO complexes has been the subject of several studies. The simplest picture of the metal-metal bonding in these complexes 102,104 is provided by noting that within each of the two local octahedra that combine to form the ESBO there are three d orbitals (t<sub>2g</sub> orbitals) that do not possess suitable lobal structure for participation in metal-ligand of bonding. These three d-orbitals have the proper symmetry to form one  $\sigma$  bond, one  $\pi$  bond, and one  $\delta$  bond. Purely on the basis of the differing extents of overlap, the relative energies of the orbitals are expected to increase in the following order  $\sigma << \pi < \delta < \delta^* < \pi^* < \sigma^*$ , as shown in Figure 4.1. If this simple picture were reliable, a bond order of three would be predicted for d<sup>3</sup>—d<sup>3</sup> dimolybdenum ESBOs on the basis of the  $\sigma^2\pi^2\delta^2$  electronic configuration. However, as Hoffmann<sup>105</sup> et al first reported, interactions between the pure metal orbitals and ligand based orbitals may render such a simple picture, and hence the predictions made from it, incorrect. The  $\delta$ -bonding combination of metal orbitals and the  $b_{3g}$   $\pi$  orbitals on the  $\mu$ -Cl ligands of  $M_2Cl_6(PP)_2$  (M = Nb, Ta, Mo, Re and Ru; PP = dppm and dmpm; dmpm = dimethylphosphinomethane) complexes, are of proper symmetry to interact. Because there is no combination

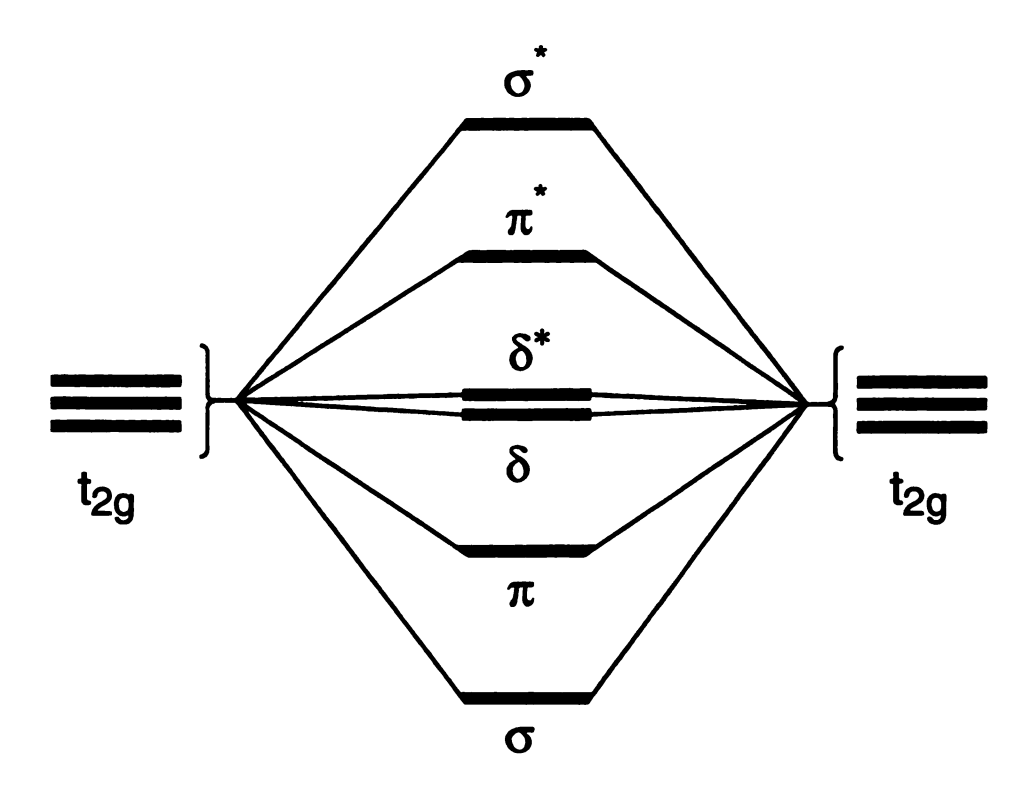


Figure 4.1 Qualitative molecular orbital diagram for ESBO complexes.

of ligand orbitals that has the same symmetry as the  $\delta^*$  anti-bonding orbital (a<sub>u</sub>), the energy of the  $\delta$  orbital may be raised above that on the  $\delta^*$  orbital to give an energy ordering of:  $\sigma \ll \pi < \delta^* < \delta < \pi^* \ll \sigma^*$ . Cotton and coworkers have addressed the question of the  $\delta/\delta^*$  ordering experimentally  $^{102,106}$  by examining how the M-M distance changes with the d-electron count on the metal centers of a homologous series of compounds. The M-M distance in the M<sub>2</sub>Cl<sub>6</sub>(PP)<sub>2</sub> complexes varies with the number of d electrons contributed by each metal in a manner that is consistent with  $\delta > \delta^*$ . The results of Fenske-Hall calculations <sup>104</sup> carried out on Mo<sub>2</sub>(µ-SH)<sub>2</sub>(SH<sub>2</sub>)<sub>4</sub> for a range of Mo-Mo distances show that the two levels are close together and that at longer Mo-Mo distances  $\delta^*$  lies below δ. An SCF-Xα-SW calculation<sup>104</sup> carried out on the same molecule using an Mo-Mo distance of 2.68 Å also places the two levels close together, however,  $\delta$  is below  $\delta^*$ . The two levels are so close in energy that it is unlikely that either calculation can be trusted to provide the correct ordering. Regardless of the exact ordering, both the  $\delta$  and  $\delta^*$  orbitals are virtually nonbonding and the Mo-Mo bond order in the d<sup>3</sup>—d<sup>3</sup> ESBOs is essentially two. Temperature dependent magnetic susceptibility measurements confirm that the energy difference between  $\delta^*$  and  $\delta$  is relatively small. The singlet-triplet  $(\sigma^2 \pi^2 \delta^{*2} / \sigma^2 \pi^2 \delta^* \delta)$ separations range from 1100-1400 cm<sup>-1</sup> for the Mo<sub>2</sub>X<sub>6</sub>(dppm)<sub>2</sub> complexes.<sup>68</sup>

Unfortunately, there have been few spectroscopic studies to complement the theoretical model developed for ESBO complexes. The UV-vis spectra of Mo<sub>2</sub>X<sub>6</sub>(dppm)<sub>2</sub> complexes<sup>68</sup> were reported by Cotton and coworkers. Yet, the spectra are complicated and no effort was made to assign the transitions. On the

basis of the qualitative molecular orbital diagram, electronic transitions such as  $\pi \to \delta^*$ ,  $\pi \to \delta$  and  $\delta^* \to \pi^*$  are predicted for ESBO complexes.

ESBO complexes are formed upon either thermal<sup>68,104,106,107</sup> or photochemical<sup>55,56</sup> oxidative addition to quadruply bonded metal-metal complexes with  $D_{2h}$  symmetry,  $M_2X_4(PP)_2$  (M= Mo, W, X= halide, and PP = bridging phosphine). The photochemical oxidative addition of a substrate (YZ) to a M<sup>4</sup>M complex, with D<sub>2h</sub> symmetry, to yield an ESBO product is illustrated in Figure 3.1a. The reduction of Mo<sub>2</sub>X<sub>6</sub>(dppm)<sub>2</sub> complexes<sup>68</sup> is consistent with formation of simple quadruply bonded species. Each of the three complexes displays one or more redox process(es), but the majority are irreversible, presumably because they lead to qualitative changes in structure. The only electrochemical process observed for Mo<sub>2</sub>Cl<sub>6</sub>(dppm)<sub>2</sub> is an irreversible oneelectron reduction. In contrast, Mo<sub>2</sub>I<sub>6</sub>(dppm)<sub>2</sub> has four irreversible processes, two oxidation and two reduction. The only complex in the series to show reversible electrochemical behavior is Mo<sub>2</sub>Br<sub>6</sub>(dppm)<sub>2</sub>; the one-electron reduction process is reversible, however, the second reduction is irreversible. On this basis, if the reduction of the metal core can be photochemically initiated by MMCT or LMCT excitation, then the potential exists for reductive elimination of halide. Accordingly, this Chapter focuses on photoinduced reductive elimination from Mo<sub>2</sub>X<sub>6</sub>(dppm)<sub>2</sub> ESBO complexes.

The selection of  $Mo_2X_6(dppm)_2$  (X = Cl, Br, I) complexes for photochemical study was based on several factors. Whereas, oxidative addition to both quadruply bonded dimolybdenum and ditungsten (D<sub>2h</sub>) complexes results in ESBO products, the dimolybdenum congeners should be more

favorable toward reductive elimination because Mo is more easily reduced than W. In addition, a homologous series,  $Mo_2X_6(dppm)_2$ , can be complexes synthesized by oxidative addition of the appropriate halogen to  $Mo_2X_4(dppm)_2$ . Finally, the expected products of two-electron reductive elimination,  $Mo_2X_4(dppm)_2$ , are well characterized,  $^{69-71}$  providing a solid foundation on which to build a photochemical investigation. One major limitation of the  $Mo_2X_6(dppm)_2$  complexes is their low solubility in most common solvents.

## **B. Photochemistry**

## 1. $Mo_2I_6(dppm)_2$

The first member of the  $Mo_2X_6(dppm)_2$  series studied photochemically was  $Mo_2I_6(dppm)_2$ .  $Mo_2I_6(dppm)_2$  was chosen on the basis of Mo-X bond strengths. The weakest bond, Mo-I, should be the easiest to cleave. Benzene solutions of  $Mo_2I_6(dppm)_2$  and the radical trap 2,3-dimethyl-1,3-butadiene (DMB), are indefinitely stable at 45 °C, a slow decomposition reaction occurs at 60 °C, in the absence of light. Irradiation with  $\lambda > 435$  nm, of benzene solutions of  $Mo_2I_6(dppm)_2$  and DMB, as monitored by UV-vis spectroscopy, resulted in a decrease in the intensity of bands due to the starting material,  $\lambda_{max} = 550(sh)$ , 525(sh), 460 and 420 nm, and a concomitant increase in the intensity of a band at 440 nm. The lowest energy transition, ~ 710 nm, exhibits very little change during the course of photolysis. Isobestic points were not maintained during the

reaction. The photochemistry goes to completion in approximately 2 days. No appreciable photochemical reaction is observed if the irradiation is carried out in the absence of DMB. Photolysis of benzene solutions of  $Mo_2I_6(dppm)_2$  and DMB with  $\lambda > 530$  nm resulted in a slow partial conversion; no photochemistry occurs when irradiation is carried out using a 630 nm high energy cutoff filter. There were no changes observed in the absorption spectrum of photolyzed solutions stored at room temperature, in the dark indicating that the photoproduct does not undergo a thermal back reaction. The photoproduct was identified by the preparation of the authentic complex. The absorption spectrum of the photoproduct ( $\lambda_{max} = 713$ , 440 nm) is identical to that of  $Mo_2I_4(dppm)_2$ , which was prepared by literature methods ( $\lambda_{max} = 713$ , 440 nm). The  $^{31}P\{^{1}H\}$  NMR spectrum of the isolated photoproduct,  $\delta = 13.11$  (s) ppm, is consistent with that of  $Mo_2I_4(dppm)_2$  (12.70 ppm, CDCl<sub>3</sub>). Figure 4.2 shows the absorption spectra of the starting material, the photoproduct and independently prepared  $Mo_2I_4(dppm)_2$ .

The photoreaction was also studied in THF. Irradiation of THF solutions of  $Mo_2I_6(dppm)_2$  and DMB  $\lambda > 335$  nm, also resulted in the production of  $Mo_2I_4(dppm)_2$ . However, the low solubility of  $Mo_2I_6(dppm)_2$  in THF precluded further photochemical study in this solvent.

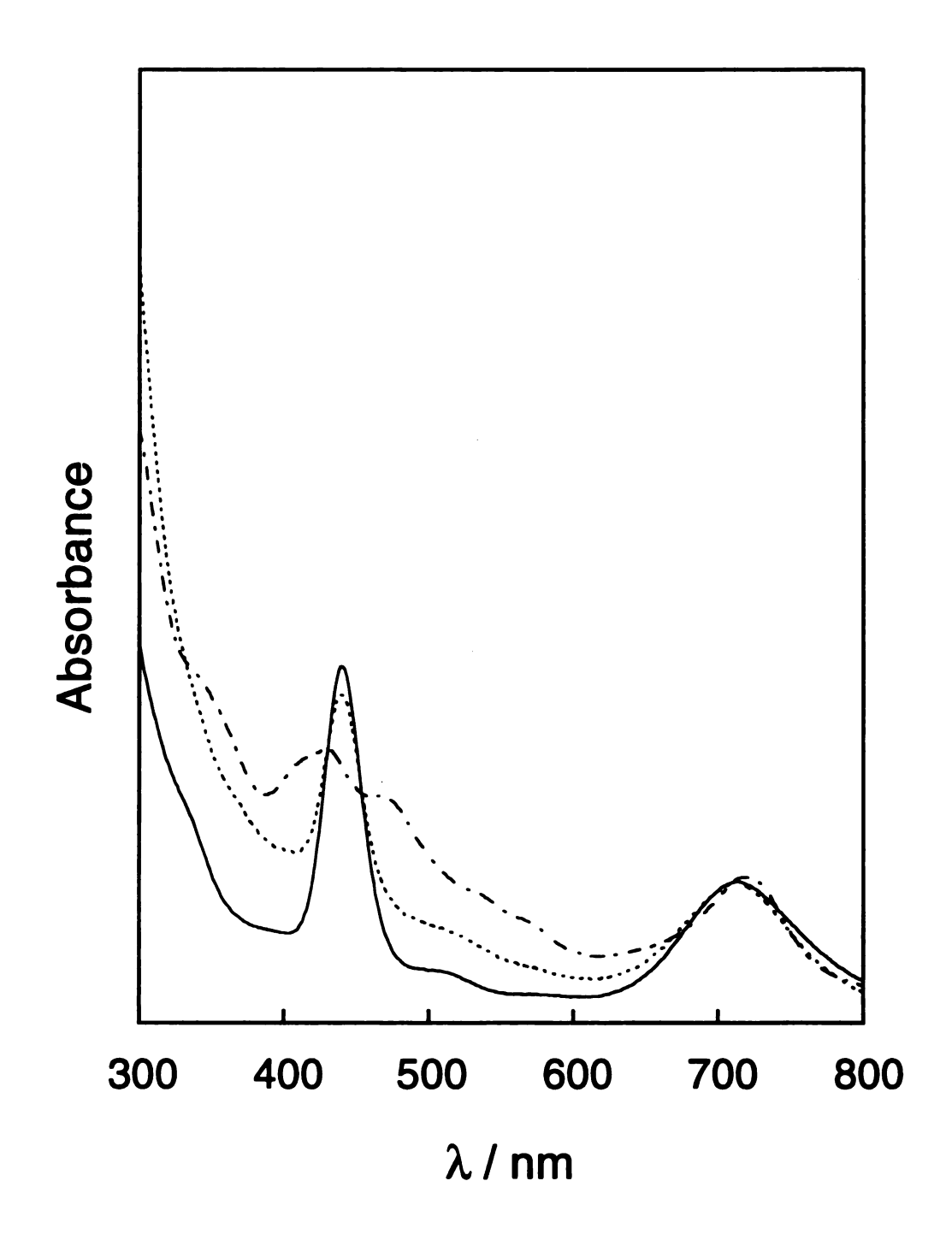


Figure 4.2 Electronic absorption spectra of (a)  $Mo_2I_6(dppm)_2$ ,  $(-\cdot -)$  (b) product from the irradiation ( $\lambda_{exc} > 435$  nm) of benzene solutions of  $Mo_2I_6(dppm)_2$  with DMB (—) and (c) independently prepared  $Mo_2I_4(dppm)_2$ , (----).

### 2. $Mo_2Br_6(dppm)_2$

In the absence of light, DMF solutions of Mo<sub>2</sub>Br<sub>6</sub>(dppm)<sub>2</sub> and DMB are indefinitely stable at room temperature, however, heating these solutions to 80 °C produced decomposition products that were not characterized. Photolysis, as followed by absorption spectroscopy, of DMF solutions of Mo<sub>2</sub>Br<sub>6</sub>(dppm)<sub>2</sub> and DMB,  $\lambda > 335$  nm, resulted in the disappearance of bands due to the starting material ( $\lambda_{max} = 590, 427, 326 \text{ nm}$ ) and the growth of bands at 457 nm and 612 nm. There were no further changes in the absorption spectra after 26 h of photolysis. Irradiation of solutions of Mo<sub>2</sub>Br<sub>6</sub>(dppm)<sub>2</sub> and DMB with wavelengths higher than 435 nm does not result in a photochemical reaction. The disappearance quantum yield ( $\lambda = 366$  nm) is small, an upper limit for the value is  $1 \times 10^{-4}$ . The photoreduction of Mo<sub>2</sub>Br<sub>6</sub>(dppm)<sub>2</sub> in DMF proceeds at approximately the same rate in the absence of the trap. The identity of the photoproduct was established by comparison of its spectral features with those of a genuine sample of Mo<sub>2</sub>Br<sub>4</sub>(dppm)<sub>2</sub>.<sup>70</sup> The <sup>31</sup>P{<sup>1</sup>H} NMR spectrum of the isolated photoproduct,  $\delta = 14.47$  (s) ppm, is virtually identical to that of Mo<sub>2</sub>Br<sub>4</sub>(dppm)<sub>2</sub>, 14.45 ppm in CDCl<sub>3</sub>. The absorption spectrum of the photoproduct, when the reaction was carried out in the absence of DMB,  $(\lambda_{max})$ = 463, 619 nm) is virtually identical to that of  $Mo_2Br_4(dppm)_2$  ( $\lambda_{max}$  = 465, 620 nm). Figure 4.3 shows the spectral changes associated with the photolysis of DMF solutions of  $Mo_2Br_6(dppm)_2$ ,  $\lambda > 335$  nm, in the absence of DMB and the absorption spectrum independently of prepared  $Mo_2Br_4(dppm)_2$ .

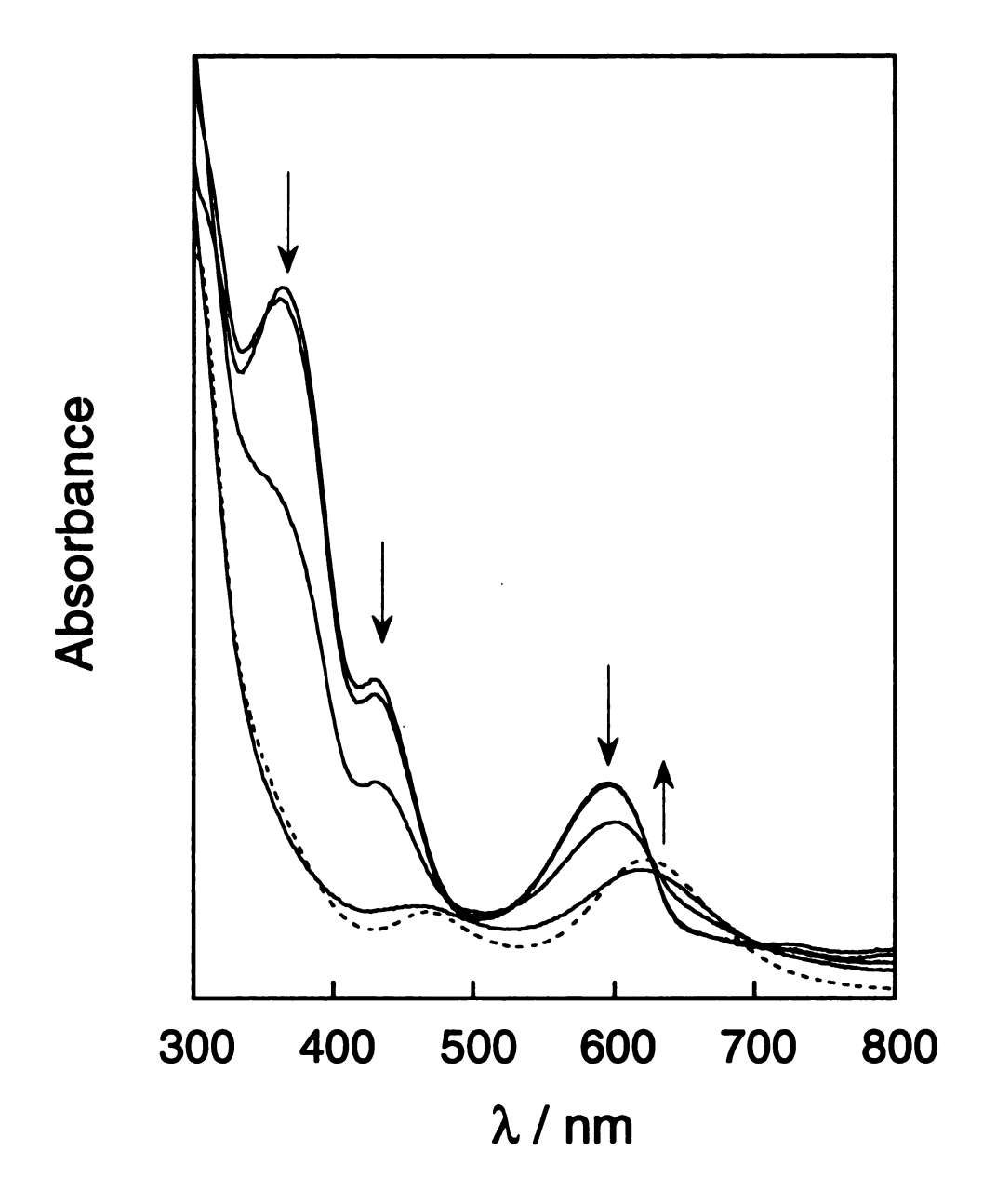


Figure 4.3 Electronic absorption spectral changes during the photolysis  $(\lambda_{\rm exc} > 335 \text{ nm})$  of  $Mo_2Br_6(dppm)_2$  in deoxygenated DMF at 20 °C. Spectra were recorded after 90 m, 3, 6, 16 h. The absorption spectrum of independently prepared  $Mo_2Br_4(dppm)_2$  is shown as a dashed line for comparison.

The photoreductive elimination chemistry was also investigated in THF. The Irradiation,  $\lambda > 335\,$  nm, of THF solutions of Mo<sub>2</sub>Br<sub>6</sub>(dppm)<sub>2</sub> and DMB results in similar photochemistry to that observed in DMF, however, the low solubility of Mo<sub>2</sub>Br<sub>6</sub>(dppm)<sub>2</sub> in THF makes any further studies in this solvent impossible.

## 3. Mo<sub>2</sub>Cl<sub>6</sub>(dppm)<sub>2</sub>

Although solutions of Mo<sub>2</sub>Cl<sub>6</sub>(dppm)<sub>2</sub> and DMB are indefinitely stable at room temperature and below (decomposition is observed when these solutions are heated to 80 °C) in the absence of light, excitation with  $\lambda > 335$  nm results in the spectral changes shown in Figure 4.4. The UV-vis spectrum of Mo<sub>2</sub>Cl<sub>4</sub>(dppm)<sub>2</sub> is shown, for comparison, as a dashed line overlaid on the spectra of the photoreaction. The <sup>31</sup>P{<sup>1</sup>H} NMR spectrum of the isolated product consisted of a singlet at 15.27 ppm which is in excellent agreement with that of the independently prepared Mo<sub>2</sub>Cl<sub>4</sub>(dppm)<sub>2</sub> 15.29 ppm (CDCl<sub>3</sub>).<sup>69</sup> The  $\lambda_{\text{max}}$  of the lowest energy band in the photoproduct, 602 nm, is not coincident with the maximum for the  $\delta \rightarrow \delta^*$  peak of Mo<sub>2</sub>Cl<sub>4</sub>(dppm)<sub>2</sub>, 611 nm. In the absence of DMB, the photoreduction of Mo<sub>2</sub>Cl<sub>6</sub>(dppm)<sub>2</sub> ( $\lambda > 335$  nm, DMF) proceeds at a slower rate and has a lower chemical yield.

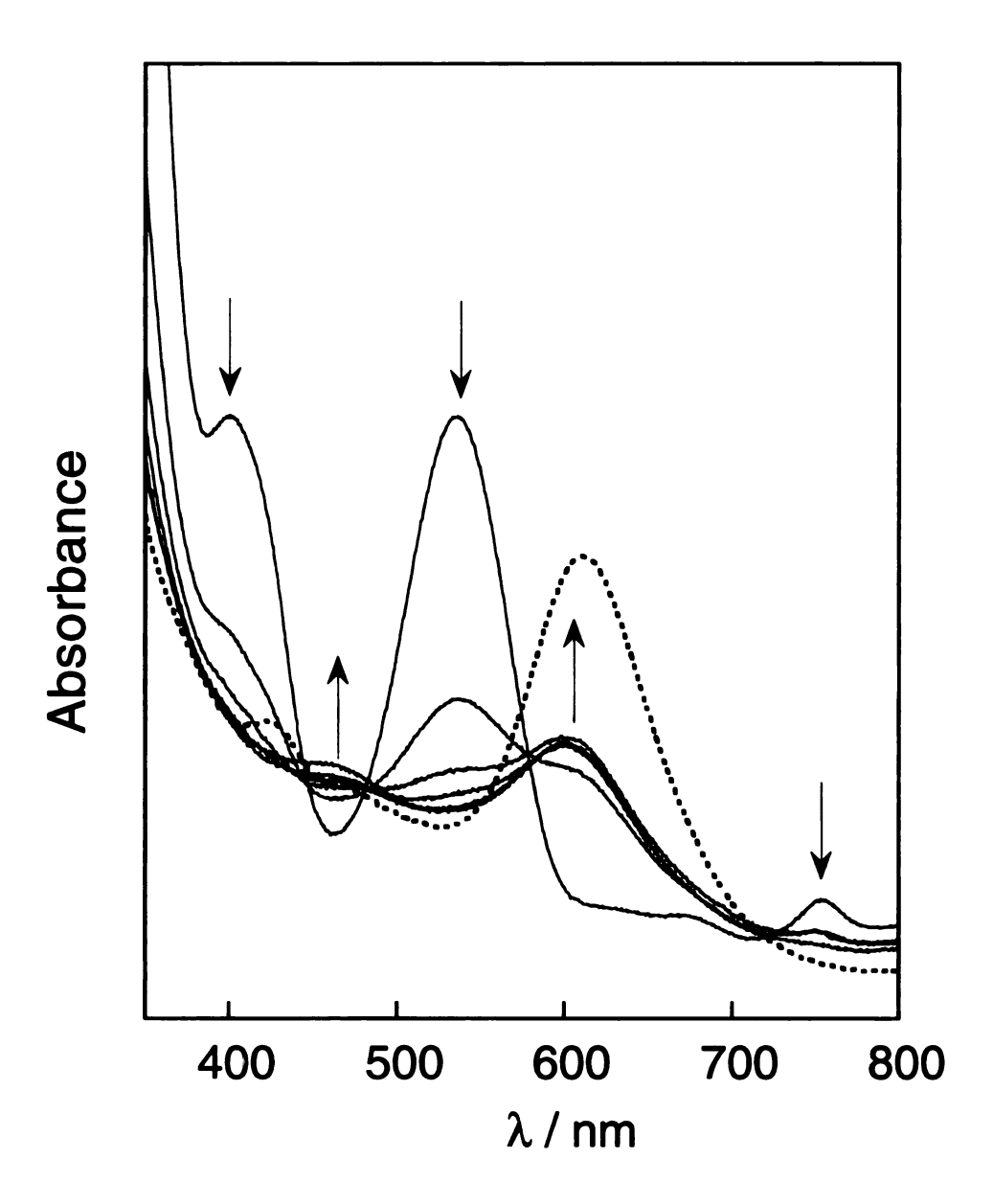


Figure 4.4 Electronic Absorption spectral changes during the photolysis  $(\lambda_{\rm exc} > 335 \text{ nm})$  of  $Mo_2Cl_6(dppm)_2$  with DMB in deoxygenated DMF at 20 °C. Spectra were recorded after 0, 4, 8, 13 and 19 h. The absorption spectrum of independently prepared  $Mo_2Cl_4(dppm)_2$  is shown as a dashed line for comparison.

#### C. Discussion and Conclusions

The photochemistry of Mo<sub>2</sub>X<sub>6</sub>(dppm)<sub>2</sub> complexes, in the presence of DMB trap, is two-electron reductive elimination to give the quadruply bonded Mo<sub>2</sub>X<sub>4</sub>(dppm)<sub>2</sub> complexes. The formation of a quadruply bonded metal-metal complex via photoinduced reductive elimination, while extremely rare is not without precedent. Chisholm and coworkers have previously reported the photoinduced reductive elimination of R<sup>\*</sup> from the axial positions of W<sub>2</sub>R<sub>2</sub>(O<sub>2</sub>CH)<sub>4</sub> to form the quadruply bonded ditungsten complex W<sub>2</sub>(O<sub>2</sub>CH)<sub>4</sub> (R = neopentyl, benzyl). The photoinduced two-electron reductive elimination chemistry reported here is significant in that it represents the first time a quadruply bonded metal-metal complex has been regenerated from a two-electron oxidation product with bioctahedral geometry. This result is important since the overwhelming majority of the M<sup>4</sup>-M two-electron oxidation products possess bioctahedral geometry.

This photochemistry is also noteworthy because two metal-halide bonds are broken in the reaction. As discussed previously, the strength of the metal-halide bond represents a significant obstacle to achieving two-electron reductive elimination. In this case, the energy of a photon was used to overcome the barrier to metal-halide elimination. Experimental and theoretical studies place Mo—Cl bond energy at approximately 75 kcal/mol. The fact that the photoreduction of Mo<sub>2</sub>Cl<sub>6</sub>(dppm)<sub>2</sub> and Mo<sub>2</sub>Br<sub>6</sub>(dppm)<sub>2</sub> requires higher energy light than the photoreduction of Mo<sub>2</sub>I<sub>6</sub>(dppm)<sub>2</sub> is in agreement with the fact that Mo–Cl and Mo–Br bonds are harder to break than a Mo–I bond. The

absorption spectra of Mo<sub>2</sub>Cl<sub>6</sub>(dppm)<sub>2</sub> photoreaction indicate that the reaction does not proceed to completion. The failure of the photoinduced reductive elimination reaction to go to completion in the case of Mo<sub>2</sub>Cl<sub>6</sub>(dppm)<sub>2</sub> may be due to the greater strength of the Mo-Cl bond, relative to Mo-Br and Mo-I. The product of Mo<sub>2</sub>I<sub>6</sub>(dppm)<sub>2</sub> photolysis has an absorption spectrum identical to that of Mo<sub>2</sub>I<sub>4</sub>(dppm)<sub>2</sub>, while the spectrum of Mo<sub>2</sub>Br<sub>4</sub>(dppm)<sub>2</sub> and the photoproduct of the Mo<sub>2</sub>Br<sub>6</sub>(dppm)<sub>2</sub> reaction, in the absence of DMB, differ only slightly. The determination of chemical yields from photolysis spectra of Mo<sub>2</sub>X<sub>6</sub>(dppm)<sub>2</sub> is compromised by the low solubility of these complexes and possibly by absorption contributions from the products of secondary reactions.

The absence of isobestic points in the absorption spectra of the photoreactions is likely due to one of several reasons. The inefficient trapping of  $X_2/X^*$  could have resulted in a secondary reaction involving the untrapped  $X_2/X^*$ . Alternatively, the  $Mo_2X_4(dppm)_2$  photoproducts might have undergone subsequent thermal or photochemical decomposition. The photoeliminated  $I_2/I^*$  is the most difficult of the halogens to trap with unsaturated hydrocarbons, such as DMB. The iodination of double bonds is slower than either chlorination or bromination. Under free radical conditions iodination occurs more easily. The change in free energy for the iodination of alkenes is usually small. Consequently, an equilibrium is established and incomplete conversion to the diiodide is typically observed. The observation that the photoreaction of  $Mo_2I_6(dppm)_2$  is the slowest of the three reactions, despite the fact that the  $Mo_-I$  bond is the weakest, and that the  $Mo_2I_6(dppm)_2$  photoreduction does not appear to proceed as cleanly as the other two reactions is consistent with the

trapping of  $I_2/I^{\bullet}$  being less efficient than  $Br_2/Br^{\bullet}$  or  $Cl_2/Cl^{\bullet}$ . The poor solubility of  $Mo_2X_6(dppm)_2$  might also have contributed to the lack of isobestic points.

This study leaves several unanswered questions. The first is whether or not the elimination of X<sub>2</sub> occurs via a concerted mechanism. The adjacent terminal halide ligands in the Mo<sub>2</sub>X<sub>6</sub>(dppm)<sub>2</sub> ESBOs are close enough to each other that a concerted mechanism is theoretically possible. However, no evidence has been obtained that either supports or refutes a concerted mechanism. The nature of the excited state(s) responsible for the photochemistry is also unknown. The absence of assignments for transitions in the absorption spectra of Mo<sub>2</sub>X<sub>6</sub>(dppm)<sub>2</sub> make exact determination of the photoactive state impossible. The lowest energy band can ruled out as the photoactive state because no reaction is observed when solutions of the complexes are irradiated with wavelengths coincident with this transition. An excited state with significant halide to metal charge transfer character would be favorable toward reductive elimination of halide ligands. As discussed previously, the photolytic cleavage of Pt-X in Pt<sub>2</sub>(pop)<sub>4</sub> $X_2^{4-}$  is promoted by the X  $\rightarrow$  Pt(III) charge transfer character of its  $(\sigma)^1(d\sigma^*)^1$  state.<sup>38</sup> LMCT excitation of PtCl<sub>6</sub><sup>2-</sup> likewise results in the cleavage of the Pt-Cl bond.<sup>39</sup> Another question yet to be answered definitely is from which positions on the ESBO are the two X ligands eliminated. This question could, in principle, be addressed by examining the products of photoinduced reductive elimination from a series of Mo<sub>2</sub>X<sub>4</sub>Y<sub>2</sub> (Y= halide different from X) complexes synthesized by Cotton and coworkers.<sup>68</sup> However, X-ray structural analysis of Mo<sub>2</sub>Cl<sub>4</sub>I<sub>2</sub>(dppm)<sub>2</sub> was unable to differentiate between Cl and I in the two crystallographically independent terminal halogen positions. The refinement suggested that each of two crystallographically independent positions are occupied by both Cl and I (each atom is assigned 0.5 occupancy).

Transient absorption spectroscopic studies of the  $Mo_2X_6(dppm)_2$  complexes will be essential to the further study of this photochemistry. (Initial attempts to obtain the transient absorption spectra of these complexes ( $\lambda_{exc}$  = 532 nm) yielded spectra with very poor signal-to-noise ratios.) Indeed, transient absorption spectroscopy has provided some clues about the converse reaction pathway, photooxidative addition to  $M_2X_4(PP)_4$  complexes. The  $M_2X_4(PP)_4$  complexes exhibit long-lived, non-luminescent transients whose absorption spectra are similar to those of  $M_2X_6(PP)_2$  ESBO complexes. This led to the proposal that the transient arises from chemical distortion to an edge-sharing intermediate like the one shown in Figure 1.9. Two-electron photooxidative addition of substrate occurs at the open coordination site on the reduced metal site. The photoinduced reductive elimination may initially result in a similar structure which subsequently rearranges to form the quadruply bonded metal-metal complex.

In spite of these unanswered questions, the two-electron photoinduced reductive elimination from  $Mo_2X_6(dppm)_2$  represents an important step in the development of a photocatayltic system based on  $M^{-4}$ M complexes. The next step is to try to generalize this reaction by attempting to eliminate different types of ligands from a variety of ESBOs. One possible choice of leaving group is an alkyl halide (RX). Photochemical oxidation of RX to  $W_2Cl_4(dppm)_2$  (R = CH<sub>3</sub>, CH<sub>3</sub>CH<sub>2</sub>; X = I) has been reported.<sup>56</sup> However, photooxidative addition of RX

to Mo<sub>2</sub>Cl<sub>4</sub>(dppm)<sub>2</sub> has not been observed. Therefore, it will be necessary to first synthesize a dimolybdenum ESBO complex, Mo<sub>2</sub>X<sub>4</sub>(R)(X), that contains an alkyl ligand. It may be possible to synthesize Mo<sub>2</sub>X<sub>5</sub>CH<sub>3</sub>(dppm)<sub>2</sub> by reacting Mo<sub>2</sub>X<sub>6</sub>(dppm)<sub>2</sub> with a methylating agent such as methyl lithium, methyl magnesium bromide or dimethyl zinc. The ultimate achievement would be to oxidatively add one species and reductively eliminate a different product. This capability would have important implications for both synthetic, it would lead to the formation of bonds between carbon and other elements, and energy conversion applications.

Although the internuclear distances between ligands in FSBOs are almost certainly too long to permit reductive elimination to occur via a concerted mechanism, it may be possible for these complexes to undergo reductive elimination reactions by a radical mechanism. A series of FSBOs, Mo<sub>2</sub>X<sub>6</sub>(PR<sub>3</sub>)<sub>3</sub> (X = Cl, Br, I; R<sub>3</sub>= Et<sub>3</sub> or Me<sub>2</sub>Ph)<sup>114-117</sup> have been synthesized and structurally characterized. As was the case with the ESBOs described in this Chapter, one of the biggest obstacles in carrying out photochemical studies on these FSBOs is there low solubility in most common solvents. Another significant limitation is lack of detailed spectroscopic studies of these complexes. Nevertheless, it would be interesting to see if FSBOs display photochemistry similar to that observed for their ESBO counterparts. The variances in metal-metal bonding between FSBOs and ESBOs may result in FSBOs having significantly different photochemistry.

## CHAPTER 5

# PHOTOINDUCED TWO-ELECTRON REDUCTIVE ELIMINATION OF HALOGEN FROM A SINGLY BONDED DIRHODIUM COMPLEX

# A. Background

The occurrence of authentic two-electron mixed-valence complexes is rare. The preparation of multielectron mixed valence species require that a ligand system stabilize metals in high and low oxidation states of different coordination geometries. The work of King and co-workers in the mid-1970s indicated that the bis(difluorophosphino)methylamine (dfpma) ligand was capable of stabilizing binuclear metal cores with formal oxidation states differing by two. The ability of the dfpma ligand to stabilize metal centers in a variety of oxidation states and coordination geometries is probably best exemplified by the dicobalt complex  $Co_2(dfpma)_3(CO)_2$ , which can be oxidized with  $Br_2$  to the  $Co_2(II,II)$  complex,  $Co_2(dfpma)_3(CO)_2^{2-.119}$  In this system, the dfpma ligand has stabilized the metal core through an overall six-electron change in the formal oxidation state.

Joel Dulebohn in the Nocera group was the first to show that the dfpma ligand could lead to the preparation of authentic two-electron complexes. 59,60 The Rh<sup>0</sup>Rh<sup>II</sup> complexes, Rh<sub>2</sub>X<sub>2</sub>(dfpma)<sub>2</sub>L (X = Cl, Br, I; L = PF<sub>3</sub>,  $\eta^1$ -dfpma), are obtained upon addition of dfpma to [RhX(PF<sub>3</sub>)<sub>2</sub>]<sub>2</sub>.<sup>59,61</sup> The overall reaction corresponds to an intramolecular disproportionation of the RhIRhI starting material to yield a Rh<sup>0</sup>Rh<sup>II</sup> mixed-valence complex. The two-electron mixedvalence character of the Rh<sup>0</sup>Rh<sup>II</sup> core is established unequivocally by the coordination geometry about the individual metal centers within the dirhodium complex. The inner coordination sphere of Rh<sub>2</sub>Br<sub>2</sub>(dfpma)<sub>3</sub>( $\eta^1$ -dfpma) is represented in Figure 5.1b. Pseudooctahedral and trigonal-bipyramidal geometries are structural benchmarks for metal-metal bonded rhodium in divalent and zero oxidation states, respectively. 120 The Rh<sup>0</sup> center, of the Rh<sup>0</sup>Rh<sup>II</sup>X<sub>2</sub>, complex can be oxidized by two electrons with X2 to give the symmetrical X<sub>2</sub>Rh<sup>II</sup>Rh<sup>II</sup>X<sub>2</sub> complex, Rh<sub>2</sub>(dfpma)<sub>3</sub>X<sub>4</sub>. Pseudooctahedral geometry is observed about both rhodium centers in Rh<sub>2</sub>(dfpma)<sub>3</sub>X<sub>4</sub>, the inner coordination sphere of Rh<sub>2</sub>(dfpma)<sub>3</sub>Br<sub>4</sub> is shown in Figure 5.1c. Conversely, the Rh<sup>II</sup> center in Rh<sup>0</sup>Rh<sup>II</sup>X<sub>2</sub> can be reduced by two electrons with cobaltacene, under a PF<sub>3</sub> atmosphere to produce the Rh<sup>0</sup>Rh<sup>0</sup> complex, Rh<sub>2</sub>(dfpma)<sub>3</sub>(PF<sub>3</sub>)<sub>2</sub>. Figure 5.1a shows the inner coordination sphere of Rh<sub>2</sub>(dfpma)<sub>3</sub>(PF<sub>3</sub>)<sub>2</sub>, which has a trigonal bipyramidal arrangement about both rhodium centers.

The ability of the ligand to stabilize two-electron mixed valence cores results from both electronic and structural origins. The remarkable flexibility of the dfpma ligand enables it to accommodate the coordination asymmetry that must exist for metals in formal oxidation states that differ by greater than 1. The

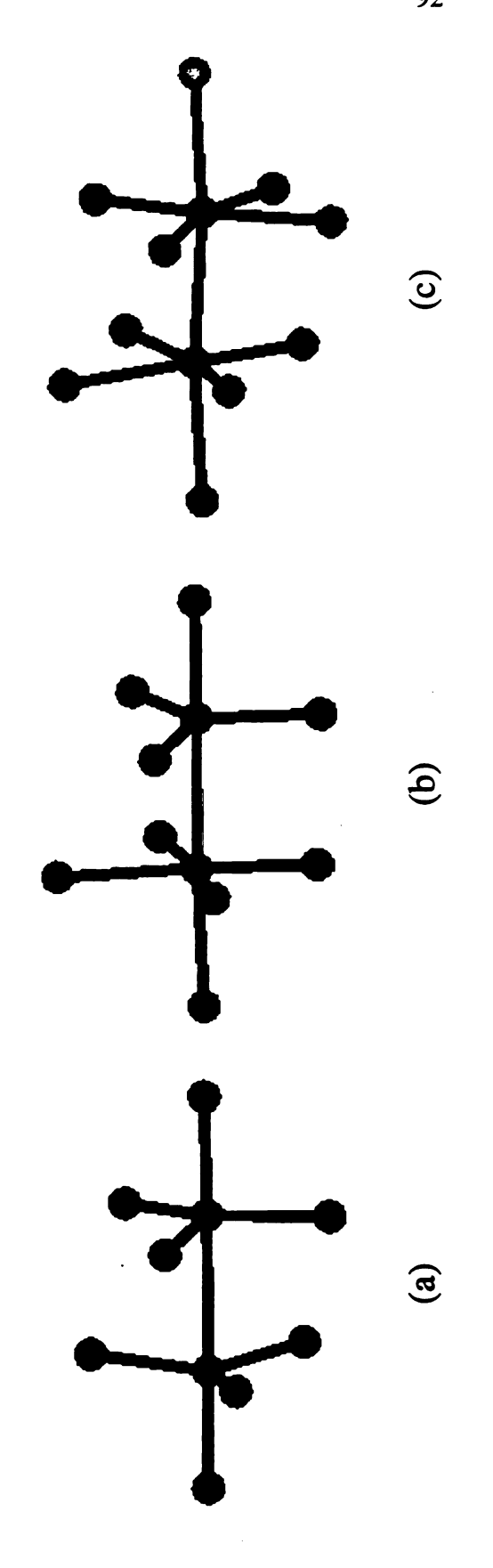


Figure 5.1 A skeletal view of the inner coordination spheres of (a) Rh<sub>2</sub>(dfpma)<sub>3</sub>(PF<sub>3</sub>)<sub>2</sub> (b) Rh<sub>2</sub>(dfpma)<sub>3</sub>Br<sub>2</sub>(η<sup>1</sup>-dfpma) (c) Rh<sub>2</sub>(dfpma)<sub>3</sub>Br<sub>4</sub>. (Ref. 60 and 61)

electronic properties of the ligand also play a crucial role in the stabilization of  $Rh^0Rh^{II}$  mixed-valence complex. Although the dfpma ligand is itself symmetrical, upon coordination to the dirhodium core, the lone pair electrons on the bridging nitrogen atom allow the ligand to function asymmetrically. The asymmetric behavior of dfpma ligand is manifested as disparate N—P bond lengths. Specifically, the three N—P bonds adjacent to P—Rh<sup>II</sup> are 0.03 Å shorter than the N—P bonds adjacent to the P—Rh<sup>0</sup>. This asymmetry in the ligand backbone can be explained in terms of differences in N  $\pi p$  donation to the P d $\pi$  orbitals. The shorter N—P(Rh<sup>II</sup>) distances are consistent with the donation of N lone pair electrons to the d $\pi$  orbitals of P, thereby decreasing the  $\pi$ -withdrawing ability of the PF<sub>2</sub> groups bonded to the Rh<sup>II</sup>. This feature serves to stabilize the high oxidation state of the Rh<sup>II</sup> center. The channeling away of N lone pair electron density from the PF<sub>2</sub> groups bonded to the Rh<sup>0</sup> center helps to maintain the strong d $\pi$  accepting properties of the PF<sub>2</sub> group and hence stabilize the Rh<sup>0</sup> center.

The qualitative molecular orbital diagrams for the series of dirhodium fluorophosphine complexes, shown in Figure 5.2, provide insight into the structural and spectroscopic properties of these complexes. The central panel of Figure 5.2 shows the qualitative molecular orbital diagram for  $Rh^0Rh^{II}X_2$  complex, which is constructed by interacting a  $C_{3v}$   $Rh^0P_4$  fragment with a  $C_{4v}$   $Rh^{II}P_3X_2$  fragment. Molecular orbital treatments  $^{121}$  suggest that in the  $d^9$   $Rh^0P_4$  fragment eight electrons reside in  $\pi(d_{xz}, d_{yz})$  and  $\delta(d_{xy}, d_{x^2-y^2})$  orbitals while the odd electron occupies the  $\sigma(d_{z^2})$  orbital. In the case of the  $d^7$   $Rh^{II}P_3X_2$  fragment, the  $d_{x^2-y^2}$  level is displaced to very high energy owing to the destabilizing  $\sigma^*$ 

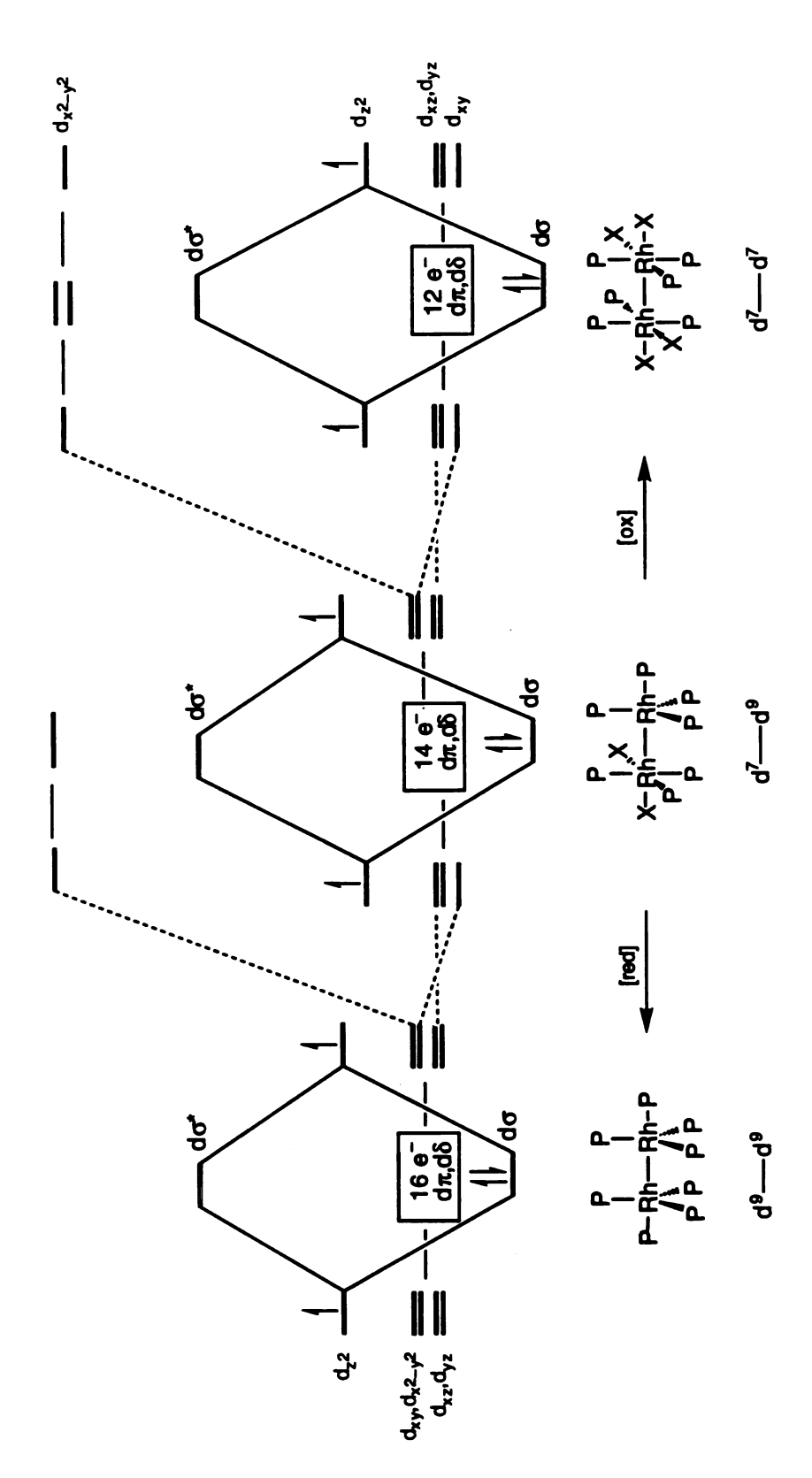


Figure 5.2 Qualitative energy level diagrams for Rh<sup>0</sup>Rh<sup>0</sup>, Rh<sup>0</sup>Rh<sup>II</sup>, and Rh<sup>II</sup>Rh<sup>II</sup> generated by the interaction of the appropriate C<sub>3</sub>v Rh<sup>0</sup>P<sub>4</sub> and C<sub>4</sub>v Rh<sup>II</sup>P<sub>3</sub>X<sub>2</sub> fragments.

interactions of the metal with the ligands in the equatorial plane. Accordingly, six electrons occupy the lower energy  $\pi(d_{xz}, d_{yz})$  and  $\delta(d_{xy})$  orbitals and the odd electron, as was the case for the Rh<sup>0</sup>P<sub>4</sub> fragment, resides in the  $\sigma(d_{2})$  orbital. The Rh—Rh single bond is formed by the pairing of the electrons contained in the spatially directed d<sub>7</sub>2 orbitals of the individual fragments. Therefore, the delectron count of the  $Rh^0Rh^{II}X_2$  complex is best represented as  $(d^6)d^1$ — $d^1(d^8)$ . The lowest energy excited states in Rh<sup>0</sup>Rh<sup>II</sup>X<sub>2</sub> complexes result from the promotion of an electron to the  $d\sigma^*$  orbital. The electronic consequences of the two-electron oxidation or reduction of Rh<sup>0</sup>Rh<sup>II</sup>X<sub>2</sub> are also illustrated in Figure 5.2. The d<sub>x2-y2</sub> orbital is emptied and destabilized upon the oxidation of the Rh<sup>0</sup> center of the mixed-valence complex, to give the X<sub>2</sub>Rh<sup>II</sup>Rh<sup>II</sup>X<sub>2</sub> product. Conversely, upon the reduction of the Rh<sup>II</sup> center, to form the Rh<sup>0</sup>Rh<sup>0</sup> complex. the d<sub>x</sub>2<sub>-y</sub>2 orbital is occupied and stabilized. Consequently, the electronic structures of the  $d^7$ — $d^7$  [( $d^6$ ) $d^1$ — $d^1$ ( $d^6$ )] and  $d^9$ — $d^9$  [( $d^8$ ) $d^1$ — $d^1$ ( $d^8$ )] complexes differ only slightly from that of the d<sup>7</sup>—d<sup>9</sup> [(d<sup>6</sup>)d<sup>1</sup>—d<sup>1</sup>(d<sup>8</sup>)] complex, with lowest energy transitions arising from the population of the  $d\sigma^*$  orbital.

The absorption and luminescence spectroscopy of the dirhodium fluorophosphine complexes are in accordance with this simple electronic structure model. The band shapes and energy trends of the absorption profile observed for the dirhodium fluorophosphine complexes are characteristic of complexes possessing an electronic structure dominated by excited states with dσ\* parentage. The absorption and luminescence spectra vary little across the Rh<sup>0</sup>Rh<sup>0</sup>, Rh<sup>0</sup>Rh<sup>II</sup>X<sub>2</sub> and Rh<sup>II</sup>Rh<sup>II</sup>X<sub>4</sub> series. As suggested by the molecular orbital diagram in Figure 5.2, the higher energy absorption bands correlate to states

arising from promotion of an electron to the  $d\sigma^*$  level from configurationally mixed  $d\sigma$  and  $X\sigma$  levels; the lowest energy transition is consistent with a  $d\pi^* \to d\sigma^*$  assignment. Kadis and Nocera have shown that excitation into this absorption manifold produces a long-lived red luminescence<sup>61</sup> from crystalline solids ( $\lambda_{em,max} = 760\text{-}850$  nm across the Rh<sup>0</sup>Rh<sup>0</sup>, Rh<sup>0</sup>Rh<sup>II</sup>X<sub>2</sub> and Rh<sup>II</sup>Rh<sup>II</sup>X<sub>4</sub> series) with spectral features characteristic of a  $d\sigma^*$  parentage. In all cases, the luminescence lifetime is 100's of microseconds at low temperatures. The lifetime is temperature independent up to 80-120 K, followed by a sharp monotonic decrease with increasing temperatures. This behavior is characteristic of excited states of  $d\sigma^*$  parentage.

Previous work by Kadis and Nocera<sup>79</sup> showed that the dσ\* excited state is photoactive. Irradiation (λ > 375 nm) of THF solutions of Rh<sup>0</sup>Rh<sup>II</sup>Cl<sub>2</sub> in the presence of the Cl\* trap, 2,3-dimethyl-1,3-butadiene (DMB) resulted in the appearance and subsequent disappearance of a band at 570 nm in the UV-vis spectrum.<sup>79</sup> It was postulated, based on the results of studies carried out on the photoreactivity of Rh<sub>2</sub>(bridge)<sub>4</sub><sup>2+</sup>,<sup>36</sup> that the 570 nm band is indicative of dimerization of one-electron mixed-valence binuclear species, though the products were not equivocally identified. These results led us to consider whether the dσ\* excited state could be used to interconvert among the two-electron bimetallic cores of this series of compounds. Because the Rh<sup>0</sup>Rh<sup>II</sup>Br<sub>2</sub> should undergo reductive elimination of halogen more readily than Rh<sup>0</sup>Rh<sup>II</sup>Cl<sub>2</sub>, owing to the weaker metal-halide bond, the photochemistry of the former dimer was investigated. This Chapter describes the photoinduced reductive elimination of bromine from Rh<sup>0</sup>Rh<sup>II</sup>Br<sub>2</sub> to give a Rh<sup>0</sup>Rh<sup>0</sup> photoproduct.

# **B. Photochemistry**

The absorption spectrum of Rh<sub>2</sub>Br<sub>2</sub>(dfpma)<sub>3</sub>( $\eta^1$ -dfpma) in THF, shown in Figure 5.3, is dominated by three bands  $(\lambda_{\text{max}}/\text{nm}(\epsilon/\text{M}^{-1}\text{cm}^{-1}) = 300 (12,300), 358$ (9800) and 415 (8600). Definitive assignments for the electronic transitions in this and other dirhodium fluorophosphine complexes, based on the spectral trends of previously assigned D<sub>4h</sub> M-M complexes are tenuous<sup>61</sup> because configuration interaction between metal- and ligand based orbitals is more extensive in the lower symmetry dirhodium complexes. Nevertheless, the energy trends of the halide series led to the assignment of the higher energy bands at 300 and 358 nm to configurationally mixed d $\sigma \to d\sigma^*$  and  $X\sigma \to d\sigma^*$ transitions. The lowest energy transition at 415 nm is characteristic of a  $d\pi^* \rightarrow$ dσ\* assignment. Excitation into at any wavelength encompassed by this absorption manifold produces a long-lived red luminescence ( $\lambda_{em,max} = 760$  nm) from of crystalline solids; the luminescence spectrum is shown in Figure 5.3.61 As discussed above, the spectral trends of this luminescence is consistent with a dσ\* parentage. The luminescence lifetime of 190(10) μs is temperature independent up to 90 K, which is followed by a sharp monotonic decrease with increasing temperatures. In contrast, luminescence is not detected from solutions at temperatures equivalent to those at which crystalline solids emit. Moreover, luminescence is promptly lost from solutions at temperatures above glassing transitions. These results suggest a dominant nonradiative decay pathway for the  $d\sigma^*$  excited state that involves bond dissociation.

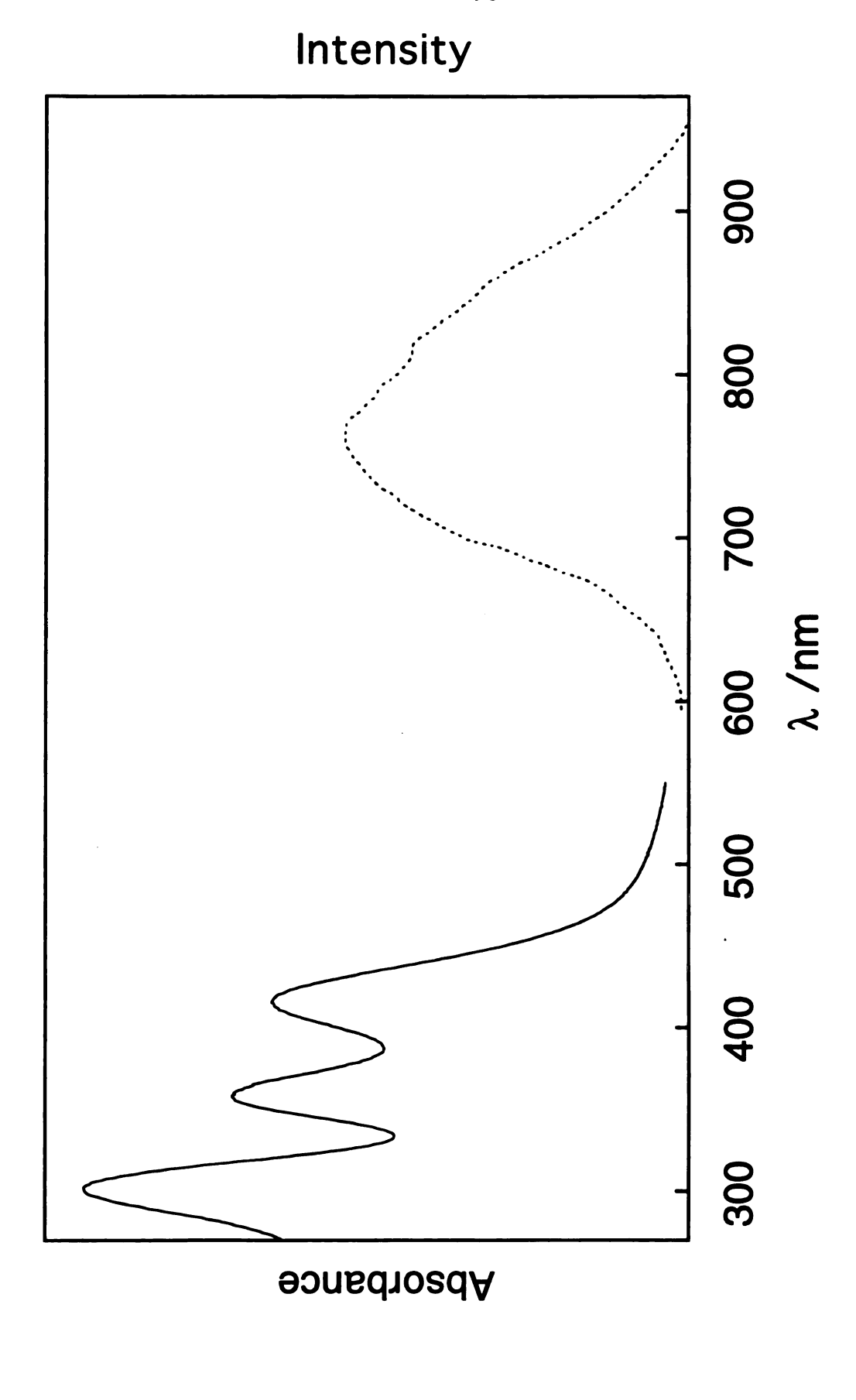


Figure 5.3 Electronic absorption spectrum of Rh<sub>2</sub>(dfpma)<sub>3</sub>Br<sub>2</sub>(η<sup>1</sup>-dfpma) in THF. The corrected emission spectrum of the crystalline complex at 77 K is shown as a dashed line.

The spectral changes associated with the irradiation of THF solutions ( $\lambda$  > 305 nm, T = 0 °C) of Rh<sub>2</sub>Br<sub>2</sub>(dfpma)<sub>3</sub>(n<sup>1</sup>-dfpma) in the presence of a large excess of dfpma are shown in Figure 5.4. Under the same conditions as those used for photolysis, solutions are thermally stable; as solutions are warmed (T > 30 °C) however, a slow thermal reaction occurs to yield an unidentified product  $(\lambda_{max} = 340 \text{ nm})$ . Initially two isobestic points are maintained but are lost with continued photolysis, indicating the presence of a secondary photochemical reaction, which becomes important at long times. The photoproduct has an absorption spectrum that matches that of Rh<sub>2</sub>(dfpma)<sub>3</sub>L<sub>2</sub>, which has been structurally characterized for L = PF<sub>3</sub>. The absorption spectrum of Rh<sub>2</sub>(dfpma)<sub>3</sub>(PF<sub>3</sub>)<sub>2</sub> displays an intense band at 305 nm attributable to the allowed  $d\sigma \rightarrow d\sigma^*$  and a broader, much less intense band at lower energy consistent with  $d\pi^* \to d\sigma^*$  promotion. The dfpma ligand was used in place PF<sub>3</sub> for the photochemical studies discussed in this Chapter because the former is a liquid and can be more readily purified and rigorously deoxygenated prior to use. The photoproduct was isolated and characterized by electrospray mass spectrometry (ES/MS), shown in Figure 5.5. Molecular ion peaks observed at MH<sup>+</sup> m/z = 974 and 906 amu correspond to Rh<sub>2</sub>(dfpma)<sub>3</sub>( $\eta^{1}$ dfpma)(F<sub>2</sub>PCH<sub>3</sub>NH) and Rh<sub>2</sub>(dfpma)<sub>3</sub>(F<sub>2</sub>PCH<sub>3</sub>NH)<sub>2</sub>, respectively. Efforts to obtain crystals of the photoproduct that were suitable for x-ray crystallographic analysis were unsuccessful.

These results are in good agreement with previous studies<sup>79</sup> in which a THF solution of  $Rh_2Br_2(dfpma)_3(\eta^1-dfpma)$  was photolyzed in the presence of both excess dfpma and DMB. The fast-atom-bombardment mass spectrum of the

Figure 5.4 Electronic absorption spectral changes during the photolysis  $(\lambda_{exc} > 305 \text{ nm})$  of  $Rh_2(dfpma)_3Br_2(\eta^1\text{-dfpma})$  in THF with excess dfpma. Spectra were recorded after 0, 5, 20, 50, 85, 210, 420, 1260 min. The spectrum of independently prepared  $Rh_2(dfpma)_3(PF_3)_2$  is shown as a dashed line. The open circles are quantum yields for the photoreaction at the specified wavelengths.

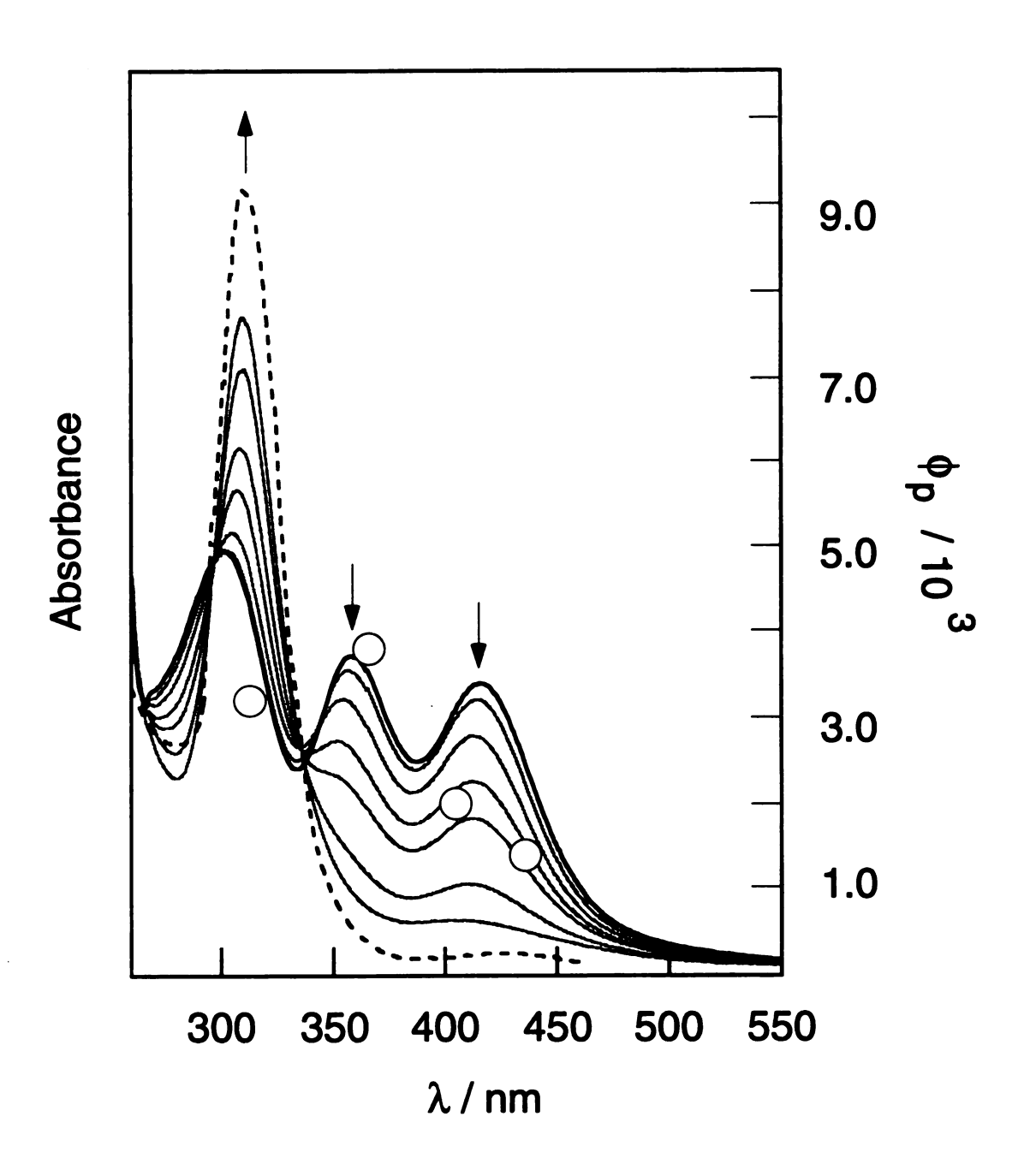


Figure 5.4

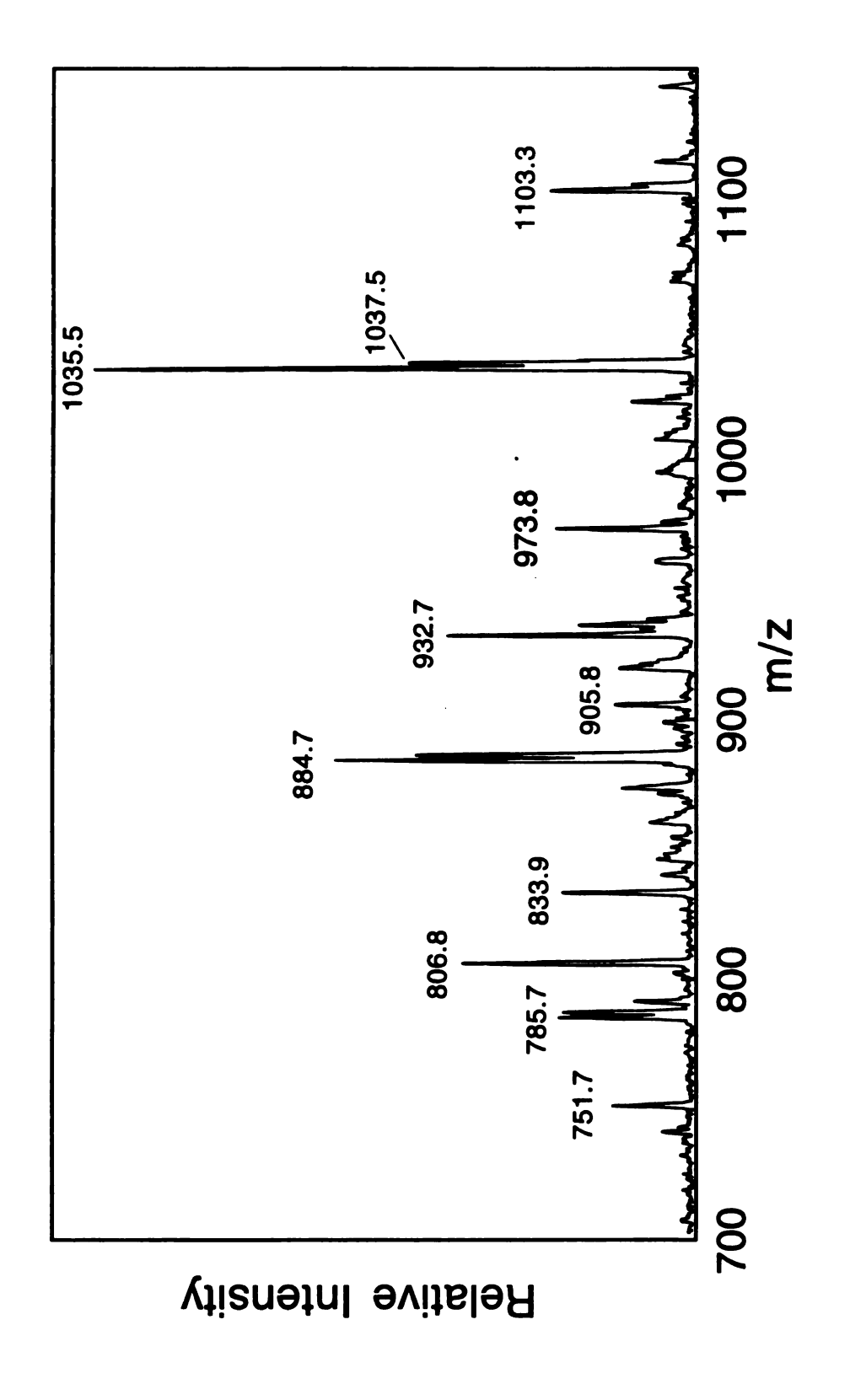


Figure 5.5 ES-MS spectrum of the final products resulting from the photolysis ( $\lambda_{\rm exc} > 305$  nm) of Rh<sub>2</sub>(dfpma)<sub>3</sub>Br<sub>2</sub>(η<sup>1</sup>-dfpma) in THF with excess dfpma.

the molecular ion peak for Rh<sub>2</sub>(dfpma)<sub>3</sub>( $\eta^{1}$ photoproduct contains 976 dfpma)(F<sub>2</sub>PCH<sub>3</sub>NH) amu and fragmentation peaks at from Rh<sub>2</sub>(dfpma)<sub>3</sub>(F<sub>2</sub>PCH<sub>3</sub>NH)<sub>2</sub> and the Rh<sup>0</sup>Rh<sup>II</sup>Br<sub>2</sub> starting material. The FAB mass spectrum of the products from the photolysis of THF solutions of Rh<sub>2</sub>Br<sub>2</sub>(dfpma)<sub>3</sub>( $\eta^1$ -dfpma) in the presence of DMB but without excess dfpma does not show any evidence of Rh<sub>2</sub>(dfpma)<sub>3</sub>(n<sup>1</sup>-dfpma)(F<sub>2</sub>PCH<sub>3</sub>NH), no product with a mass higher than 905 amu was observed. Molecular ion peaks were detected for Rh<sub>2</sub>(dfpma)<sub>3</sub>(F<sub>2</sub>PCH<sub>3</sub>NH)<sub>2</sub> and Rh<sub>2</sub>(dfpma)<sub>3</sub>(F<sub>2</sub>PCH<sub>3</sub>NH)(F<sub>2</sub>PH) at 905 and 874 amu, respectively. A comparison of these FABMS results clearly shows that photoproducts with unhydrolyzed  $\eta^1$ -dfpma ligands are only obtained when irradiation is carried out in the presence of excess dfpma. The occurrence of photoproducts where the N—P bond of the unligated PF<sub>2</sub> has been hydrolyzed could be the result of a secondary reaction between photogenerated HBr and  $\eta^1$ -dfpma.

$$PF_2N(CH_3)PF_2 + HBr \longrightarrow PF_2N(CH_3)H$$
 (5.1)

The HBr, which subsequently hydrolyzes the  $\eta^1$ -dfpma ligand, could be generated by the reaction of photoeliminated bromine atoms with THF. The homolysis of the N—P bond in F<sub>2</sub>PNR<sub>2</sub> to form [R<sub>2</sub>NH<sub>2</sub>]Br is known to be readily promoted by HBr. <sup>121</sup>

$$F_2PNR_2 + 2HBr \longrightarrow [R_2NH_2]Br$$
 (5.2)

The quantum yield for photolyses carried out in the presence of excess dfpma, shown as open circles in Figure 5.4, is invariant with wavelength in the UV but slowly decreases as the excitation wavelength is extended into the visible region ( $\Phi_p^{311} = 0.0032$ ,  $\Phi_p^{366} = 0.0038$ ,  $\Phi_p^{405} = 0.0020$ ,  $\Phi_p^{436} = 0.0014$ ). The photochemical action spectrum is consistent with the photoreaction occurring from the two higher energy transitions, which involve the promotion of an electron from configurationally mixed  $X\sigma$  and  $d\sigma$  orbitals to  $d\sigma^*$ . A common theme in the photochemistry of  $d^7$ — $d^7$  and  $d^9$ — $d^9$  bimetallic complexes is that population of the  $d\sigma^*$  orbital leads to significant weakening of σ framework and bond homolysis. In the case of Rh<sup>0</sup>Rh<sup>II</sup>Br<sub>2</sub>, bond homolysis is further promoted by a ligand-to-metal charge transfer  $(X\sigma \to d\sigma^*)$  contribution, which results in the depopulation of the Rh—Br( $\sigma$ ) orbitals. The lowest-energy transition in Rh<sup>0</sup>Rh<sup>II</sup>X<sub>2</sub> is consistent with a  $d\pi^*d\sigma^*$  transition. The loss of charge transfer character, in this transition, is reflected in the lower quantum yields as the excitation wavelength is shifted to the red. The quantum yield for the photoreductive elimination of halogen from Pt<sub>2</sub>(pop)<sub>4</sub>X<sub>2</sub><sup>4</sup> displays a similar wavelength dependence.<sup>38</sup> Specifically, the quantum yields are highest when excitation wavelengths are coincident with the  $\sigma \to d\sigma^*$  transition ( $\sigma$  refers to a combination of  $\sigma_x$  and d $\sigma$  orbitals).

At a given wavelength ( $\lambda$  = 366 nm), the quantum yield decreases dramatically when photolysis is carried out in the absence of excess dfpma ( $\Phi_p^{THF}$  = 0.00058,  $\Phi_p^{xsdfpma}$  = 0.0038). This observation is consistent with the coordination chemistry of the dirhodium fluorophosphine series, which shows that the dfpma ligand is a good monodentate ligand for the reduced rhodium

center. In the photoreaction, the dfpma ligation of the rhodium center can impede the back reaction of eliminated bromine atoms at the site from which they were produced thereby allowing them to be chemically trapped. In contrast, the addition of DMB as a bromine atom trap has relatively little affect on the quantum yield ( $\Phi_p^{DMB} = 0.00048$ ,  $\Phi_p^{xsdfpma/DMB} = 0.0019$ ). These data suggest that photoeliminated bromine atoms are readily trapped by THF at neat solvent concentrations and DMB is not required to promote the photochemistry. The product of the trapping reaction is HBr, which in turn undergoes facile reaction with the noncoordinated end of the dangling dfpma ligand to yield the observed Rh<sup>0</sup>Rh<sup>0</sup> photoproduct. This argument is bolstered by previous studies,<sup>79</sup> which showed that no significant thermal back reaction occurred, over a period of 10 days, in THF solutions of Rh<sup>0</sup>Rh<sup>II</sup>Br<sub>2</sub> that had been photolyzed without DMB or excess dfpma. The work reported here confirms this result; no thermal back reaction was observed when samples of Rh<sup>0</sup>Rh<sup>II</sup>Br<sub>2</sub> that had been photolyzed in THF with excess dfpma were heated to 40 °C, protected from room light, for one week. Solvent dependent photochemical studies are also in accordance with the contention that THF is acting as a bromine radical trap. No photoreaction is observed when photolysis is carried out in either neat CH<sub>2</sub>Cl<sub>2</sub> or neat CH<sub>3</sub>CN. The photoelimination reaction does occur, however, when dichloromethane solutions are irradiated in the presence of the halogen trap DMB. The reaction in dichloromethane, shown in Figure 5.6, does not appear to proceed as cleanly. The addition of excess dfpma accelerates the reaction but does not result in a clean reaction. DMB is insufficiently soluble in CH<sub>3</sub>CN to carryout photochemical experiments. Transient absorption spectroscopy may be able to

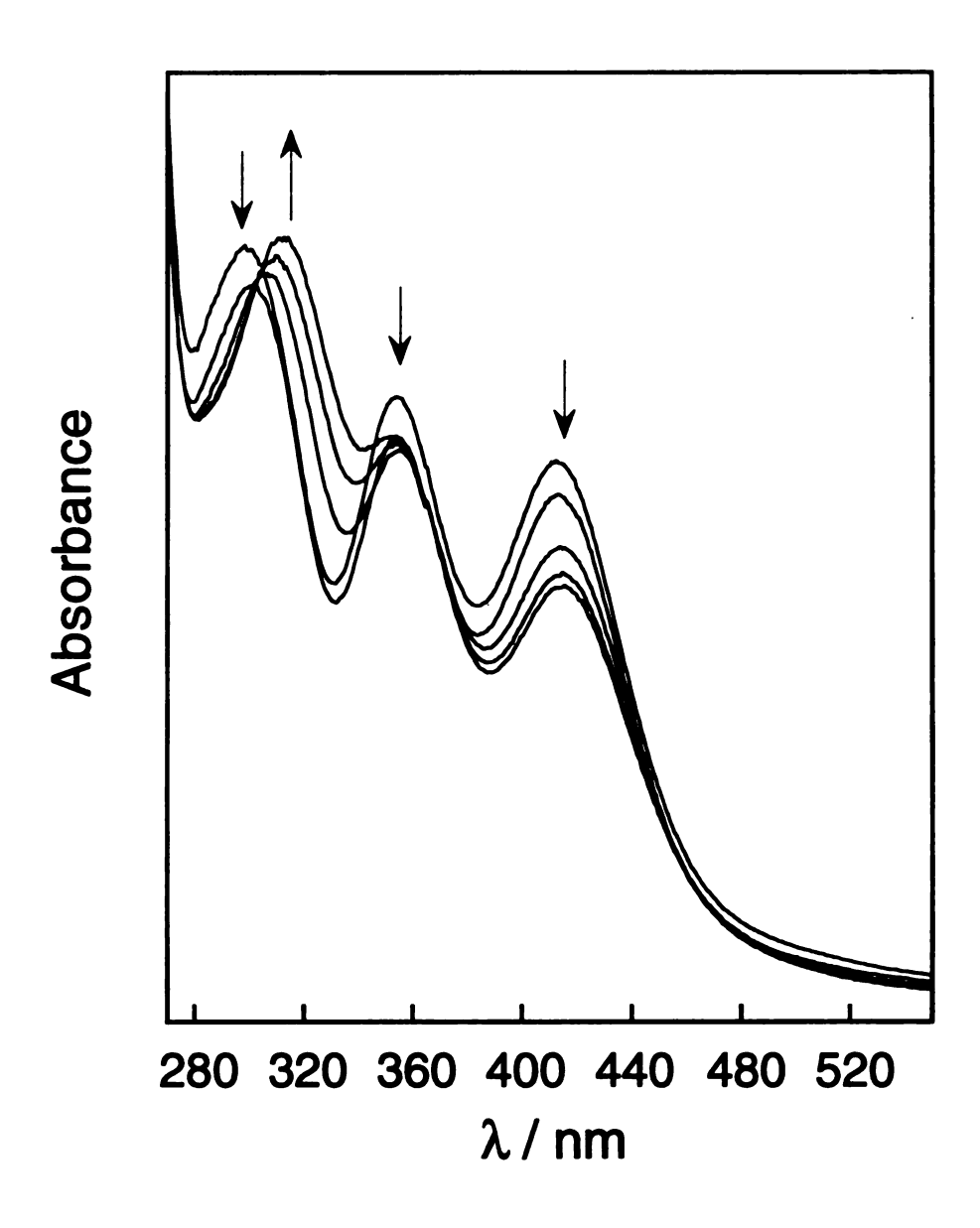


Figure 5.6 Electronic absorption spectral changes during the photolysis  $(\lambda_{eXC} > 305 \text{ nm})$  of Rh<sub>2</sub>(dfpma)<sub>3</sub>Br<sub>2</sub>( $\eta^1$ -dfpma) in CH<sub>2</sub>Cl<sub>2</sub> in the presence of DMB. Spectra were recorded after 0, 10, 90, 180 and 240 min.

provide even further insight into the mechanism of the photoelimination of bromine from  $Rh^0Rh^{II}Br_2$ . However, initial attempts at obtaining transient absorption spectra ( $\lambda_{exc} = 355$  nm) of  $Rh^0Rh^{II}Br_2$  were throated by fluorescence from the spectroscopic cells.

### C. Conclusion

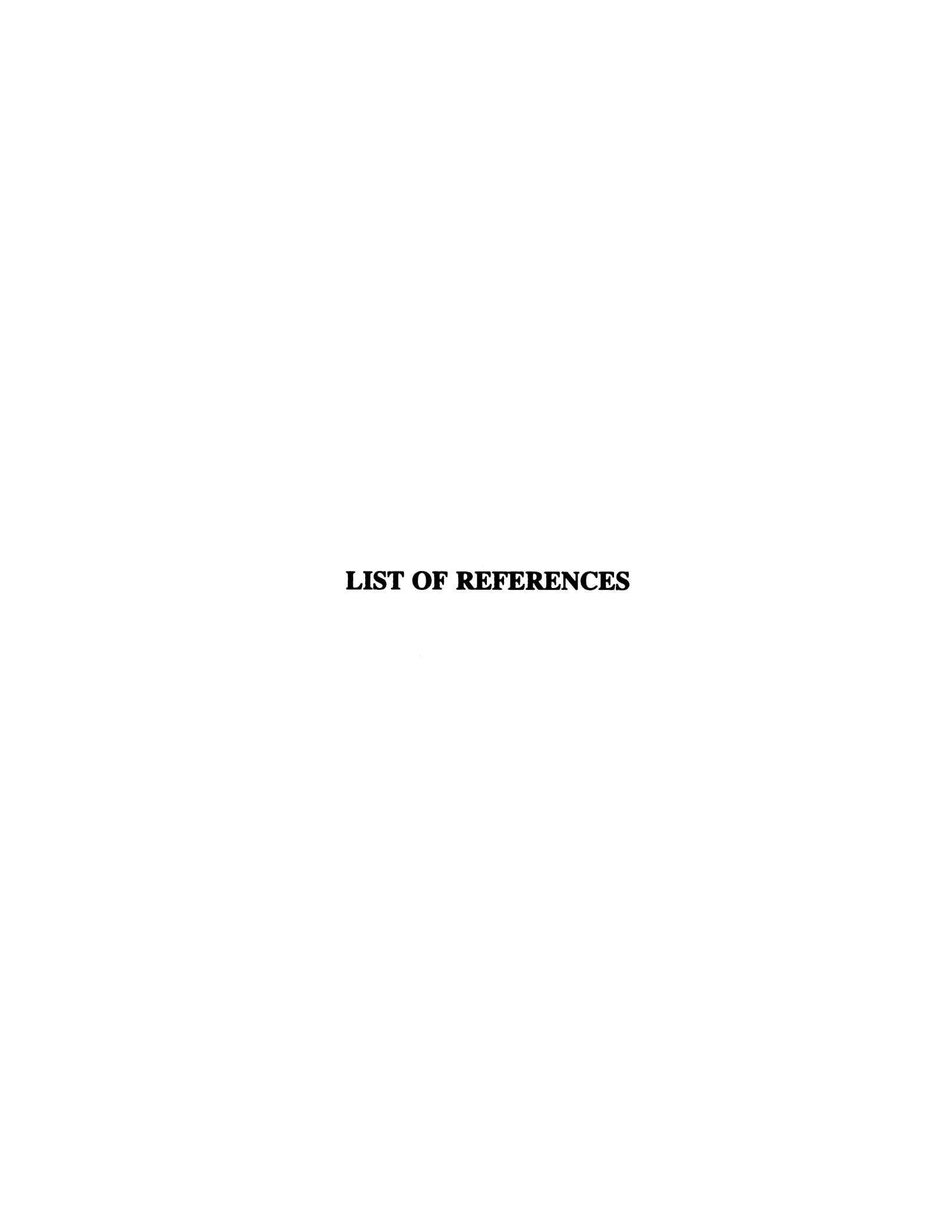
The two-electron photoinduced reductive elimination of bromine from  $Rh^0Rh^{II}Br_2$  is noteworthy because a metal-halide bond usually represents a kinetic and/or thermodynamic sink in energy conversion cycle. It probably does in this case too, but the reactive  $d\sigma^*$  excited state permits us to overcome the barrier to halide elimination. Unlike previous studies of transition metal systems, photo-reductive elimination of halogen is prompted from a  $d\sigma^*$  excited state with two-electron mixed-valence character.

The photoactivity of the  $d\sigma^*$  excited state and the fact that it is preserved across a four-electron series, offers the possibility of interconverting among the  $Rh^0Rh^0$ ,  $Rh^0Rh^{II}X_2$  and  $X_2Rh^{II}Rh^{II}X_2$  cores via two-electron steps. The work described herein clearly demonstrates that the  $d\sigma^*$  excited state permits the photochemical conversion of  $Rh^0Rh^{II}X_2$  to  $Rh^0Rh^0$ . The lowest-energy  $d\sigma^*$  excited state, which is preserved across the four-electron series, also offers the possibility of photochemically converting the  $X_2Rh^{II}Rh^{II}X_2$  complex to  $Rh^0Rh^{II}X_2$ . The next logical step, therefore, is to study the photochemistry of  $Rh_2(dfpma)_3Br_4$ . This reaction would represent the realization of a four-electron

series, in which the  $d\sigma^*$  excited state allows photo-reductive elimination to occur in two-electron steps.

The ultimate goal, in the photochemistry of dirhodium fluorophosphine complexes is to replace X<sub>2</sub> with HX. This goal could, in principle, be attained by adding two equivalents of HX to the Rh<sup>0</sup>Rh<sup>0</sup> complex to produce a  $(H)(X)Rh^{II}Rh^{II}(H)(X)$  hydrido-halide species and use the  $d\sigma^*$  excited state of  $Rh^0Rh^{II}X_2$  and  $Rh^{II}Rh^{II}X_4$  complexes to reductively eliminate  $H_2$  and  $X_2$ . The splitting of HX is a highly endergonic reaction and would therefore be a useful energy storage system. The first significant challenge in the development of such a system is the synthesis of (H)(X)Rh<sup>II</sup>Rh<sup>II</sup>(H)(X). The next major obstacle is to ensure that reductive elimination leads to H2 and X2 and not HX. While the research described in this dissertation initially focused achieving reductive elimination via concerted pathways, the ability to produce halogen by free radical photoelimination may be advantageous in the elaboration of energy conversion cycles. According to the principle of microscopic reversibility, oxidative addition of HX to metal followed by concerted reductive elimination will likely lead to HX again, which is an energetically trivial reaction. A system where HX oxidative addition is followed by radical elimination may be required for the successful development of H<sub>2</sub> and X<sub>2</sub> cycles. The photochemistry observed here for Rh<sup>0</sup>Rh<sup>II</sup>Br<sub>2</sub> is consistent with bromine atom dissociation, which is what is expected from a  $d\sigma^*$  excited state. However, it still must be determined whether the same holds true for the RhIIRhII hydrido-halide complexes. Therefore, once synthesized, photophysical studies of the

(H)(X)Rh<sup>II</sup>Rh<sup>II</sup>(H)(X) species will be necessary in order to determine the nature of its excited states, prior to undertaking any photochemical studies.



### LIST OF REFERENCES

- 1. (a) Energy Resources through Photochemistry and Catalysis; Grätzel M., Ed.; Academic Press: New York, 1983. (b) Photochemical Conversion and Storage of Solar Energy; Connolly, J. S. Ed.; Academic Press: New York, 1981. (c) Photochemical Energy Conversion; Norris, J. R., Jr.; Meisel, D., Eds.; Elsevier: New York, 1989.
- 2. Kutal, C. J. Chem. Ed. 1983, 60, 882.
- 3. Bard, A. J.; Fox, M. A. Acc. Chem. Res. 1995, 28, 141.
- 4. Gratzel, M. Acc. chem. Res. 1981, 14, 376.
- 5. Meyer, T. J. Acc. Chem. Res. 1989, 22, 163.
- 6. Stryer, L.; Biochemistry; W. H. Freeman & Co.: New York, 1988.
- 7. Youvan, D. C.; Marrs, B. L. Sci. Am. 1987, 256(6), 42.
- 8. (a) Kuhlbrandt, W.; Wang, D. N. *Nature* **1991**, *350*, 130. (b) Kuhlbrandt, W.; Wang, D. N. Fujiyoshi, Y. *Nature* **1994**, *367*, 614.
- 9. Hoganson, C. W.; Babcock, G. T. In Metal Ions in Biological Systems, Vol. 30, "Metaloenzymes Involving Amino Acid-Residue and Related Radicals," H. Sigel and A. Sigel, eds.; Dekker: New York, 1994.
- 10. ERDA/NASA Report 1022-77/16 on terrestrial photovoltaic measurement procedures.
- 11. Kutal C. In *Inorganic and Organometallic Photochemistry;* Wrighton, M. S. Ed.; Advances in Chemistry 168; American Chemical Society: Washington, DC, 1978.; pp158-173.
- 12. Lewis, N.S. In *Progress In Inorganic Chemistry Vol. 41*, Karlin, K. D., Ed.; John Wiley Sons: New York, 1994; pp 21-144.

- 13. (a) O'Reagan, B.; Grtäzel, M. Nature 1991, 353, 737. (b) Grätzel, M. Comments Inor. Chem. 1991, 12, 93.
- 14 (a) Kiwi, J.; Gratzel, M. *Nature*. 1979, 657. (b) Kiwi, J.; Gratzel, M. *J. Am. chem. Soc.* 1979, 101, 7214.
- Kalyanasundaram, K.; Gratzel, M. Angew. Chem. Int. Ed. Engl. 1979, 18, 701.
- 16. (a) Brown, G.M.; Chan, S. F.; Creutz, C.; Schwartz, H. A.; Sutin, N. J. Am. Chem. Soc. 1979, 101, 7638. (b) Gratzel, M. Isr. J. Chem. 1979, 18, 3.
- 17. (a) Kiwi, J.; Gratzel, M. J. Am. Chem. Soc. 1978, 100, 6314. (b) Wilner, L; Ford, W. E.; Otvoos, J. W.; Calvin, M. Nature. 1979, 280, 823.
- (a) Shafirovich, V. Y.; Shilov, A. E. Isr. J. Chem. 1988, 38, 149.
   (b) Zamaraev, K. II.; Lymar, S. V. Khramov, M. I.; Parmon, V. N. Pure Appl. Chem. 1988, 60, 1039.
- 19 Gratzel, M. In *Photochemical Conversion and Storage of solar Energy*; Connolly, J. S. Ed; Academic Press: New York, 1981; pp 131-160.
- 20. (a) Gust, D.; Moore, T. A.; Moore, A. L. Acc. Chem. Res. 1993, 26, 198.
  (b) Gust, D.; Moore, T. A.; Moore, A. L.; Lee, S.-J.; Bittersmann, E.; Luttruull, D. K.; Rehms, A. A.; DeGraziano, J. M.; Ma, X. C.; Gao, F.; Belford, R. E.; Trier, T. T. Science 1990, 248, 199.
- 21. Roundhill, D. M.; Photochemistry and the Photophysics of Metal Complexes, Plenum Press: New York, 1994.
- 22. Electron Transfer in Biology and Solid State; Johnson, M. K., King, R. B., Kurtz, D. M., Jr., Kutal, C., Norton, M. L. Scott, R. A., Eds.; Advances in Chemistry 226; American Chemical Society: Washington, DC, 1990.
- 23. Electron Transfer in Inorganic, Organic and Biological Systems; Bolton, J., Mataga, N., McLendon, G., Eds.; Advances in Chemistry 228; American Chemical Society: Washington, DC, 1992.
- 24. Photoinduced Electron Transfer; Fox, M. A., Chanon, M. Eds.; Elsevier: Amsterdam, 1988; Parts A-D.
- (a) Roundhill, D. M.; Gray, H. B.; Che, C-M. Acc. Chem. Res. 1989, 22, 51.
  (b) Smith, D. C.; Gray, H. B. Coord. Chem. Rev. 1990, 100, 169.
- 26. Roundhill, D. M. J. Am. Chem. Soc. 1985, 107, 4354.

- 27. Harvey, E. L.; Stiegman, A. E.; Vlcek, A. Jr.; Gray, H. B. J. Am. Chem. Soc. 1987, 109, 5233.
- 28. Roundhill, D. M.; Atherton, S. J.; Shen, Z-P. J. Am. Chem. Soc. 1987, 109, 6076.
- 29. Marshall, J. L.; Stiegman, A.E.; Gray, H. B. Excited States and Reactive Intermediates; Lever. A. B. P., Ed.; ACS Symposium Series 307; American Chemical Society: Washington, DC, 1986; pp 166-76.
- 30. (a) Vlcek, Jr., A.; Gray, H. B. J. Am. Chem. Soc. 1987, 109, 286. (b) Vlcek, Jr., A.; Gray, H. B. Inorg. Chem. 1987, 26, 1997.
- 31. Geffroy, G. L. In *Progress In Inorganic Chemistry*, Vol. 27; Lippard, S. J. Ed.; John Wiley & Sons: New York, 1980. pp 124-134.
- 32. Geoffroy, G. L.; Pierantozzi, R. J. Am. Chem. Soc. 1976, 98, 8054.
- 33. Geoffroy, G. L.; Hammond, G. S.; Gray, H. B. J. Am. Chem. Soc. 1975, 97, 3933.
- (a) Giannotti, C.; Green, M. L. H. J. Chem. Soc., Chem. Comm. 1972, 1114.
  (b) Elmitti, K.; Green, M. L. H.; Forder, R. A.; Jefferson, I.; Prout, K. J. Chem. Soc., Chem. Comm. 1974, 747.
  (c) Farruga, L.; Green, M. L. H. J. Chem. Soc., Chem. Comm. 1975, 416.
  (d) Green, M. L. H.; Berry, M.; Couldwell, C.; Prout, K. Nouv. J. Chim. 1977, 1, 187.
- 35. Janowicz, A. H.; Bergman, R. G. J. Am. Chem. Soc. 1983, 105, 3929.
- (a) Mann, K. R.; Lewis, N. S.; Miskowski, V. M.; Erwin, D. K.; Hammond, G. S.; Gray, H. B. J. Am. Chem. Soc. 1977, 99, 5525-6. (b) Miskowski, V. M.; Sigal, I. S.; Mann, K. R.; Gray, H. B. J. Am. Chem. Soc. 1979, 101, 4383. (c) Sigal, I. S.; Mann, K. R.; Gray, H. B. J. Am. Chem. Soc. 1980, 102, 7252.
- 37. Caspar, J. V.; Gray, H. B. J. Am. Chem. Soc. 1984, 106, 3029.
- 38 Che, C-M.; Lee, W-M.; Cho, K-C. J. Am. Chem. Soc. 1988, 110, 5407.
- 39. Wright, R. C.; Laurence, G. S. J. Chem. Soc., Chem. Comm. 1972, 132.
- (a) Vogler, A.; Quett, C.; Paukner, A.; Kunkely, H. J. Am. Chem. Soc. 1986, 108, 8263.
   (b) Vogler, A.; Paukner, A. J. Photochem. Photobio. A 1989, 46, 227.
   (c) Becht, A. Vogler, A. Inorg. Chem. 1993, 32, 2835.
- 41. Blazejowski, J.; Szchlinski, J. J. Phochem. 1979, 10, 451.

- 42. Vogler, A.; Nikol, H. Pure Appl. Chem. 1992, 64, 1311.
- 43. Bell, T. N.; Boonstra, M.; Dobud, P. A. J. Am. Chem. Soc. 1970, 92, 4521.
- 44. Vogler, A.; Paukner, A. Inorg. Chim. Acta, 1989, 163, 207.
- 45. Vogler, A.; Paukner, A. Kunkely, H. Coord. Chem. Rev. 1990, 97, 285.
- 46. Geffroy, G. L.; Wrighton, M. S.; Organometallic Photochemistry; Academic Press: New York, 1979.
- 47 Nocera, D. G. Acc. Chem. Res. 1995, 28, 209.
- 48. Cotton, F. A.; Walton, R. A.; Multiple Bonds Between Metal Atoms 2nd ed. Claredon Press: Oxford, 1993.
- 49. Trogler, W. C.; Gray, H. B. Acc. Chem. Res. 1978, 11, 232.
- 50. Hay, P. J. J. Am. Chem. Soc. 1982, 104, 7007.
- 51. Cotton, F. A. Polyhedron 1987, 6, 667.
- 52. Poli, R.; Torralba, R. C. Inorg. Chim. Acta 1993, 212, 123.
- 53. Winkler, J. R.; Nocera, D. G.; Netzel, T. L. J. Am. Chem. Soc. 1986, 108, 4451.
- Partigianoni, C. M.; Turro, C.; Shin, Y-g. K.; Motry, D. H.; Kadis, J.; Dulebohn, J. I.; Nocera, D. G. In *Mixed-Valency Systems: Applications in Chemistry, Physics and Biology; Presides*, K. Ed.; NATO ASI Series C: Mathematical and Physical Sciences-Vol. 343; Kluwer Academic: Doordrecht, 1991; pp 91-106.
- 55. Hsu, T.-L. C.; Helvoigt, S. A.; Partigianoni, C. M; Turro, C.; Nocera, D. G. *Inorg. Chem.* **1995**, *34*, 6186.
- 56. Partigianoni, C. M.; Nocera, D. G. Inorg. Chem. 1990, 29, 2033.
- Partigianoni, C. M.; Turro, C.; Hsu, T.-L.; Chang, I-J.; Nocera, D. G. In *Photosensitive Metal-Organic Systems*; Kutal C., Serpone, N., Eds.; Advances in Chemistry 238; American Chemical Society: Washington, DC, 1993; pp 147.
- 58. Helvoigt, S. A. Ph. D. Dissertation, Michigan State University, 1997.

- 59. Dulebohn, J. I.; Ward, D. L.; Nocera, D. G. J. Am. Chem. Soc. 1988, 110, 4059.
- 60. Dulebohn, J. I.; Ward, D. L.; Nocera, D. G. J. Am. Chem. Soc. 1990, 112, 2969.
- 61. Kadis, J.; Shin, Y.-g.; Dulebohn, J. I.; Ward, D. L.; Nocera, D. G. *Inorg. Chem.* 1996, 35, 811.
- 62. Harwood, W. S.; Kennedy, S. M.; Lytle, F. E.; Qi, J-s.; Walton, R. A. *Inorg. Chem.* 1987, 26, 1784.
- 63. San Filppo, J. Jr. Inorg. Chem. 1972, 11, 3140.
- 64. Glicksman, H. D.; Hamer, A. D.; Smith, T. J.; Walton, R. A. *Inorg. Chem.* 1976, 15, 2205.
- 65. Bursten, B. E.; Kaufmann, G. B. *Inorg. Chem.* **1985**, 24, 1165.
- 66. Fanwick, P. E. Inorg. Chem. 1985, 24, 258.
- 67. Canich, J. M.; Cotton, F. A.; Dunbar, K. R.; Falvello, L. R. *Inorg. Chem.* 1988, 27, 804.
- 68. Cotton, F. A.; Daniels, L. M.; Dunbar, K. R.; Falvello, L. R.; O'Connor, C. J.; Price, A. C. *Inorg. Chem.* 1991, 30, 2509.
- 69. Best, S. A.; Smith, T.J.; Walton, R. A. Inorg. Chem. 1978, 17, 99.
- 70. Campbell, F. L.; Cotton, F. A.; Powell, G. L. *Inorg. Chem.* 1984, 23, 4222.
- 71. Cotton, F. A.; Dunbar, K. R.; Poli, R. Inorg. Chem. 1986, 25, 3700.
- 72. Nixon, J. F. J. Chem. Soc. A 1968, 2689.
- 73. Bennett, M. A.; Patmore, P. J. Inorg. Chem. 1971, 10, 2387.
- 74. Kadis, J.; Nocera, D. G. unpublished results.
- 75. Mussel, R. D.; Nocera, D. G. J. Am. Chem. Soc. 1988, 110, 2764.
- 76. Saari, E. A. Ph. D. Dissertation, Michigan State University, 1997.
- 77. Van Houten, T.; Watts, R. J. J. Am. Chem. Soc. 1976, 98, 4853.
- 78. Demas, N. J.; Crosby, G. A. J. Phys. Chem. 1971, 75, 996.

- 79. Bowman, L. E.; Berglund, K. A.; Nocera, D. G. Rev. Sci. Instrum. 1993, 64, 338.
- 80. Kadis, J. Ph. D. Dissertation, Michigan State University, 1993.
- 81. Ferraudi, G. J. Elements of Inorganic Photochemistry; Wiley: New York, 1988; Chapter 1.5.
- 82. Calvert, J. G.; Pitts, J. N. Photochemistry Wiley: New York, 1966.
- 83. Chang, I-J Ph. D. Dissertation, Michigan State University, 1988.
- 84. Nocera, D. G. J. Cluster Sci. 1994, 5, 185.
- 85. Hsu, T.-L. C.; Engebretson, D. S.; Helvoigt, S. A.; Nocera, D. G. *Inorg. Chim. Acta* 1995, 240, 551.
- 86. Cotton, F. A.; Dunbar, K. R.; Verbruggen, M. G. J. Am. Chem. Soc. 1987, 109, 5498.
- 87. Shih, K.; Fanwick, P.E.; Walton, R. A. Inorg. Chem. 1992, 31, 3663.
- 88. Wu, J.; Fanwick, P. E.; Kubiak, C. P. J. Am. Chem. Soc. 1989, 111, 7812.
- 89 Hopkins, M. D.; Gray, H. B. J. Am. Chem. Soc. 1984, 106, 2468.
- 90. Miskowski, V. M.; Goldbeck, R. A.; Kilger, D. S.; Gray, H. B. *Inorg. Chem.* 1979, 18, 86.
- 91. Zietlow, T. C.; Hopkins, M. D.; Gray, H. B. J. Solid State Chem. 1985, 57, 112.
- 92. Ballhausen, C. J. Molecular Electronic Structures of Transition Metal Complexes; McGraw-Hill: New York, 1979; Chapter 1.
- 93. Manning, M. C.; Troggler, W. C. J. Am. Chem. Soc. 1983, 105, 5311.
- 94. Miskowski, V. M.; Dallinger, R. F.; Christopher, G. C.; Morris, D. E.; Spies, G. H.; Woodruff, W. H. *Inorg. Chem.* 1987, 26, 2127.
- 95. Cotton, F. A.; Dunbar, K. R.; Falvello, L. R.; Tomas, M.; Walton, R. A. J. Am. Chem. Soc. 1983, 105, 4950.
- 96. Hsu, T.-L. C.; Chang, I-J.; Ward, D. L.; Nocera, D. G. *Inorg. Chem.* 1994, 33, 2932.

- 97. Hopkins, M. D.; Miskowski, V. M.; Gray, H. B. J. Am. Chem. Soc. 1988, 110, 1787.
- 98. Miskowski, V. M.; Gray, H. B.; Hopkins, M. D. Inorg. Chem. 1992, 31, 2885.
- 99. Cotton, F. A.; Hong, B.; Shang, M.; Stanley, G. C. *Inorg. Chem.* 1993, 32, 3620.
- 100. Kerbaol, J. M.; Furet, E.; Guerchais, J. E.; LeMest, Y.; Saillard, J. Y.; Sala-Pala, J.; Toupet, L. *Inorg. Chem.* 1993, 32, 713.
- 101. Acho, J. A.; Lippard, S. J. Inorg. Chim. Acta 1995, 229, 5.
- Chakravarty, A. R.; Cotton, F. A.; Diebold, M. P.; Lewis, D. B.; Roth, W. J. J. Am. Chem. Soc. 1986, 108, 971
- 103. CRC Handbook of Physics of Chemistry and Physics, 65th ed.; Weast, R. C. Ed.; CRC Press: Boca Raton, FL, 1984; p D-191.
- 104 Cotton, F. A.; Diebold, M. P.; O'Connor, C. J. Powell, G. L. J. Am. Chem. Soc. 1985, 107, 7438.
- 105 Shaik, S. Hoffmann, R.; Fisel, C. R.; Summerville, R. H. J. Am. Chem. Soc. 1980, 102, 4555.
- 106 Canich, J. A. M.; Cotton, F. A.; Daniels, L. M.; Lewis, D. B. *Inorg. Chem.* 1987, 26, 4046.
- (a) Agaskar, P. A.; Cotton, F. A.; Dunbar, K. R.; Favello, L. R.; O'Connor, C. J. Inorg. Chem. 1987, 26, 4051. (b) Cotton, F. A.; Powell, G. L. J. Am. Chem. Soc. 1984, 106, 3371.
- 108 Chisholm, M. H.; Clark, D. L.; Huffman, J. C.; Van Der Sluys, W. G.; Kober, E. M.; Lichtenberger, D. L.; Bursten, B. E. J. Am. Chem. Soc. 1987, 109, 6796.
- 109 Adedeji, F. A.; Cavell, K. J.; Cavell, S.; Connor, J. A.; Pilcher, G.; Skinner, H. A.; Zafarani-Moattar, M. T. J. Chem. Soc. Faraday Trans. I 1979, 75, 603.
- 110 Ziegler, T. J. Am. Chem. Soc. 1983, 105, 7543.
- 111 (a) March, J. Advanced Organic Chemistry, 4th ed.; Wiley Interscience: New York, 1992. (b) Sumrell, G.; Wyman, B. M.; Howell, R. G.; Harvey,

- M. C. Can. J. Chem. 1964, 42, 2710. (c) Zanger, M.; Rabinowitz, J. C. J. Org. Chem. 1975, 40, 248.
- 112 (a) Skell; Pavis J. Am. Chem. Soc. 1964, 86, 2956. (b) Ayres; Michejta; Rack J. Am. Chem. Soc. 1971, 93, 1389.
- 113 The Chemistry of Double-Bonded Functional Groups, Part 2; Patai, S. Ed.; Wiley Interscience: New York, 1977.
- 114 Cotton, F. A.; Luck, R. L; Son, K.-A. Inorg. Chim. Acta 1990, 173, 131.
- 115 Poli, R.; Mui, H. D. J. Am. Chem. Soc. 1990, 112, 2446.
- 116 Gordon, J. C.; Mui, H. D.; Poli, R.; Ahmed, K. J. *Polyhedron* **1991**, *10*, 1667.
- 117 Kraatz, H-B.; Boorman, P. M. Coord. Chem. Rev. 1995, 143, 35.
- Prassides, K. In Mixed-Valency Systems: Applications in Chemistry, Physics and Biology; Presides, K. Ed.; NATO ASI Series C: Mathematical and Physical Sciences-Vol. 343; Kluwer Academic: Doordrecht, 1991; p. 202.
- 119 King, R. B. Acc. Chem. Res. 1980, 13, 243.
- Jardine, F. H.; Sheridan, P. S. In Comprehensive Coordination Chemistry; Wilkinson, G.; Girard, R. D., McCleverty, J. A., Eds.; Pergamon Press: Oxford, 1987; Vol. 4, chapter 48.
- Albright, T. A.; Burdett, J. K.; Whangbo, M.-H. Orbital Interactions in Chemistry; Wiley-Interscience: New York, 1985; Chapters 15-19.
- 122 Morse, J. G.; Cohn, K.; Rudolph, R. W.; Parry, R. W. *Inorg. Synth.* 1967, 10, 147.